TEMPORAL CHARACTERIZATION OF A THREE-DIMENSIONAL BIOPRINTED MODEL PROVIDES NEW INSIGHT INTO EARLY EVENTS UNDERLYING COMPOUND-INDUCED FIBROTIC LIVER INJURY

Leah M. Norona

A dissertation submitted to the faculty at the University of North Carolina at Chapel Hill in partial fulfillment of the requirements for the degree of Doctor of Philosophy in the Curriculum in Toxicology in the School of Medicine.

Chapel Hill
2017

Approved by:

Paul B. Watkins

William B. Coleman

David A. Gerber

Stephanie Padilla

Carol A. Otey

Sharon C. Presnell

ABSTRACT

Leah M. Norona: Temporal Characterization of a Three-Dimensional Bioprinted Model Provides New Insight into Early Events Underlying Compound-Induced Fibrotic Liver Injury (Under the direction of Paul B. Watkins)

Hepatic fibrosis develops from a series of complex and cumulative interactions among resident and recruited cells in response to sustained injury, making it a challenge to replicate using standard preclinical models. To understand early resident cell-mediated events that occur during this response, we took a three-dimensional approach using commercially available bioprinted liver tissues (ExVive3D™ Human Liver, Organovo) composed of primary human hepatocytes (HCs), endothelial cells (ECs), and hepatic stellate cells (HSCs). Because these cultures sustain important cell interactions and liver-specific functions over an extended period, we assessed the utility to recapitulate fundamental aspects of fibrogenesis following exposure to prototype fibrogenic agents. We first demonstrate compelling evidence of methotrexate-, TGF-β1-, and thioacetamide-induced fibrogenesis following two weeks of exposure with the rapid accumulation of collagen accompanied by transient cytokine release, HSC activation, and time-dependent upregulation of fibrosis-associated genes. To resolve early compound-induced effects, tissues were maintained post-manufacturing and allowed to reach steady-state cytokine production prior to dosing. Although tissue viability/function was not significantly altered, collagen deposition was attenuated suggesting the cytokine milieu post-manufacturing may influence the progression of the response. Temporal differences in LDH (general injury) and ALT (HC-specific injury)

suggest HC injury precedes general, sustained injury following repeated methotrexate exposure. To understand the role of resident macrophages in modulating this response, Kupffer cells (KCs) were incorporated into the model. The pattern of general injury in the modified model suggests KCs shorten the injury window and reduce collagen deposition at the mid timepoint. These findings implicate the modulatory role of KCs during early exposure but suggest they may play a bimodal role during later phases where increased collagen deposition was observed. Because fibrosis is a dynamic response, recovery was also assessed. Monitoring of injury/functional markers following removal of the etiological agent suggests the model retains some biochemical capacity to recover. However, the two-week recovery timeframe may not have been sufficient to visualize collagen regression. This work lays the foundation for a well-defined, dynamic model of compound-induced liver fibrosis that will provide mechanistic insight into the early events underlying fibrogenesis and may inform the development of therapeutic strategies to prevent or reverse fibrosis.

Wheresoever you go, go with all your heart.

- Confucius

ACKNOWLEDGEMENTS

The road to obtaining your Ph.D. is not only a quest for new knowledge but one of self-enlightenment. Perhaps most importantly, it includes the unconditional support of family and friends as well as the people you meet along your journey. Although my graduate school experience has been what some may call a tumultuous journey, every experience, obstacle, interaction, setback, and opportunity has helped shape me into the scientist you see standing before you. The completion of this dissertation would not have been possible without the assistance, support, and guidance from many people in my life and I am extremely grateful for that!

Thank you, mom and dad, for believing in me and supporting me every step of the way. You taught me the value of hard work, persistence, and how to keep your cool no matter what life throws your way. Your endless encouragement even during my worst days is what kept me going. To my awesome brothers Chris and Justin- thank you for always being there for me and always challenging me to do better. I'm so proud of you for all that you have accomplished and know that you will continue to do great things! Thank you, Skippy, aka Mama Dog, for the barks of reassurance over the phone and for always being the first to greet me with a wagging tail when I visited home.

Thank you to my family, for all of your unconditional love and support. Grandma, Grandpa, Abuelita, Aunt Viola and Aunt Idella- you played a huge part in raising me and

helped me become the person I am today. I am so grateful for all you have done to support me and my endeavors. Thank you, Uncle Larry, for all of the helpful advice and nuggets of wisdom throughout the years that have helped me put things in perspective. Aunt Maria, I could never thank you enough for your selfless gift- you not only put our worries at ease but also gave my mom the gift of a better quality of life and the chance to watch me defend!

My existence as a scientist would not have been possible without the support and encouragement from my first mentor, Miguel Garcia-Diaz. Thank you for taking a chance on someone with absolutely no prior research experience and for fostering my development as a scientist!

Ed LeCluyse, everything I've accomplished up to this point would not have been possible without your help! Despite joining your lab with limited cell culture experience, I have learned a tremendous amount about the art of primary cell isolation/culture as well as organotypic model development. Your enthusiasm for the research and attention to detail is what sparked my interest in *in vitro* toxicology and the advancement of cell culture platforms. Thank you for the opportunity to develop a great project and the chance to interact and work with lots of great people in the field. Thank you to past LeCluyse Lab members for your help and support and all of the people who taught me various techniques: Kirstin Willie, Manda Edwards, Kelly Rose, Kristina Wolf, Blair Bradford, Angela Green, Jenny Pedersen, Rhiannon Hardwick, Valerie Soldatow, Joel LeCluyse, Tammy Stone, Tristan Thomas, Lola Reid, Eliane Wauthier, Linda Pluta, and Josh Harrill. You ultimately helped me view my research in a new light!

I would also like to thank the members of my committee Paul Watkins, Bill Coleman, David Gerber, Stephanie Padilla, Carol Otey, and Sharon Presnell. When tasked to assemble

a committee, I carefully selected (and even convinced) each and every one of you because of your unique perspectives and expertise. I truly enjoyed presenting my work and having great discussions during our many update meetings. I would like to give a special thanks to my committee chair, Bill Coleman, for always having an open door and for the helpful conversations that have helped me navigate through graduate school.

Thank you so much to Paul Watkins and Merrie Mosedale and the Watkin's lab for taking me on as a student without hesitation when The Hamner Institutes closed and for giving me the opportunity to continue to pursue my project and learn from the best!

A majority of the work described in this dissertation took place at Organovo, Inc. While this involved living out of a suitcase for up to 6 months at a time, the people and the science is what really made it a great experience! This dissertation would not have been possible without Deb Nguyen and Sharon Presnell. I cannot thank you ladies enough for the incredible opportunity to develop and pursue such an exciting project. I don't think any graduate student has been as lucky to have had such a unique experience and great role models. I am truly grateful for your unwavering support to continue the project but also make sure I was fully funded despite the closing of The Hamner Institutes. I would also like to thank all of the awesome past and present Organovo employees for making my visits welcoming and for including me in all of your company socials and parties. It has truly been a pleasure getting to know and work with you all! Special thanks to Candace Grundy, Preeti Bangalore, Ryan Smith, Dean Perusse, Julie Weisse, Elizabeth Paffenroth, Jenny Waters, Sara Aranda, and Jack Goodlaxson (Organovo, Tissue Testing Team) for hosting me at Organovo; Wayne Hardy, Krystal Moon, Roland Cabading, Xin Zhang, and Christine Beckett (Organovo, Manufacturing Team); Chris Young, and Rhiannon Hardwick

(Organovo, R&D) for facilitating the experiments discussed herein; Jeff Nickel, Amber Keeton, Susan Kelly, Vina Keophilaone, and Erika Hong (Organovo, Histology); and Delorise Williams (The Hamner Institutes Histology Core) for providing awesome histological support and technical assistance.

A big thank you to Sharon Presnell, Michael Presnell, Rose Presnell, and animals for graciously offering me a place to stay (for 5+ months!) while I completed my studies at Organovo. I had so much fun with you all and I miss you terribly!

I would like to also acknowledge the friends that I have made here in Chapel Hill over the past five years. Alisa Suen, Matt Wallach, Emma Bowers, Aaron Wesley, Mike Henderson, and Andres Henriquez, thank you for all of the adventures, funny moments, and being there for me and supporting me in more ways than you know. I couldn't have asked for better friends.

And last but not least, thank you to my best friend, soul mate, and companion Michael Pulkoski-Gross. Even though I decided to pursue graduate school 500+ miles away you've always been there for me no matter what. These past 5 years apart have been difficult but my accomplishments as a research scientist would have not been possible without your unconditional love and support. I love you so much!

For all of the family and friends I have not been able to individually thank in this limited space, thank you! You have helped me become the person I am today and make me feel like I can accomplish anything!

PREFACE

The research described in this dissertation was performed in collaboration with Organovo, Inc. to apply a previously developed 3D bioprinted liver model (ExVive 3D™ Human Liver) to examine the early events underlying compound-induced liver injury leading to fibrosis. Direct research support was provided by Organovo which included extended site visits to perform the experiments presented herein but also to gain additional experience and training on various endpoint assays and techniques to better understand the effect of repeated compound exposure on fibrogenic outcome. Parts of Chapter 1 were adapted from a second author book chapter which is currently under editorial review. The subjects covered were outlined by Dr. Edward LeCluyse (former advisor) with additional input from all authors. Contributions to the book chapter were made primarily within the section entitled "Beyond hepatocytes: The putative roles of non-parenchymal cells in human DILI" and subsections describing the roles of Kupffer cells and hepatic stellate cells in maintaining normal liver physiology and their roles during injury. Additional contributions were made in the form of figures, integrating all author's contributions into one cohesive document, and supplementing writing within sections discussing advanced three-dimensional *in vitro* models. Below is the information regarding the book chapter and the list of authors as submitted:

> LeCluyse, E.L., Norona, L.M., Akingbasote, J.A., Howell, L.S., Woodhead, J.L., Cross, M.J., Roth, A.B., Goldring, C.E. (2017) Leading Edge Approaches for *In Vitro* Hepatotoxicity Evaluation. *Comprehensive Toxicology,* Third Edition.

Permission to include/modify minor subsections of the article was retained from Edward LeCluyse.

Chapter 2 represents a first author publication under the guidance of Drs. Edward LeCluyse (former advisor), David Gerber (clinical co-mentor), Sharon Presnell, and Deborah Nguyen (Organovo advisors). A majority of the experiments were performed at Organovo (San Diego, CA) during site visits with follow-up analyses performed at The Hamner Institutes (now Institute for Drug Safety Sciences, RTP, NC). The Organovo Manufacturing Team produced the tissues utilized for all studies, the Tissue Testing Team provided technical guidance on the care and dosing of tissues, and the Organovo and Hamner Histology Cores provided assistance with tissue processing, sectioning, and staining. All authors on the manuscript provided mentoring, direction, and help with revising the manuscript. The data presented in Chapter 2 was published prior to writing the dissertation and can be located using the following citation:

> Norona, L.M., Nguyen, D.G., Gerber, D.A., Presnell, S.C., and LeCluyse, E.L. (2016) Modeling Compound-Induced Fibrogenesis *In Vitro* Using Three-Dimensional Bioprinted Human Liver Tissues. *Toxicological Sciences.* (2016) 154(2): 354-367.

Permission to include the article in its entirety was retained from Oxford University Press as explained here:

https://global.oup.com/academic/rights/permissions/autperm/?cc=gb&lang=en.

Chapters 3 and 4 represent unpublished work with the intent to publish as separate manuscripts. To ensure there were enough tissues from a particular lot to compare the standard model to a modified version containing Kupffer cells, validation of LOT B was performed prior to conducting subsequent studies to ensure consistent biochemical response profiles with LOT A presented in Chapter 2. Methods optimization and lot validation are

described in Appendix 2. The research presented in Chapter 3 was performed under the guidance of Drs. Paul Watkins (current advisor), Merrie Mosedale (co-advisor), David Gerber (clinical co-mentor), Sharon Presnell, and Deborah Nguyen (Organovo advisors). The majority of experiments were performed on site at Organovo with assistance from the Organovo Manufacturing Team, technical guidance from the Tissue Testing Team, and assistance from the Organovo Histology Core. Follow-up experiments were performed at the Institute for Drug Safety Sciences (IDSS). The research presented in Chapter 4 was conceptualized under the guidance of Drs. Edward LeCluyse, Sharon Presnell, and Deborah Nguyen and performed on site at Organovo. Additional follow-up experiments were performed at the Institute for Drug Safety Sciences under the guidance of Drs. Paul Watkins and Merrie Mosedale. The microarray studies and measurement of miR-122 as a hepatocyte-specific marker of injury described in both chapters will be performed with assistance from the UNC Functional Genomics core and under the guidance of Dr. Rachel Church and J. Scott Eaddy (IDSS/UNC Biomarker core), respectively.

.

TABLE OF CONTENTS

LIST OF TABLES

LIST OF FIGURES

LIST OF ABBREVIATIONS

2D	Two-dimensional
3D	Three-dimensional
AA	Allyl alcohol
ACTA2	α-smooth muscle actin
ALT	Alanine aminotransferase
ANOVA	Analysis of variance
AOP	Adverse outcome pathway
APAP	Acetaminophen
APC	Antigen presenting cell
α-SMA	α-smooth muscle actin
ATP	Adenosine triphosphate
BDL	Bile duct ligation
CCl_4	Carbon tetrachloride
CD	Cluster of differentiation
COL1A1	Collagen, type 1, α1
CYP	Cytochrome P450
DAMPS	Damage-associated molecular patterns
DAPI	4’, 6-diamidino-2-phenylindole
DC	Dendritic cell
DILI	Drug-induced liver injury
DMN	Dimethylnitrosamine

DMSO	Dimethyl sulfoxide
EC	Endothelial cell
ECM	Extracellular matrix
EH	Entrapped hepatocytes
ELISA	Enzyme-linked immunosorbent assay
EMT	Epithelial to mesenchymal transition
EtOH	Ethanol
FGF	Fibroblast growth factor
Flt-1	Fms-related tyrosine kinase-1
$GdCl_3$	Gadolinium chloride
HC	Hepatocyte
H&E	Hematoxylin and eosin
HGF	Hepatocyte growth factor
HPRT	Hypoxanthine guanine phosphoribosyl transferase
HRP	Horseradish peroxidase
HSC	Hepatic stellate cell
IHC	Immunohistochemistry
iHSC	Inactivated hepatic stellate cell
IL-1	Interleukin-1
IL-6	Interleukin-6
IMSD	Initiative for Maximizing Student Diversity
JRC	Joint Research Centre
KC	Kupffer cell

LC	Lethal concentration
LDH	Lactate dehydrogenase
LSEC	Liver sinusoidal endothelial cell
MCP-1	Monocyte chemotactic protein-1
MHC	Major histocompatibility complex
MIE	Molecular initiating event
MMP	Matrix metalloproteinase
MPCC	Micropatterned co-culture
MRP	Multidrug resistance-associated protein
MSD	Meso Scale Discovery
MTX	Methotrexate
NADH	Nicotinamide adenine dinucleotide hydride
NASH	Non-alcoholic steatohepatitis
NF	Nodular fibrosis
NFκB	Nuclear factor kappa B
NIEHS	National Institute of Environmental Health Sciences
NIH	National Institutes of Health
NK	Natural killer
NKT	Natural killer T
NOX	Nicotinamide adenine dinucleotide phosphate oxidase
NPC	Non-parenchymal cell
PCLS	Precision-cut liver slices
PCNA	Proliferating cell nuclear antigen

PF	Pericellular fibrosis
RIN	RNA integrity number
ROS	Reactive oxygen species
Rx	Recovery day
RQ	Relative quantity
SD	Standard deviation
SE	Standard error
TAA	Thioacetamide
TASO	Thioacetamide sulfoxide
TGF-β1	Transforming growth factor-beta 1
TIMP	Tissue inhibitor of metalloproteinases
TSA	Tyramide signal amplification
TNF-α	Tumor necrosis factor-alpha
Tx	Treatment day
VEGF	Vascular endothelial cell growth factor

CHAPTER 1 – INTRODUCTION

The prediction of human toxicity from animal or *in vitro* data continues to be a significant challenge not only for the evaluation of drug liability, but also risk assessment in the broader chemical space (Landesmann, 2016, Olson et al., 2000). In particular, adverse outcomes which manifest in the setting of chronic liver injury (*i.e.*, liver fibrosis) are difficult to predict given the latency to onset, limited mechanistic insight, lack of predictive biomarkers, and species differences in the progression and severity of the response (Starkel and Leclercq, 2011). During the past decade, our understanding of the underlying mechanisms of drug- and chemical-induced liver injury has grown immensely along with a greater appreciation for the biological complexities and multicellular interactions that occur during compound exposure that cause, alleviate, or exacerbate perturbations of normal liver function. As human risk and safety assessment strategies have shifted from the traditional high-dose, acute exposure testing in animals, there is an ongoing effort to develop a balanced strategy using an integrated approach of *in vivo*, *in vitro,* and *in silico* model systems to understand the toxicological implications of drugs and the vast array of chemicals with limited toxicity data (Andersen et al., 2010, Judson et al., 2009, Krewski et al., 2010). As such, there are scientific, regulatory, and practical drivers that require more effective and efficient strategies and tools to understand and predict the human response to drug and chemical exposure.

Over the past few years there has been an unprecedented surge in the development of novel organotypic liver culture platforms to investigate the complex interactions of pathways and functions of the liver, as well as mechanisms of action for compound-induced liver injury (Ebrahimkhani et al., 2014, Godoy et al., 2013, LeCluyse et al., 2012, Soldatow et al., 2013). The use of *in vitro* models to assess more physiologically relevant exposure scenarios also presents the challenge of maintaining and exposing cells over longer durations to adequately assess chronic toxicity. In the case of compound-induced liver injury leading to fibrosis, the lack of predictive assays and sufficiently complex models comprising cells intimately involved in the response has limited our understanding of the initial series of events that mediate this outcome and our ability to effectively screen and identify potential fibrogenic drugs and chemicals (Landesmann, 2016, Van de Bovenkamp et al., 2007).

Improvement towards more physiologically-relevant culture systems has been accomplished by incorporating additional liver cell types, such as hepatic stellate cells (HSCs), liver sinusoidal endothelial cells (LSECs) and Kupffer cells (KCs). Additionally, the arrangement of these cells into three-dimensional (3D) tissue-like structures, also supports the long-term culture of primary hepatocytes (HCs) (Godoy et al., 2013). Recent publications have shown that such *in vitro* models have the potential to detect *in vivo*-like liver toxicities not typically achieved or observed with standard two-dimensional (2D) monolayers and represent a significant innovation for the systematic evaluation of more complex adverse outcomes such as liver fibrosis (Achilli et al., 2012, Messner et al., 2013).

This intent of this introductory chapter is to: (i) provide a background on the structural and functional complexities of the liver, (ii) briefly review the main non-parenchymal cells involved in mediating the liver's response to injury, (iii) highlight the

cellular and molecular underpinnings of hepatic fibrosis, (iv) discuss the limitations of recapitulating fibrotic injury using conventional *in vitro* modeling approaches, (v) introduce 3D bioprinted liver tissues and their potential for modeling hepatic fibrosis, and (vi) outline the scope of the dissertation.

1.1 Liver Primer

The development of relevant cell culture models for hepatic toxicity assessment first requires an appreciation for the structural and functional complexities of the liver and a basic understanding of the intricate homeostatic roles of the various resident cell types of which it is comprised. The liver is a highly-vascularized organ strategically positioned at the nexus of blood flow between the gastrointestinal tract and the systemic circulation (Klaassen et al., 2013). As the major site of detoxication processes, resident liver cells are exposed to significant concentrations of exogenous compounds on the order of 10-50 times the concentration measured in the plasma (Ferslew and Brouwer, 2014). The inherent anatomical and physiological design of the liver enables the efficient removal and metabolism of xenobiotics arising from the gut. Consequently, it is also the primary site of potential toxicity (Klaassen et al., 2013).

The liver is further organized on a microstructural level into polygonal units called lobules within which hepatocytes radiate from a central vein (Bioulac-Sage et al., 2008). As blood percolates from the portal tract towards the central vein, blood constituents in the sinusoid transverse the fenestrated sinusoidal endothelium and enter the space of Disse where hepatic stellate cells (HSCs) and hepatocytes (HCs) reside. HCs are functionally demarcated into three zones based on their position along the acinus (Figure 1.1). Within each zone,

unique microenvironments such as gradients in oxygen tension, matrix chemistry, and solute concentrations ultimately influence distinct zonal differences in gene expression, cellular phenotype, and functional capabilities (Gebhardt, 1992, Smith and Wills, 1981, Ugele et al., 1991). Although HCs comprise approximately 60% of the total cell population, there are many other non-parenchymal cell (NPC) types that intimately define their molecular and structural environment (Bioulac-Sage et al., 2008, Kmiec, 2001). These microenvironments and heterotypic cellular interactions mediate the necessary gene expression required for not only for metabolic homeostasis, differentiation, and maturation, but also HC response to insult (Lindros, 1997, Reid et al., 1992, Turner et al., 2011). As such, the maintenance of normal liver function is critically dependent on the interplay among resident cell types as well as the context or microenvironment within which these interactions take place (Cox and Erler, 2011).

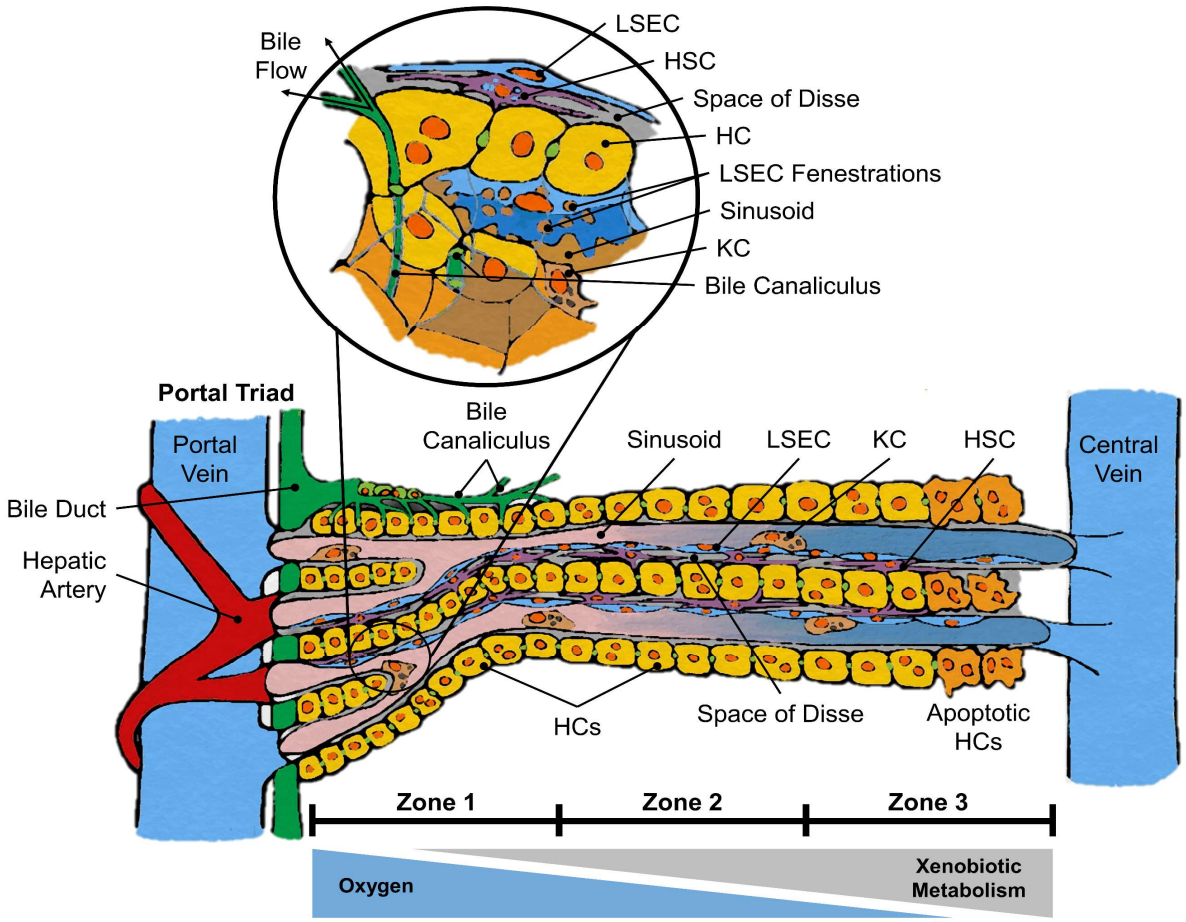

	Periportal	Transitional	Pericentral
Primary Function	β-Oxidation, Gluconeogenesis, Glycogen Synthesis (from lactate), Cholesterol Biosynthesis	Mixture of Zone 1 and Zone 3 functions	Glycogen Synthesis (from glucose), Glycolysis, Lipogenesis, Ketogenesis, Bile Acid Synthesis, Glutamine Synthesis, Heme Synthesis, Xenobiotic Metabolism

Figure 1.1 *Structural zonation of the liver.* Discrete microenvironments or zones of the liver between the portal triad (periportal region) and central vein (pericentral region) illustrating the differences in hepatocyte (HC) phenotype. Due to the flow of mixed blood from the portal vein and hepatic artery towards the central vein, inherent gradients are formed that vary in oxygen tension, nutrient concentrations, and the levels of soluble and bound factors. These gradients are thought to play a role in the creation of localized differences in HC gene expression profiles and phenotypes. Non-parenchymal cells are closely associated with HCs and perform complementary roles necessary to maintain liver homeostasis. The sinusoidal vessels are patrolled by resident macrophages or Kupffer cells (KC) which act as a first line of innate immune defense. Fenestrated liver sinusoidal endothelial cells (LSEC) comprise the sinusoidal walls and form a selective barrier between the sinusoidal blood and HCs. Hepatic stellate cells (HSCs) reside between LSECs and HCs within the space of Disse and perform numerous functions to maintain the hepatic sinusoid on a structural, physical, and chemical basis. Adapted from Turner et al. (2011).

1.2 How is the Liver Equipped to Deal with Injury?

Research investigations geared towards understanding liver injury have focused mainly on the role and involvement of parenchymal cells or hepatocytes (HCs), being the most abundant cell type of the liver, responsible for the clearance of most compounds, and a primary target of toxicity (Klaassen et al., 2013, Rodés, 2007). The liver's ability to cope with injury involves a complex, finely orchestrated interplay among resident hepatic cell types within defined niche microenvironments, with the main goal of restoring normal liver architecture and function.

During both acute and chronic liver injury, non-parenchymal cells (NPCs) including Kupffer cells (KCs), liver sinusoidal endothelial cells (LSECs), and hepatic stellate cells (HSCs) play key roles as immediate responders to injury by mediating the local liver response and facilitating recovery from exposure to drugs and other xenobiotics (Kmiec, 2001). Only recently have we begun to appreciate and account for the numerous and diverse functions of NPCs in shaping the liver's response to injury and role in precipitating more complex adverse outcomes such as hepatic fibrosis-- a process which manifests as an imbalance in reparative processes (Bataller and Brenner, 2005). In the following subsections, the roles of the key resident NPC types in maintaining normal liver function and modulating HC injury are presented in the order by which these cells are organized in the liver traversing the sinusoidal lumen to the perisinusoidal space.

1.2.1 Kupffer Cells: Sinusoidal Sentinels

As a major site for detoxication, the liver is constantly exposed to pathogens, waste products, chemicals, and metabolites via intestinal blood from the portal vein and hepatic arteries (Klaassen et al., 2013). As the primary fixed-tissue macrophage in the liver

accounting for 80-90% of total macrophages in the body, Kupffer cells (KCs) lie at a critical interface between portal and systemic circulation, and play an important role in immune tolerance and surveillance as a first line of innate defense (Bilzer et al., 2006, Ju and Tacke, 2016). KCs possess a high endocytic and phagocytic capacity, efficiently engulfing foreign particles such as bacterial endotoxin and maintaining the sinusoid clear of cellular debris (Bilzer et al., 2006). In addition to their scavenger roles, they also play an important part in normal iron, cholesterol, and bilirubin metabolism (Krenkel and Tacke, 2017).

KCs not only help maintain normal liver physiology and function but also influence acute and chronic responses following their activation during compound-induced injury (Roberts et al., 2007). Much of the cellular crosstalk that occurs amongst KCs and other cell types in the liver is dependent on an array of cell signaling mediators such as reactive oxygen species (ROS), TNF-α, IL-1β, and IL-6. However, cytoplasmic extensions can also traverse LSEC fenestrations making direct contact with HCs and HSCs to mediate cell survival and death (Hoebe et al., 2001, Kolios et al., 2006). KC-derived superoxide radicals via NOX2 and production of TNF-α can enhance collateral damage to surrounding cells and potentiate liver injury via the disruption of cellular homeostasis. While HCs are normally resistant to the cytotoxic effects of TNF-α due to the NF-κB induction of antioxidant gene transcription programs and downstream signaling molecules, perturbations in redox mechanisms sensitize HCs to TNF-α-mediated cytotoxic activity from KCs and other inflammatory cells recruited to the liver during injury (Han et al., 2013).

ROS not only play a role in cellular stress mechanisms, but also mediate KC antigen presentation through the initiation and amplification of major histocompatibility (MHC) complex II and co-stimulatory molecule expression as second messengers (Maemura et al.,

2005). Due to the position of KCs within the sinusoidal space they are uniquely situated to encounter circulating T-lymphocytes entering the liver. Compared to other antigen presenting cells (APCs), such as splenic dendritic cells (DCs), naïve KCs express significantly lower levels of antigen presentation and co-stimulatory molecules, such as MHC II, B7-1 (CD80), B7-2 (CD86), and CD40, making them less potent compared to their professional counterparts in evoking T-cell responses (You et al., 2008). Thus, KCs play an integral part in mediating or remediating pathogenic responses related to injury by adapting their phenotype and cytokine profiles to different environmental cues/soluble stress signals and serve as gatekeepers to facilitate immune responses when appropriate (Tacke and Zimmermann, 2014).

During both acute and chronic liver injury, there is a substantial shift in the proportion of resident versus recruited macrophages (Pellicoro et al., 2014). Thus, the precise role of KCs during the initiation, progression, and remediation of injury has been elusive primarily due to the inability to specifically target specific macrophage subsets during injury (*i.e.*, resident versus recruited) (Tacke and Zimmermann, 2014). Many studies have demonstrated that inhibition or depletion of macrophages using a battery of techniques (*i.e.*, gadolinium chloride, glycine, clondronate-encapsulated liposomes, transgenic approaches) significantly attenuates compound-induced liver injury and fibrosis in rodent models (Duffield et al., 2005, Ramachandran and Iredale, 2012). Contrary to these findings, other studies have reported increased toxicity with KC depletion following acute acetaminophen (APAP) exposure in mice due to the absence of macrophage-mediated compensatory mechanisms such as the upregulation of hepatic transporters (*e.g.,* MRP4), during initial insult to limit APAP toxicity (Campion et al., 2008, Ju et al., 2002). Furthermore, KCs are

capable of modulating the basic functions and metabolic activity of HCs via production of inflammatory cytokines (*e.g.*, IL-1, IL-6 and TNF-α) that induce the expression of acute phase proteins while causing the down-regulation of genes involved in the metabolism and clearance of xenobiotics (Hoebe et al., 2001, Morgan, 2009, Zinchenko et al., 2006). The contradictory roles that have been ascribed to KCs suggest, they may play an initial protective role and that impairment of KC function during injury may lead to a heightened immune response in the liver and further exacerbate compound-induced injury. While the role of resident KCs in mediating injury has not been extensively studied in detail, it is something that can be potentially addressed with advanced *in vitro* modeling approaches as described further in Chapter 3.

1.2.2 Sinusoidal Endothelial Cells: Dynamic Barriers

Liver sinusoidal endothelial cells (LSECs) represent morphologically distinct cells that discontinuously line the sinusoid and lie at the interface between blood flowing into the sinusoid and the hepatic parenchyma. These cells comprise about 50% of the total number of NPCs and are unique to the liver in that they are the only mammalian endothelial cells that possess open transcellular pores or fenestrations and lack an organized basement membrane (DeLeve, 2011, Hang et al., 2012). The presence of fenestrations (50-150 nm in diameter) facilitate parenchymal oxygenation, the passive transport of solutes, the coordinated exchange of particulates such as lipoproteins between the circulating blood and perisinusoidal space, and efficient clearance of xenobiotics (Deleve et al., 2004, Fraser et al., 1995, Stolz, 2011).

As a first point of contact with macromolecules and antigens entering the portal circulation, LSECs play a complementary role to KCs as a scavenger system in the clearance

of xenobiotics and act as a selective barrier for transvascular exchange. While KCs phagocytose larger, insoluble particulates, LSECs remove colloids, macromolecules, and soluble components which are less than 0.23 μm in size from the blood via receptor-mediated endocytosis (Elvevold et al., 2008, Shiratori et al., 1993, Smedsrod et al., 1990). Controlled by the actin cytoskeletal network, the diameters of the fenestrae are dynamic and can be adjusted by the pressure of blood flowing through the sinusoid and the effects of vasoactive substances such as alcohol, drugs, and other toxicants (Braet et al., 1996). In uninjured liver, LSECs produce factors that help preserve phenotypic features of other NPCs. For example, HSC quiescence is maintained via LSEC-derived nitric oxide (Deleve et al., 2008). Furthermore, recent evidence has shown that the permissibility of these fenestrations play a key role in cellular signaling events between adjacent cell types during both health and disease (Beninson and Fleshner, 2014, De Maio, 2011, Robbins and Morelli, 2014).

During the onset of liver injury (*e.g.*, alcoholic liver disease, fibrosis, cirrhosis), LSECs undergo a dedifferentiation process and acquire a more vascular phenotype with the formation of an organized basement membrane (Deleve et al., 2004). Other factors that contribute to the loss of fenestrations or capillarization of the endothelium as seen in these phenomena include generation of reactive oxygen species (ROS) and depletion of endogenous antioxidants (*e.g.*, glutathione) (Cogger et al., 2004, Stolz, 2011). Although LSECs are involved in HSC quiescence, when stimulated by TGF-β1, they can produce basement membrane-like ECM components like laminin, fibronectin, and collagen type IV (Rieder et al., 1993). The dedifferentiation of LSECs results in the activation of HSCs further leading to the excess production of ECM within space of Disse and progressive fibrogenesis. Consequently, this can lead to poor oxygenation of the parenchyma and impairment of the

movement of solutes and particles across the endothelium.

1.2.3 Hepatic Stellate Cells: Versatile Modulators of the Hepatic Microenvironment

Hepatic stellate cells (HSCs), also known as lipocytes, fat-storing cells, or Ito cells, are liver-resident pericytes that reside within the space of Disse. Although HSCs constitute about 5-10% of the total liver cell population, they exhibit numerous and diverse functions to maintain the hepatic microenvironment on a structural, physical, and chemical basis (Friedman, 2008). In uninjured liver, HSCs primarily reside in a quiescent state characterized by a dendritic morphology, perinuclear retinyl ester containing lipid droplets, condensed nuclear chromatin, and expression of intermediate filaments (*i.e.*, desmin, vimentin), and neuroendocrine markers (*i.e.*, synaptophysin, nestin, glial fibrillary acidic protein) (Friedman, 2008, Puche et al., 2013). HSCs synthesize a basement membrane-like matrix within the perisinusoidal space and maintain local microenvironments by synthesizing matrix proteins such as collagens III, IV, and laminin (Reid et al., 1992). Matrix turnover and the modulation of biologically active molecules (*i.e.*, cytokine, chemokines, growth factors, and cell surface proteins) are tightly regulated processes via the production of matrix metalloproteinases (MMPs) and tissue inhibitors of metalloproteinases (TIMPs) by both HSCs and KCs (Arpino et al., 2015, Parks et al., 2004). HSC function is further modulated by neighboring parenchymal and NPC types, gradients of circulating substrates, cellular metabolic byproducts, hormones, and extrahepatic factors across the acinus (Friedman, 2008).

Within the space of Disse, HSCs lie at a critical junction which allows them to interact with all the major resident cell types spanning the hepatic sinusoid and function as sinusoidal sensors that constantly survey the surrounding microenvironment (Friedman, 2008). HSCs produce a myriad of factors to help maintain the differentiated phenotypic

features of neighboring cells. Their dendritic processes partially embrace adjacent LSECs and may even extend into the sinusoidal space making contact with resident KCs. The close association between HSCs and LSECs mutually maintain the unique phenotypic features of each cell type (Deleve et al., 2008, Deleve et al., 2004). HSCs have also been implicated in regulating sinusoidal tone due to their contractile properties and the production vascular endothelial growth factor (VEGF), a key mediator involved in maintaining the fenestrated phenotype of LSECs in culture (Deleve et al., 2004, Rockey, 2001). Thus, HSCs play an important role in modulating sinusoidal blood flow and can potentially lead to impairment and increased intrahepatic resistance particularly during injury and disease states where HSCs become activated (Ekataksin and Kaneda, 1999).

HSCs exhibit a dynamic phenotype in response to activating stimuli; their transition from a quiescent to activated phenotype and vice versa is important for orchestrating the wound healing response and resolution following injury (Friedman, 2012, Friedman, 2008). During both acute and chronic liver injury, the integration of signals received from damaged HCs, other NPCs, and the surrounding microenvironment perpetuate HSC activation and transdifferentiation into myofibroblasts. This activation process is characterized by a host of changes, including cell spreading, pro-fibrotic/inflammatory mediator production, proliferation, and the synthesis/deposition of ECM components (Friedman, 2008).

During acute injury, the transient activation of HSCs results in the production of fibrillar collagens and other ECM components which not only act to protect the site of injury from further damage but also form a basic scaffold on which liver cells can repopulate and remodel following injury (Yin et al., 2013). HSCs also have been shown to produce oxidant scavengers to provide a coping mechanism to mediate HC oxidative stress as a result of

compound-induced injury and collateral damage caused by activated KCs and infiltrating extrahepatic inflammatory cells (Jameel et al., 2010). Furthermore, HSC-derived cytokines and growth factors during their transient activation help promote the regeneration of parenchymal cells and coordinate the reconstitution of normal liver architecture (Kalinichenko et al., 2003). Studies in rodent models have suggested a close association between HSCs and the progenitor cell compartment that promotes the expansion, differentiation, and maturation of parenchymal cells via matrix remodeling and the production of growth factors such as fibroblast growth factor 7 (FGF7) and hepatocyte growth factor (HGF) (Pintilie et al., 2010). While wound healing processes are initiated with repair as the primary intention, persistent damage disrupts this tightly regulated response program which ultimately leads to the derangement of normal liver architecture and impaired liver function.

1.3 Hepatic Fibrosis Arises from the Setting of Chronic Injury

1.3.1 Fibrosis is an Abnormal Wound Healing Response

The liver is well-equipped to deal with injury through a highly-orchestrated interplay among resident hepatic cell types which act as the first responders to injury. In the setting of chronic liver injury, this response manifests as a maladaptive wound healing response and can occur on the order of months to years (Bataller and Brenner, 2005). Fibrosis is a dynamic process during which simultaneous damage and repair processes ultimately lead to a net increase in the formation of scar tissue. As depicted in Figure 1.2, some of the major hallmarks of the response include: HC injury, presence of HSC-derived myofibroblasts, an imbalance in the deposition/degradation of ECM, inflammation in the form of resident KC

activation but also the recruitment of inflammatory cells, and the sustained production of growth factors and cytokines (Iredale, 2007). The microenvironmental context of injury (*i.e.*, paracrine factors produced by other cell types, autocrine factors, ECM composition/rigidity) plays a major role in initiating and sustaining a fibrogenic response (Bataller and Brenner, 2005, Friedman, 2008). As a result, these factors drive the progressive displacement of the liver parenchyma with scar tissue leading to a distortion of normal tissue architecture and ultimately a perturbation of normal liver function if the underlying etiology is not identified and removed/corrected.

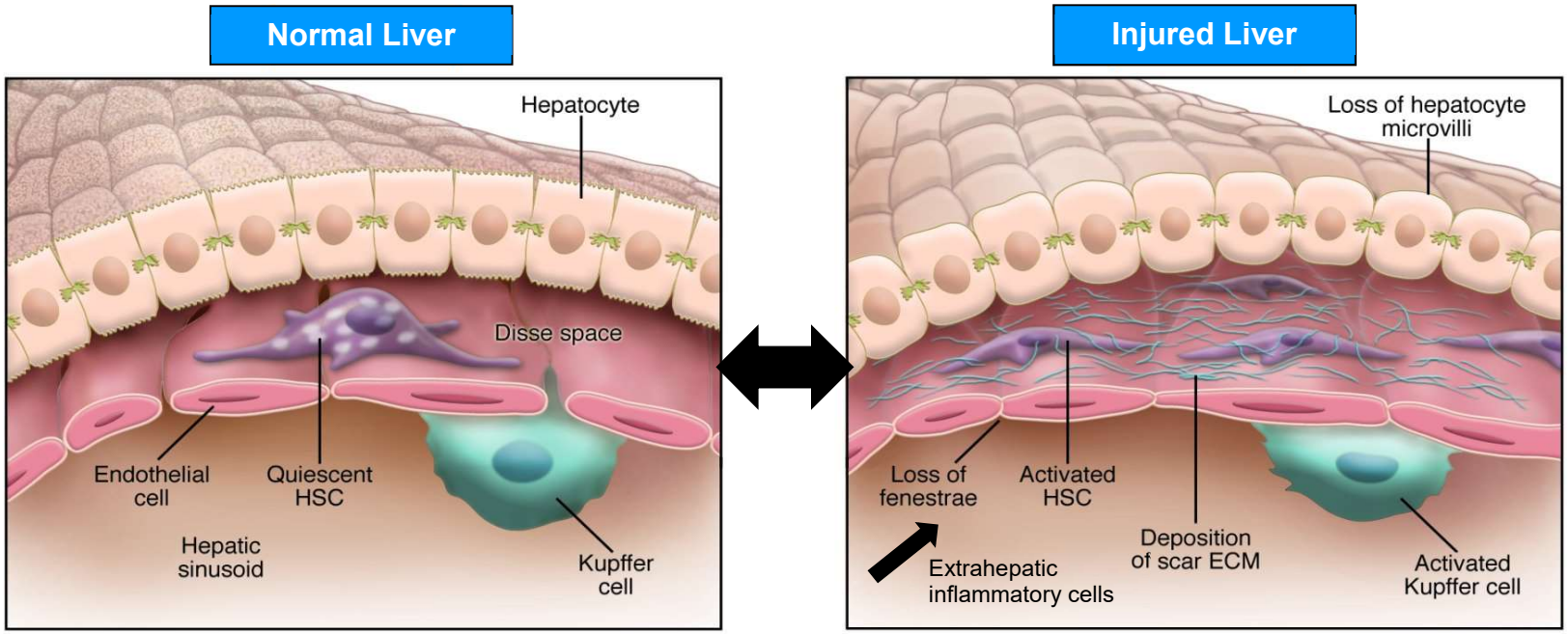

Figure 1.2 *Hallmarks of hepatic fibrosis*. Some of the major hallmarks include: capillarization of the sinusoidal endothelium, hepatocellular damage, activation of hepatic stellate cells (HSCs), a net increase in scar extracellular matrix (ECM), activation of resident macrophages or Kupffer cells, and recruitment of extrahepatic cells to the site of injury. In addition, fibrosis is a bidirectional process. Adapted from Friedman (2000) and Iredale (2007).

1.3.2 Lessons Learned from Animal Models: Current Concepts

Much of our current understanding and major advances in the field have been gleaned from rodent models of fibrotic liver injury employed over the past several decades. The most common rodent models involve iterative toxic damage as a result of compound exposure and bile duct ligation to mimic hepatotoxic and cholestatic injury, respectively (Starkel and Leclercq, 2011). The use of different agents and exposure regimens evoke patterns of fibrotic injury that are similar in some respects to the human pathology (*e.g.*, periportal versus pericentral fibrosis, bridging fibrosis, pericellular fibrosis, steatohepatitis, compensatory proliferation) (Crespo Yanguas et al., 2016, Starkel and Leclercq, 2011). Furthermore, these models can mimic disease aspects such as lipid accumulation observed in non-alcoholic steatohepatitis (NASH) via special diets (*i.e.*, methionine and choline deficiency) (Crespo Yanguas et al., 2016). Table 1.1 outlines the most common methods for inducing fibrosis in rodent models. While these various models exhibit features of clinically relevant fibrosis and have been a critical aspect in understanding basic mechanisms underlying the dynamic nature of the response in an intact system, no model fully recapitulates the complexities of the human pathogenesis and therefore are of limited predictive value with regards to toxicity risk assessment (Liedtke et al., 2013).

The following subsections describe some of the current concepts in hepatic fibrogenesis which are important features to consider when developing strategies for risk assessment purposes and more predictive models aimed at recapitulating the progression of the response in an *in vitro* context.

Table 1.1 *Experimental in vivo models of hepatic fibrosis*

Model	Mechanistic basis	Pattern of Injury	Advantages	Disadvantages
Alcoholic				
Ethanol (EtOH)	CYP450-mediated biotransformation to reactive metabolites	Mild centrilobular fibrosis Steatosis	Can be used to study certain aspects of alcoholic liver disease	Not a comprehensive model of alcoholic liver disease
	Enhanced immune response Increased collagen synthesis	Inflammatory infiltrate		Long time to develop (>3 months) Requires intragastric feeding
Hepatotoxic				
Carbon tetrachloride (CCl_4)	CYP2E1-mediated biotransformation to reactive metabolites	Pericentral fibrosis Inflammation Bridging fibrosis	First appearance of histological fibrosis observed after 2 to 3 weeks of exposure	Intraperitoneal administration can induce chronic peritonitis
		Cirrhosis	Robust and high reproducibility Close to human liver fibrosis	Susceptibility is variable across species and strain dependent
Thioacetamide (TAA)	CYP2E1-mediated biotransformation to reactive metabolites Immunological response	Centrilobular necrosis Pericentral and periportal fibrosis Cirrhosis	Often used as a second independent approach to confirm results obtained from other models	Long time to develop (6 weeks or longer) Slow reversibility
Dimethylnitrosamine (DMN)	CYP2E1-mediated biotransformation to reactive metabolites	Pericentral fibrosis Centrilobular fibrosis	Good model to study hepatocellular carcinoma (HCC)	Not ideal for the study of liver fibrosis due to strong mutagenic/carcinogenic properties
Cholestatic				
Common bile duct ligation (BDL)	Increased biliary pressure Infiltration of inflammatory cells Portal fibroblast activation	Periportal fibrotic injury Periductular inflammation Cholangiocyte proliferation	Reversibility after relief of the obstruction Close to human cholestatic injury	High mortality rate Variability between animals
Nutritional				
Methionine/choline-deficient diet	Impaired secretion of hepatic triglycerides Lipotoxicity	Pericellular fibrosis Steatohepatitis	Close to human non-alcoholic steatohepatitis (NASH)	Susceptibility is variable across species and strain dependent
			Rapid development of steatosis and inflammation (~2 weeks)	Lack of obesity and peripheral insulin resistance
Choline-deficient, L-amino acid-defined diet	Impaired secretion of hepatic triglycerides Lipotoxicity	Pericellular fibrosis Steatohepatitis	Mimics human obesity and peripheral insulin resistance	Development of HCC can hinder the study of liver fibrosis

Adapted from Crespo Yanguas et al. (2016), Liedtke et al. (2013), and Starkel and Leclercq (2011).

1.3.2.1 HSCs are the major contributors to fibrotic liver injury regardless of etiology

One of the major hallmark features of hepatic fibrosis is the presence of myofibroblasts. While these cells are not typically observed in uninjured liver, they are implicated in wound healing and fibroproliferative disorders as the primary source of collagen following injury (Bataller and Brenner, 2005). Over the past few years, several studies have identified potential sources of myofibroblasts in injured liver. These include recruited bone marrow-derived cells (*e.g.*, fibrocytes), epithelial to mesenchymal transition (EMT) of hepatocytes and/or cholangiocytes, portal fibroblasts, and HSCs (Lee and Friedman, 2011). Elegant fate mapping studies coupling the use of transgenic mice and bone marrow transplantation have demonstrated that myofibroblasts derived from activated portal fibroblasts and HSCs constitute the greater proportion of cells that contribute to fibrogenesis (Forbes and Parola, 2011, Taura et al., 2010). Portal fibroblasts are situated in the vicinity of the bile duct and portal vein, and help maintain vessel stability while HSCs reside distally and surround the sinusoidal vessels that direct the flow of blood throughout the liver. The anatomically distinct localization of these cells within the liver implicate there may be distinct contributions of portal fibroblast-derived and HSC-derived myofibroblasts during specific types of liver injury (*e.g.*, cholestatic versus hepatotoxic).

While myofibroblasts have generally been thought of as a homogenous population of cells, recent studies suggest not all fibrogenic cells contribute equally to the myofibroblast population and that their contribution, particularly during early injury, is dependent on their localization (Dranoff and Wells, 2010). During hepatotoxic liver injury, a majority of myofibroblasts are HSC-derived However, portal fibroblast-derived myofibroblasts constitute a greater proportion of cells following the early stages of cholestatic liver injury

(Iwaisako et al., 2014). Nonetheless, HSC-derived myofibroblasts constitute the greater proportion of cells during extended liver injury regardless of etiology (Iwaisako et al., 2014, Mederacke et al., 2013).

1.3.2.2 Liver fibrosis is a reversible wound healing response

Although the reversibility of liver fibrosis has been documented for over two decades, more recent studies have provided compelling evidence that the liver has the capacity to resolve extensive fibrotic injury (Friedman and Bansal, 2006). Spontaneous resolution has been observed in rodent models of fibrotic liver injury whereby removal (*i.e.*, cessation of treatment) or correction (*i.e.*, removal of biliary obstruction) of the underlying etiology results in remodeling and reversal to near normal liver microarchitecture (Iredale et al., 1998, Kisseleva et al., 2012, Traber et al., 2013) (Figure 1.3A). Furthermore, case studies involving patients successfully treated for chronic viral infection demonstrate that remodeling and regression of excess scar tissue is possible in humans as well (Ellis and Mann, 2012, Marcellin et al.). The regression of hepatic fibrosis is accompanied by gradual disappearance of the myofibroblast population which facilitates this process by rendering the liver matrix susceptible to remodeling by matrix metalloproteinases (MMPs) and collagenases (Pellicoro et al., 2014). What was once considered permanent scarring is now recognized as a very dynamic process and suggests that even more advanced cases of fibrotic injury such as liver cirrhosis could potentially be reversed.

1.3.2.3 Hepatic stellate cells can revert to a quiescent-like phenotype

Lending further to the idea of reversibility, the loss of activated HSCs via cell death or reversion of the phenotype is an important aspect of this process (Iredale et al., 1998). Recent fate mapping studies have confirmed that while some of these activated HSCs or

myofibroblasts undergo apoptosis during resolution, about half of these cells revert to a quiescent-like phenotype (Kisseleva et al., 2012, Troeger et al., 2012) (Figure 1.3B). This net loss in activated HSCs is critical for the self-limiting nature of the wound healing response during acute injury and is an essential step towards the reversal of fibrosis given that activated HSCs are a major source of the collagen in injured liver (Iredale et al., 1998). Interestingly, HSCs that undergo reversion exhibit a unique phenotype that is distinct from naïve quiescent HSCs. These cells, termed inactivated HSCs (iHSCs), exhibit a primed phenotype whereby they exhibit a robust fibrogenic response to re-challenge with activating stimuli (Kisseleva et al., 2012). While the functional advantage of iHSCs may be to facilitate a more effective wound healing response with subsequent insult, the dynamic nature of HSC quiescence, activation, and inactivation is still an important aspect to consider when designing advanced culture models aimed at recapitulating this response *in vitro*.

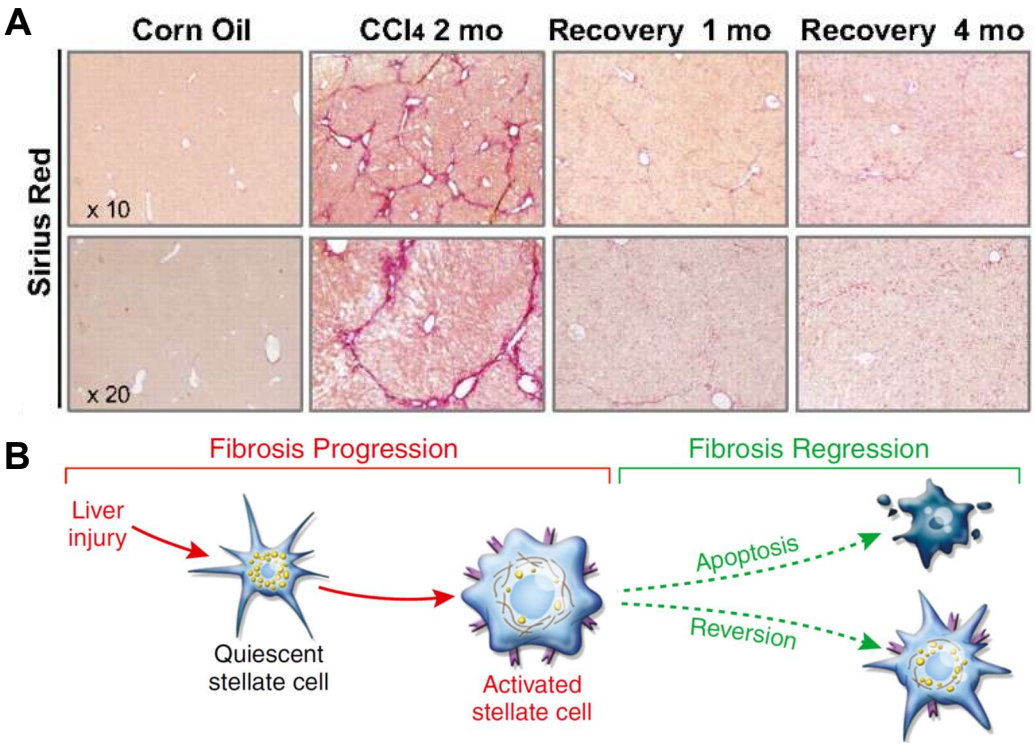

Figure 1.3 *Reversibility of fibrotic liver injury following removal of the underlying etiological agent.* (A) Cessation of treatment with a prototypical inducer of fibrogenic processes (carbon tetrachloride; CCl_4) results in a near complete resorption of excess scar tissue and recovery of normal liver tissue architecture. Collagen positive areas are highlighted with Sirius red staining. (B) The regression of hepatic fibrosis is due in part, to a loss of activated hepatic stellate cells via apoptosis or reversion to a quiescent-like phenotype. Adapted from Kisseleva et al. (2012) and Friedman (2012).

1.3.2.4 Inflammation is closely associated with the progression of fibrosis and its resolution

Pathogenic processes such as hepatic fibrosis, typically arise from an uncontrolled inflammatory state (Pellicoro et al., 2014). As the most widely studied immune cell in hepatic fibrosis, macrophages are often observed in close proximity to activated HSCs and co-localize within networks of scar tissue suggesting they may play a critical role in modulating the progression and/or resolution of fibrotic injury (Duffield et al., 2005, Fallowfield et al., 2007). The release of damage-associated molecular patterns (DAMPs) (*e.g.*, exosomes, miRNA) from compromised and dying HCs induce KC activation which culminates in the production of free radicals, cytokines, and chemotactic factors to mediate cell death, activate local NPCs, and recruit neutrophils, monocytes, NK and NKT inflammatory cells to the site of injury (Pellicoro et al., 2014).

Much of our current understanding of the role of macrophages in precipitating fibrogenic processes has stemmed from approaches targeting the general macrophage population via inhibition or depletion strategies (*i.e.*, $GdCl_3$, glycine, liposomal clondronate) in rodent models prior to or during exposure to prototype fibrogenic agents (Ide et al., 2005, Muriel et al., 2001, Muriel and Escobar, 2003, Pellicoro et al., 2014). Such studies have demonstrated a decrease in activated HSCs and overall attenuation of fibrogenic processes in rodent models indicating a pro-fibrogenic role for macrophages in this context (Ito et al., 2003, Pellicoro et al., 2014). However, such *in vivo* approaches make it largely difficult to clearly distinguish the roles of resident KCs in mediating early liver injury and fibrogenesis as they may play important roles prior to the recruitment of extrahepatic macrophages and adaptive inflammatory cells to the site of injury.

More recently, the use of transgenic mouse models to conditionally deplete

macrophages during different phases of the response has revealed that they are not only important for the initiation and progression of fibrotic injury but also its resolution (Bataller and Brenner, 2005, Duffield et al., 2005). While removal of the underlying etiology favors resolution and regression of excess ECM, depletion or inactivation of macrophages during this period largely results in persistent fibrosis and perturbations in spontaneous fibrolysis (Chávez et al., 2006). In this context, macrophages play important restorative roles including engulfment of cellular debris, de-activation/killing of myofibroblasts, production of inflammatory and fibrogenic mediators, and production of enzymes such as matrix metalloproteinases (MMPs) critical for fibrolysis/tissue remodeling and reconstitution of normal tissue architecture following injury (Pellicoro et al., 2014). The role of resident KCs in remediating hepatic fibrosis remain largely unknown primarily due to the inability to specifically target macrophages subsets *in vivo*.

1.3.3 Translation of Knowledge into a Framework Useful for Human Risk Assessment: Adverse Outcome Pathway for Liver Fibrosis

A number of precipitating factors leading to fibrotic liver injury have been gleaned from animal models. However, there are numerous challenges associated with the translation of these outcomes to humans. Species differences in drug metabolizing enzymes, transporters, hepatic drug deposition, immune response, and temporal features of the response do not typically recapitulate all features of the human condition (Chu et al., 2013, Martignoni et al., 2006). While hepatic fibrosis in humans can result from a variety of conditions/stimuli (*e.g.,* congenital, metabolic, inflammatory, parasitic, vascular, chemical/drug exposure), the underlying mechanisms are thought to be well-conserved (Friedman, 2013).

Detection and staging of fibrotic injury in humans has been vastly difficult given the latency to onset (*i.e.*, months to years) and lack of predictive biomarkers that accurately reflect the stage and progression of fibrotic events as they occur within the liver (Gressner et al., 2009). Furthermore, a number of factors influence susceptibility and progression to the pathological outcome such as age, gender, body mass index, co-morbidities, and drug/alcohol use (De Minicis et al., 2007, Mederacke et al., 2013). Clinical complications of hepatic fibrosis are most often not detected until the injury is relatively well advanced thus precluding a basic understanding of how this process manifests over time (Bataller and Brenner, 2005). Unfortunately, liver biopsy remains the gold standard method for the detection and staging of liver fibrosis in humans (Sebastiani and Alberti, 2006). However, this invasive method of assessment is prone to large sampling error (30-50%) given that a small portion of the liver (~1/50,000) is sampled at a given time, inconsistency in sample acquisition/quality, and histological observer variability (Gressner et al., 2009). While promising surrogate markers of liver fibrosis have been identified in humans (*e.g.*, N-terminal propeptide of type III collagen, hyaluronic acid, tissue inhibitor of metalloproteinase-1 [TIMP-1]), these markers are not specific to liver fibrosis and are typically useful for detecting relatively advanced stages rather than the early/intermediate phases of the response (Sebastiani and Alberti, 2006).

Many examples of compound-induced liver injury in humans stem from patients treated with drugs for extended periods of time due to chronic disorders such as rheumatoid arthritis and psoriasis (*e.g.*, methotrexate) (Bjorkman et al., 1993, Maybury et al., 2014). In addition, relatively few case studies have been reported in which the fibrogenic outcome could be attributed to exposure to a particular agent (*e.g.*, environmental/occupational

exposure to thioacetamide, vinyl chloride) ("Thioacetamide", 2000, Sherman, 2009). Given the persistent challenges associated with detecting and evaluating liver fibrosis in humans as well as the limited translatability of animal models, the evaluation of risk with respect to compound exposure is extremely difficult. Thus, there have been considerable efforts across regulatory agencies to develop and adopt more human relevant alternative testing and screening strategies that do not rely heavily on animal toxicity data (Andersen and Krewski, 2010, Knudsen et al., 2015).

In 2012, the Joint Research Center proposed an Adverse Outcome Pathway (AOP) for liver fibrosis to consolidate the main precipitating factors strongly associated with the response into an integrated framework useful for human toxicity risk assessment (Landesmann, 2016) (Figure 1.4). The AOP framework is an important aspect of compound risk assessment as it represents a comprehensive view of the pathways and networks strongly associated with an adverse outcome that occur at various levels of biological organization (Landesmann et al., 2013). This type of strategy is particularly useful for complex processes such as liver fibrosis to standardize areas of focus, inform the development of predictive risk assessment strategies, and serve as a basic mechanistic framework to guide the interpretation and integration of *in vivo*, *in vitro*, and *in silico* data for risk assessment purposes (Horvat et al., 2017). Furthermore, this "weight of evidence"-based approach incorporates essential key events at the level of detail required to identify core pathways or patterns of biological response which drive fibrogenic processes across broad sets of compounds (Mehal et al., 2011). In addition, AOP frameworks can be useful tools to improve the development of alternative *in vitro* screening strategies geared towards evaluating potential fibrogenic agents.

The development of a comprehensive AOP framework is dependent on the evaluation

of prototypical inducers of the response (Landesmann et al., 2013). For the current liver fibrosis AOP, carbon tetrachloride (CCl_4) and allyl alcohol (AA) were used to define the series of key events linking a molecular initiating event (*e.g.*, protein-alkylation/covalent protein binding) to the adverse outcome (*i.e.*, fibrosis) (Landesmann, 2016). In addition, other classified fibrogenic agents including thioacetamide (TAA), methotrexate (MTX), ethanol, and dimethyl nitrosamine (DMN), were used to provide additional weight of evidence for the proposed series of key events comprising the framework (Horvat et al., 2017). While the molecular initiating event (MIE) could be different across broad sets of compounds, they may converge on consequential HC injury and the cascade of downstream key events leading to liver fibrosis. However, by definition, an AOP framework consists of a clearly defined relationship between a single (MIE) and adverse outcome (Landesmann et al., 2013).

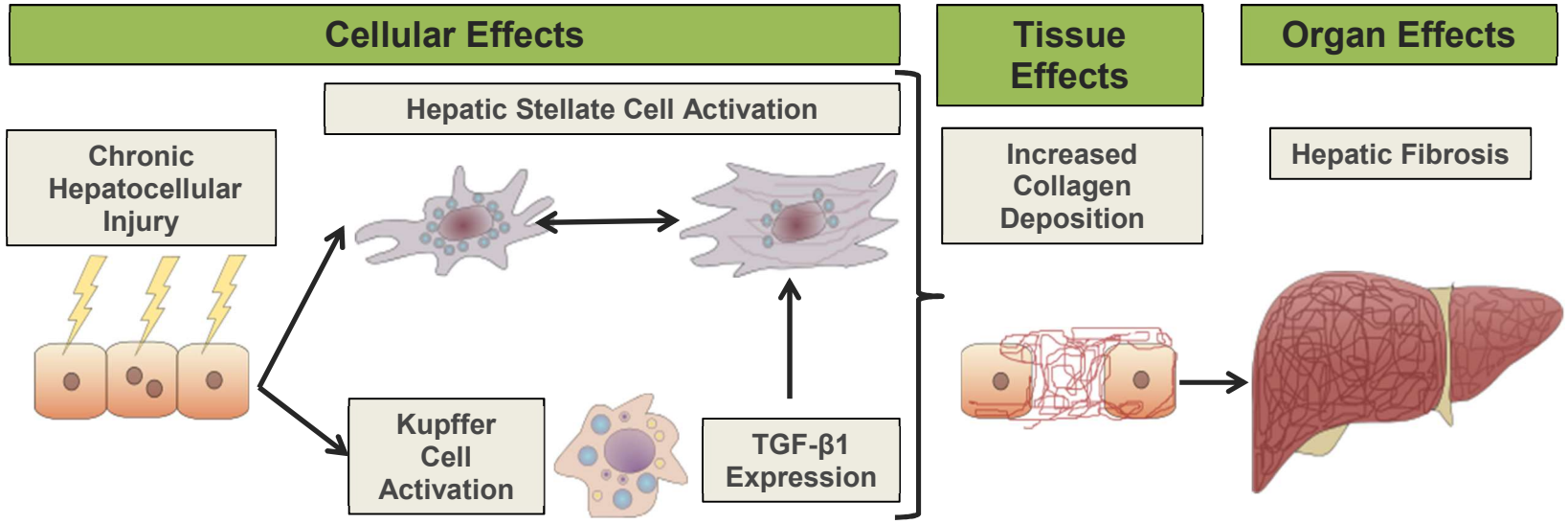

Figure 1.4 *Adverse Outcome Pathway for Liver Fibrosis*. Adapted from Landesmann (2016).

1.3.4 Knowledge Gaps

The hurdles associated with monitoring and staging fibrotic liver injury in addition to the structural and functional complexities of the liver make it difficult to deconvolute the series of events that occur and the cell types involved in the early pathogenesis and progression of fibrogenesis *in vivo* during injury. Although we have a good idea of the precipitating factors involved in the response, translation of this knowledge into a testing paradigm useful for human toxicity risk assessment remains a challenge (Horvat et al., 2017, Knudsen et al., 2015, Landesmann, 2016).

While the AOP for liver fibrosis presents a basic framework of the key factors strongly associated with the response, the series of events promoting fibrogenesis during early injury remain elusive. HCs are thought to be a major target regardless of the underlying MIE. However, the relationship between the extent of injury and perpetuation of downstream fibrogenic events has not been adequately described (Horvat et al., 2017, Landesmann, 2016). Furthermore, it is important to recognize that while many fibrogenic compounds elicit HC injury, there are a wide range of hepatotoxic agents that are not typically classified as fibrogenic agents in humans (*e.g.*, acetaminophen) (Landesmann, 2016). As such, there is a current unmet need to better understand these series of events and identify features of the response or attributes that may be unique to fibrogenic agents. Given that fibrosis is a multifactorial and dynamic response, human-based cell models that accurately reflect aspects relevant to the response but also enable an integrated assessment of how these events manifest over time will greatly improve toxicity risk assessment and screening strategies.

1.4 Modeling Hepatic Fibrogenesis *In Vitro*

1.4.1 Limitations of Conventional Culture Approaches

1.4.1.1 Two-Dimensional Monocultures

Cell culture has been used as a surrogate to dissect the mechanistic details underlying liver injury. However, conventional two-dimensional (2D) HC-based model systems typically represent a homogenous view of liver function (LeCluyse et al., 2012). The reasons for the lack of concordance between most standard 2D culture models and *in vivo* outcomes is mainly due to their limited capacity to mimic the native microenvironments and key events that cause or exacerbate toxic outcomes. Liver fibrosis rarely involves a single cell type (*i.e.*, HCs or HSCs) but rather depends on interactions of several cell types that mutually influence each other in various ways within the local microenvironments of the liver lobule (Bataller and Brenner, 2005). These biological complexities are not accurately reflected in standard sandwich cultures of HCs maintained on a simple collagen type I substratum. As a result, subacute effects of a compound, which do not overtly lead to cell necrosis or apoptosis but rather depend on these types of interactions, may be missed entirely (Astashkina et al., 2012).

Given the involvement of the hepatic stellate cell (HSC) as the major effector cell type implicated in the fibrogenic response, screening strategies have focused on evaluating compound effects in 2D monolayers comprising primary HSCs or HSC cell lines maintained on a plastic substratum (Xu et al., 2005). Although HSCs have been successfully isolated for the past two decades, a reliable *in vitro* model that is able to faithfully recapitulate and maintain the quiescent HSC phenotype observed in uninjured liver is lacking (Friedman, 2008). The maintenance of a stable quiescent HSC phenotype over an extended period of time has been difficult to achieve using standard 2D monoculture models due to the influence

of the microenvironment on the phenotypic plasticity of these cells (Olsen et al., 2011).

Once isolated, HSCs undergo a constituitive culture-induced activation process in 2D culture over a span of approximately 7 days. Even though this culture activation process reflects many of the hallmarks associated with HSC activation, it does not fully recapitulate the changes in gene expression observed *in vivo* (De Minicis et al., 2007). Furthermore, the minimal evidence of mature collagen fibril formation observed in these cultures may be due, in part, to the type of culture configuration and lack of co-factors (*e.g.*, ascorbic acid, other non-essential amino acids) required for collagen biosynthesis and deposition (Chen and Raghunath, 2009). To date, it has been particularly difficult to emulate classic features of the fibrogenic response in an *in vitro* setting.

While a 2D strategy may be useful to an extent for screening antifibrotic compounds aimed at preventing HSC activation, it does not account for the modulatory roles of the microenvironment or other cell types in the response and only provides a simplistic perspective on fibrogenic processes (Gutiérrez-Ruiz and Gómez-Quiroz, 2007). When used as a screening tool to evaluate the direct effects of potential fibrogenic agents, the constituitive activation of HSCs greatly confounds the assessment and ability to resolve direct compound effects on provoking this response. Furthermore, the relatively simplistic and non-physiologic nature of these types of culture platforms may not be able to accurately recapitulate the complex series of events that occur within the liver and, consequently, limit the ability to explore complex mechanisms underlying compound-induced liver injury leading to fibrosis for risk assessment purposes (LeCluyse et al., 2012).

1.4.1.2 Micropatterned Co-Culture Systems

As we have begun to appreciate the role of NPCs in supporting basic HC function and

modulating susceptibility to injury, 2D co-culture platforms have demonstrated toxicities not traditionally captured with HC monolayers as well as extended viability and functionality with the inclusion of stromal support cells such as fibroblasts and liver-resident NPCs (Bhatia et al., 1999, Rose et al., 2016). For example, the micropatterned co-culture (MPCC) model, which involves the selective attachment of HCs onto precisely patterned islands surrounded by stromal cells (*i.e.*, 3T3-J2 mouse embryonic fibroblasts) through surface modification of cell culture plates, has enabled the culture of primary HCs over extended periods of time while maintaining key physiological functions (Khetani and Bhatia, 2008, Ukairo et al., 2013).

While the MPCC model system is an excellent example illustrating the importance of stromal support cells in maintaining HC viability and functionality over extended periods of time, the 2D configuration of this culture system does not overcome the aforementioned limitations with regards to HSC activation and the lack of basic fibrogenic features such as collagen deposition. Nonetheless, such a configuration has proven valuable to study both drug metabolism and transport as well as drug-induced liver injury *in vitro* (Ballard et al., 2016, Khetani et al., 2013, Ramsden et al., 2014). Because of the long-term stability of the system and ease of use, addressing long-term clearance of drugs with low turnover rates has also proven particularly useful (Lin et al., 2016). Furthermore, the unique culture configuration coupled with the integration of high content imaging approaches has enabled researchers to conduct more comprehensive evaluations of the mechanisms underlying compound-induced liver injury (Tolosa et al., 2015, Trask et al., 2014).

1.4.1.3 Precision Cut Liver Slices

While the concept of precision-cut liver slices (PCLS) has been around since the early

twenties, improvements in the preparation of PCLS over the past decade has proven useful for examining drug metabolism and multicellular toxicity *ex vivo* (Olinga and Schuppan, 2013). The preparation of PCLS from a core of normal or diseased liver tissue preserves the unique architectural relationship among parenchymal and NPCs in their native ECM environment and allows for the evaluation of compound toxicity in a physiologically relevant context (Olinga and Schuppan, 2013). Many of the outcomes obtained with studies utilizing PCLS illustrate concordance with *in vivo* outcomes making it a useful tool for studying metabolic processes, enzyme induction, and predicting *in vivo* hepatotoxicity (de Graaf et al., 2007) .

With regards to fibrotic liver injury, studies utilizing both rodent- and human-derived PCLS have examined the induction of fibrogenic processes with prototype fibrogenic agents (Thiele et al., 2015, Van de Bovenkamp et al., 2007). However, one of the major limitations of this model is the rapid degeneration of HC phenotype and dedifferentiation/activation of other NPC support cells over a span of 72-96 hours (Olinga and Schuppan, 2013). While the progressive fibrogenic change observed in the model during this timeframe may be useful to evaluate the efficacy of anti-fibrotic therapeutics, it confounds the ability to resolve compound-induced fibrogenic processes over an extended period of time (Westra et al., 2016). Furthermore, the biological complexity and inability to modulate the types of cells represented hinders the ability to precisely dissect the roles of individual cell types in driving/modulating the response in this context.

1.4.1.4 Cell Seeded Scaffolds

For the past 20+ years, the tissue engineering field has pursued the construction of 3D liver tissue by seeding a pre-formed scaffold, derived from synthetic polymer or from

decellularized native tissue, with liver cells or stem cells with the intent of ultimately yielding a tissue with liver-like architecture and function (Ebrahimkhani et al., 2014, Godoy et al., 2013). These biomimetic niches and scaffolds foster the formation of 3D cell structures and provide the necessary cues for improved cell integrity and function. Such scaffolds can range from well-established, transwell-like configurations to specific structures that allow for the seeding of HCs and NPCs while minimizing the impedance of nutrient flow and exposure to drugs (Domansky et al., 2010, Kostadinova et al., 2013).

Given the importance of cell-matrix interactions, the choice of a scaffold material is particularly important to consider when utilizing these approaches to assess compound-induced toxicity. Ultrastructural and biochemical differences in the nature of the types of scaffolds utilized have a profound impact on HC morphology and function (Hammond et al., 2006). While decellularized scaffolds represent a more biologically-relevant context, the variability in the preparation of these types of scaffolds (*i.e.*, proportion of soluble and insoluble ECM components, carry over of growth factors) can lead to differences in the overall function of these tissues (Reid et al., 1992, Wang et al., 2011). On the other hand, synthetic scaffolds (*e.g.*, electrospun polystyrene, biodegradable polymers) are more useful for routine cell culture given the consistency in their fabrication.

In using these types of scaffolds, seeding of cells across the entire thickness of 3D microporous scaffolds is not user defined and may present additional challenges with incorporation of certain cell types (Baptista et al., 2011). While some of these types of cell seeded scaffolds are amenable to histological assessment, the inherent properties of scaffolds used for more routine culture applications (*i.e.*, limited biodegradability, matrix stiffness), may preclude the elucidation and assessment of basic fibrogenic features such as collagen

deposition/matrix remodeling and potentially limit an understanding this dynamic process during compound treatment.

1.4.1.5 Spheroids

Improvement towards more physiologically-relevant culture systems has been accomplished by culturing hepatic cells into 3D microsphere-like structures or spheroids. Based on the principles of self-assembly, the 3D configuration of spheroids comprising HCs alone has been useful in maintaining their viability and function out to a few weeks thus overcoming the limitations of their 2D counterparts (Bell et al., 2016, Dilworth et al., 2000). The inclusion of additional liver cell types (*i.e.*, HSCs, ECs) into these structures further support HC viability and function over an extended period of time thus allowing for the conduct of extended of repeated exposure studies and elucidation of toxicities that are multicellular in nature (Takezawa et al., 1992, Thomas et al., 2005).

Although spheroids exhibit a 3D tissue-like morphology, the underlying tissue structure is less well-defined and not user-controlled in their initial formation. However, the tissue-like cellular density in the absence of exogenous scaffolds allows cells to interact and adapt to their own microenvironment. The aggregation of cells at random via cluster- or collision-based self-assembly is followed by a period of self-sorting driven by molecular gradients and the microenvironment within the spheroid (*i.e.*, nutrient availability, oxygen tension, paracrine and autocrine factors) as well as homotypic and heterotypic cell interactions (Achilli et al., 2012). Due to their size (<200 µm cross-sectional diameter), spheroids are also amenable for high-throughput screening-based approaches (Ramaiahgari et al., 2014). Thus, these types of models may be useful for evaluating very broad sets of compounds in a biologically relevant context.

More recently, the use of this system for modeling fibrogenic processes *in vitro* was evaluated in spheroids comprising HepaRGs and HSCs (Leite et al., 2016). While HepaRGs lack a primary cell phenotype, the ability of the model to mimic compound-induced HSC activation and allow for the detection and assessment of collagen deposition in a biologically relevant context provides a useful tool to begin to tease apart the mechanisms underlying compound-induced fibrotic liver injury. The histological assessment of spheroids is a particularly useful aspect of the model because histology remains the gold standard for the detection and evaluation of fibrogenic change at the tissue level (Sebastiani and Alberti, 2006). However, given their small size and lack of a user-defined architecture, the evaluation of fibrogenic processes on a histological level can become a bit more challenging. Nonetheless, the use of 3D spheroids as a more organotypic culture platform is rapidly evolving and can be used as building blocks to create larger and more complex tissue constructs (Achilli et al., 2012).

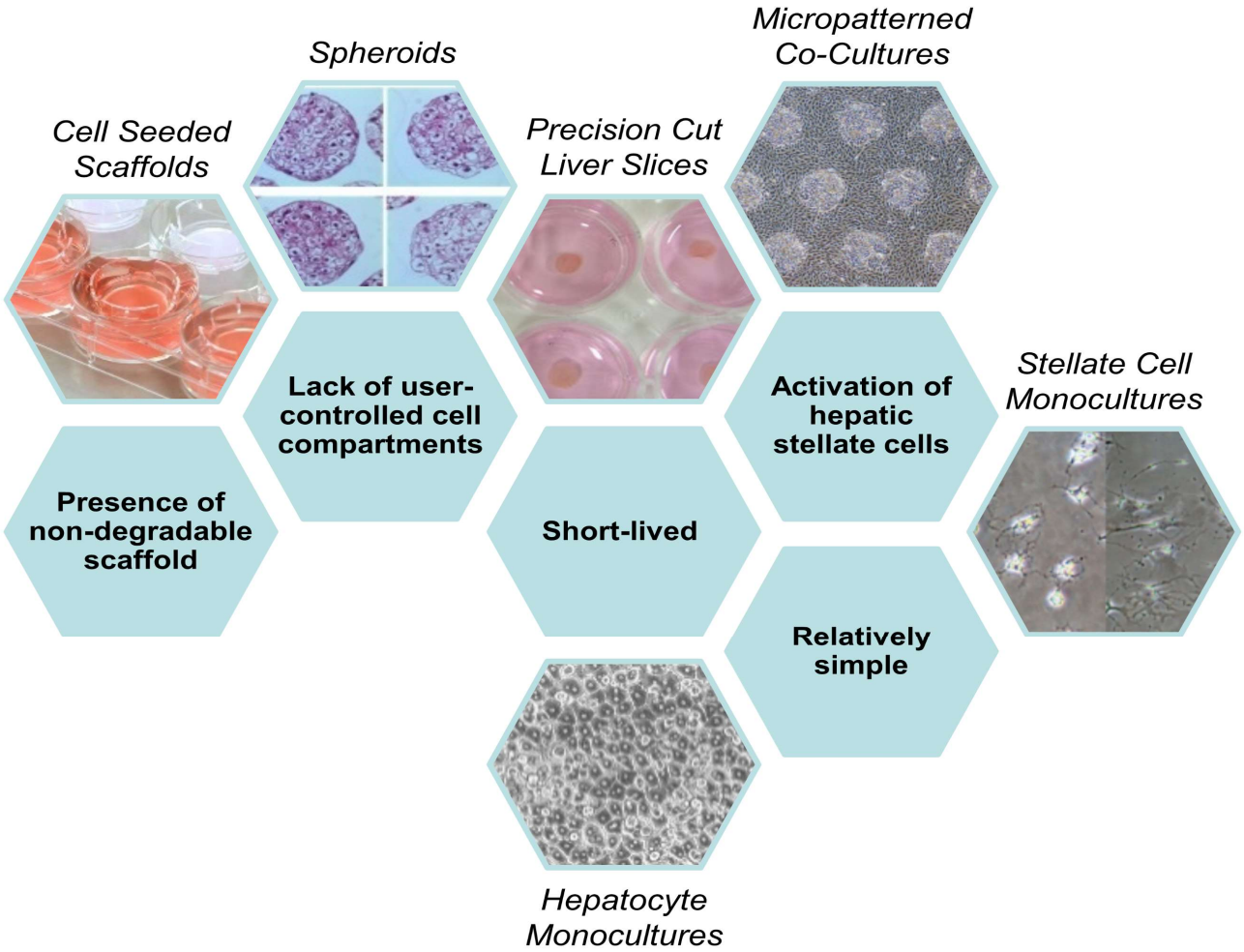

Figure 1.5 *Summary of the Limitations of Culture Systems for the Evaluation of Fibrogenesis.* A summary of some of the common traditional and advanced model systems used to evaluate toxicity *in vitro*. Limitations of each model system are represented by adjacent solid blue hexagons.

1.4.2 Culture Requirements for Recapitulating Fibrogenesis

Improved organotypic *in vitro* models that encompass key elements underlying a tissue's response to injury are needed to more accurately assess toxicity and improve our ability to accurately predict and understand the hepatotoxic and fibrogenic potential of compounds (Godoy et al., 2013, LeCluyse et al., 2012, Roth and Singer, 2014, Soldatow et al., 2013). Like any predictive model, the strengths and limitations of a system are critically important to consider when addressing specific types of research questions. From an investigative toxicology standpoint, the development of a predictive *in vitro* model for liver fibrosis should at least recapitulate some of the key events described in the proposed AOP (Knudsen et al., 2015). Given our understanding of basic fibrogenic processes, features, and the factors driving this response *in vivo*, the ability to effectively model hepatic fibrosis *in vitro* as it pertains to the AOP framework is dependent on meeting a minimum set of key criteria (Table 1.2).

Table 1.2 *Key criteria for modeling hepatic fibrosis in vitro*

Features	Justification
Multicellular and Tissue-Like Architecture	• Fibrosis is a multifactorial process • Basic fibrogenic features are best interpreted in a 3D environment
Functional and Long-Lived	• Chronic low concentration exposure scenario
Preserves Phenotypic Features of HSCs	• Resolve early compound-induced effects on perpetuating HSC activation and fibrogenic outcome

1.4.3 Compound Selection

In addition to the key criteria described in Table 1.2, the selection of agents used to validate a model system is important to consider. Although carbon tetrachloride (CCl_4) and allyl alcohol (AA) were primarily utilized to draft the AOP framework for liver fibrosis, the volatile properties of these compounds makes them less suitable for *in vitro* applications (Kim et al., 2016). Thus, the compounds evaluated as part of this dissertation were selected based on favorable physicochemical properties to enable the assessment of compound effects in an *in vitro* context. The following subsections describe each of the selected fibrogenic and hepatotoxic agents in greater detail.

1.4.3.1 Methotrexate: Classified fibrogenic agent

Methotrexate (MTX) is a folate analog well known as a chemotherapeutic agent for the treatment of several types of cancer. However, it is also useful for the treatment of rheumatoid arthritis and psoriasis at low doses for prolonged periods of time (Cronstein, 2005). While its use as a chemotherapeutic agent has not been associated with the hepatic fibrosis, studies have demonstrated a link between chronic low-dose treatment with MTX and fibrogenesis (Bjorkman et al., 1993, Shergy et al., 1988). Cumulative dose MTX toxicity is thought to be elicited primarily through accumulation of polyglutamated metabolites within HCs over an extended exposure. These metabolites act as potent inhibitors of folate-dependent enzymes and are generally long-lived in tissues (Cronstein, 2005). While MTX-induced fibrosis only accounts for approximately 20-30% of patients treated to manage inflammatory disorders, this phenomenon suggests that other confounding factors (*e.g.*, differences in pharmacokinetics and pharmacodynamics), or co-morbidities (*e.g.,* fatty and alcoholic liver disease) may play a role in the predisposition of individuals to MTX-induced

fibrosis (Cronstein, 2005).

1.4.3.2 Thioacetamide: Prototypical fibrogenic agent

TAA is an organosulfur compound commonly used in a source of sulfide ions in the synthesis of organic and inorganic compounds ("Thioacetamide", 2000). It is a widely-recognized prototype fibrogenic agent and commonly employed in rodent models of chemical-induced hepatic fibrosis that more closely mimic the human pattern of histopathology (Liedtke et al., 2013). TAA primarily elicits HC injury via CYP2E1-dependent bioactivation to the sulfoxide metabolite TASO and the highly reactive TAA-*S, S*-dioxide ($TASO_2$) metabolite, oxidative stress, inflammation, and apoptosis (Akhtar and Sheikh, 2013). Although TAA is not a therapeutic, it is documented to cause fibrotic injury in rare cases of chronic occupational/environmental exposures ("Thioacetamide", 2000).

1.4.3.3 Transforming Growth Factor-β1: Positive control

Transforming growth factor-β1 (TGF-β1) belongs to group of pleotropic cytokines that play key roles in tissue homeostatic mechanisms such as regeneration, cell differentiation, and regulation of the immune system. TGF-β1-mediated effects are influenced, in part, by the microenvironmental context of signaling and specific cell types on which it acts (Dooley and ten Dijke, 2012). In the field of fibrosis research, TGF-β1 plays a key role in mediating the wound healing response and is recognized as a major profibrogenic cytokine (Gressner and Weiskirchen, 2006). While TGF-β1 is sequestered in a latent form, activation primarily by integrins has been shown to contribute to HSC activation and drive their transdifferentiation into myofibroblasts (Hinz, 2013). During liver injury, the activation of latent TGF- β1 derived from macrophages drives the synthesis of collagen as well as the expression of HSC activation markers such as α-smooth muscle actin (α-SMA) via Smad-

dependent signaling (Leask and Abraham, 2004).

1.4.3.4 Acetaminophen: Proposed negative control

APAP is a widely-used over the counter medication used for the management of fever and pain over the course of short- and long-term periods with usage doses ranging from 2-4 grams per day. While APAP exhibits many of the hallmark attributes of a prototypical fibrogenic compound such as TAA (*i.e.*, CYP-mediated bioactivation to a reactive metabolite, HC injury, oxidative stress, glutathione depletion), liver injury due solely to the chronic ingestion of sub-therapeutic doses of APAP has not been clearly described or systematically tested (Horvat et al., 2017, Jaeschke et al., 2012, Landesmann, 2016). A majority of research studies examining APAP-induced liver injury in humans typically span acute exposure to cases of overdose. Studies that have described adverse toxicities resulting from "chronic" APAP exposure are reported on a case basis and range on the order of a couple days to several weeks (Tong et al., 2015, Watelet et al., 2007). Furthermore, the existence of a predisposing condition such as chronic alcohol use or alterations in hepatic protein metabolism (*i.e.*, nitrogen balance) and nutritional status could ultimately lead to liver fibrosis and/or consequently impact susceptibly to APAP-induced liver injury (Kondo et al., 2012, Michaut et al., 2014).

The assessment of the effects of chronic APAP exposure is challenging as clinical manifestations of liver injury typically present when the recommended daily dose of 4 grams is exceeded (Tong et al., 2015). Consequently, it remains unclear as to whether long-term administration of APAP potentially causes liver fibrosis in humans as this type of exposure scenario has been challenging to address in the general population and to date has not been adequately addressed using a human relevant *in vitro* model system. These observed

outcomes suggest that: (i) the fibrogenic potential of compounds is dependent on the context of exposure (*i.e.*, concentration/time dependent effects, co-exposures) and/or (ii) the fibrogenic potential of compounds may be intrinsic to the chemical structure and pharmacology. Further investigation is needed to better understand the mode of action underlying compound-induced liver injury leading to fibrosis and unique response signatures that provoke HSC activation and scarring of the liver.

1.5 Three-Dimensional Bioprinted Liver Tissues

1.5.1 Principles of Bioprinting

Recently, based on the demonstrated principles of cell-cell adhesion and self-assembly, an alternative strategy for achieving three-dimensionality has emerged, whereby small building blocks comprised of aggregated cells or cell mixtures are generated and placed adjacent to each other in a specific geometry using automated printing devices (Jakab et al., 2010) (Figure 1.6). Thus, 'bioprinting' allows for the fabrication of complex 3D liver tissues via the spatially defined deposition of cells that recapitulates native hepatic tissue architecture, cellular compartmentalization, and intercellular interactions in the absence of an exogenous scaffold (Khatiwala et al., 2012). Most importantly, the 3D tissue constructs generated using these approaches exhibit a broad range of highly differentiated *in vivo*-like liver features and functions *in vitro* (Nguyen et al., 2016). Given the importance of the microenvironment in modulating HSC biology as alluded to in the above sections, development of 3D co-culture models has emerged as a promising method to maintain HSCs in a quiescent-like state and also evaluate the interplay among liver resident cells during early injury (Norona et al., 2016).

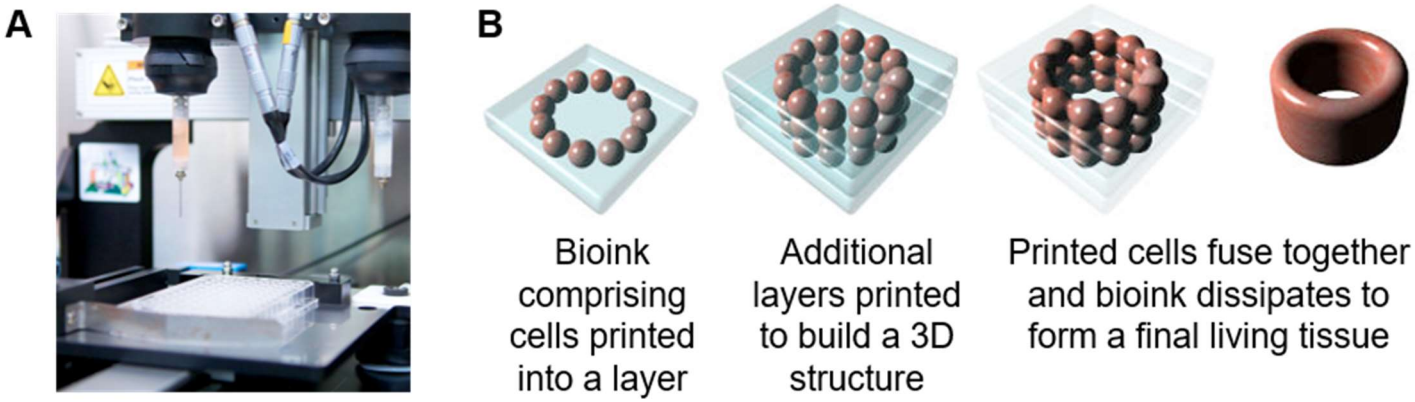

Figure 1.6 *Principles of Bioprinting.* (A) Bioink comprising cells and hydrogel is loaded onto a bioprinting platform. (B) Cells are extruded from a syringe (printed) layer by layer to create complex 3D structures. The hydrogel acts as support during the initial fabrication of the tissue but dissipates as aggregates of cells fuse together and form a tissue in the absence of an exogenous scaffold. Photo used with permission from Organovo. Cartoon adapted from ExplainingTheFuture.com.

1.5.2 Unique Model Features: ExVive™ Human Liver

Advancements in 3D multicellular culture models have demonstrated numerous advantages over simple monocultures for toxicity testing in that it maintains HC viability and function over extended periods of time, preserves phenotypic features of cells found in uninjured liver, and represents a novel approach by which compounds can be systematically evaluated (Leite et al., 2016, Nguyen et al., 2016). The model system described in this dissertation was fabricated using a novel NovoGen MMX™ bioprinting platform and represents a significant innovation in the study of chronic liver injury, as it addresses many of the shortcomings associated with traditional *in vitro* culture models and animal models. Namely, (i) it incorporates multiple key cell types into the tissue constructs (*i.e.*, HCs, HSCs, and ECs, with the flexibility of incorporating KCs and other relevant cell types as needed); (ii) it has a 3D tissue-like architecture wherein specific cell types are patterned in the x-, y-, and z-axes; (iii) it is manufactured with an automated bioprinting instrument to ensure reproducible tissue morphology; (iv) histological assessment can be performed for comparison with *in vivo* effects; and (v) it is durable *in vitro*, retaining metabolic competence and liver-specific functions for at least four weeks, thus enabling extended, low-dose treatment regimens to be investigated (Nguyen et al., 2016, Roskos et al., 2015) (Figure 1.7). Thus, the unique features of this model facilitate the investigation of low-dose, repeat exposure studies, as well as chronic disease modeling such as hepatic fibrosis as it overcomes many of the limitations described for conventional model systems.

Results from studies designed to evaluate the metabolic capacity and toxic responses to prototype drugs have shown very good reproducibility and concordance with observed outcomes *in vivo* at the functional and histological levels (Nguyen et al., 2016). Overall, the

3D bioprinting technologies are attractive as *in vitro* models for pharmaceutical and environmental health sciences due in part to the fact that they offer several added features that allow for more accurate modeling of complex diseases, such as fibrosis, NASH, and prediction of compound-induced liver injury. Currently, these technologies represent more data-rich, high-content capability with limited throughput capacity compared to simpler 2D and 3D culture platforms, such as the MPCC and spheroid model systems. However, these more biologically elaborate, but physiologically relevant, culture systems could prove to be more informative for identification of possible liver toxicities and mode of action involved in mediating more complex compound-induced hepatotoxic events.

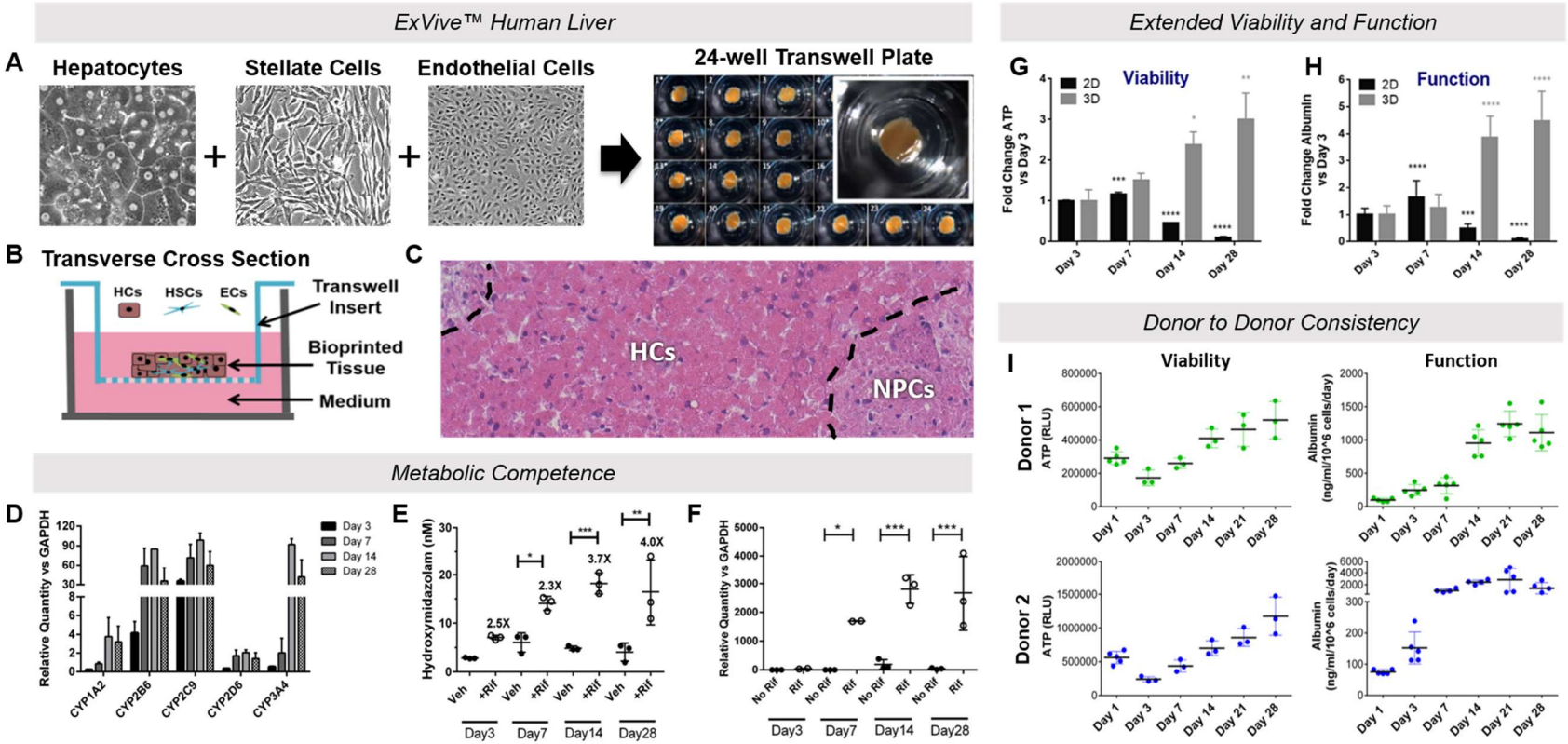

Figure 1.7 *ExVive™ Human Liver base model features.* (A) ExVive™ Human Liver tissues are composed of primary human hepatocytes (HCs), hepatic stellate cells (HSCs), and endothelial cells (ECs) printed in a 24-well transwell configuration. (B) Cartoon illustrating the compartmentalized architecture. (C) H&E-stained cross section of bioprinted liver illustrating the compartmentalized architecture. NPCs: non-parenchymal cell compartment. (D) Expression of major CYP450 enzymes in bioprinted liver over time. (E) Assessment of CYP3A4-mediated metabolism of midazolam to 4-hydroxymidazolam over time in vehicle-treated and rifampicin (CYP3A4 inducer)-treated tissues. (F) Basal and rifampicin-induced levels of *CYP3A4* transcripts over time. (G and H) Extended viability (ATP content) and functionality (albumin output) of 3D bioprinted liver tissues compared to primary human sandwich cultured hepatocyte monolayers. (I) Donor tissue consistency in basal viability and function over time. Adapted from Nguyen et al. (2016), Norona et al. (2016) and used with permission from Organovo, Inc.

1.6 Scope of the Dissertation

The present dissertation research sought to evaluate and optimize a novel 3D bioprinted liver platform developed by Organovo, Inc. (ExVive3D™ Human Liver Tissue) to model fundamental aspects of the response *in vitro* and gain insight into the early series of adaptive events and roles of resident hepatic cell types in precipitating fibrotic injury. **The overall objective of this research was to further develop a progressive model of compound-induced fibrogenesis using 3D bioprinted liver tissues to define the key events underlying the response.** *We hypothesize it will be possible to develop a model of compound-induced fibrogenesis using 3D bioprinted liver tissues that will permit an understanding of the dynamic changes that occur during abnormal wound healing and its resolution.*

This research was comprised of three specific aims. Prior to initiating this work, the application of 3D bioprinted human liver tissues to mimic aspects of compound-induced hepatic fibrogenesis was not systematically investigated. Given the unique features of the model system as described above, studies conducted within Specific Aim 1 (Chapter 2) examined the effects of repeated exposure to prototypical fibrogenic agents in the standard tissue model to support the utility of 3D bioprinted liver tissues to model progressive injury leading to fibrosis. These initial studies provide compelling evidence of mild injury profiles over a two-week timeframe with robust fibrogenic processes at a tissue, cellular, and molecular level. We further highlight the flexibility and advantage of bioprinting technology to incorporate additional cell types relevant to the response and sought to evaluate the role of resident macrophages or Kupffer cells in the modulation of the compound-induced fibrogenic response in Specific Aim 2 (Chapter 3). The incorporation of KCs into the model further implicates their important role in the modulation of progressive injury and fibrogenic

response during early compound exposure with a bimodal response during later phases of treatment. Given the dynamic nature of the injury and fibrogenic response, the capacity of the model to recover following injury was evaluated in Specific Aim 3 (Chapter 4). These data comprise the first report of compound-induced fibrogenesis using a 3D bioprinted model and provide further insight into the dynamic and temporal nature of the response. Moreover, the results from these studies indicate important parameters to consider when modeling model complex disease processes in an *in vitro* context and set the stage for further model optimization and improvement.

CHAPTER 2 – MODELING COMPOUND-INDUCED FIBROGENESIS *IN VITRO* USING THREE-DIMENSIONAL BIOPRINTED HUMAN LIVER TISSUES[1]

2.1 Introduction

Chronic liver injury progressing to fibrosis and liver failure can result from a wide range of insults including drug or chemical exposure, metabolic disease, alcoholism, or viral infection, and is a major health burden worldwide with 2% of all deaths attributable to liver cirrhosis (Lozano et al., 2012, Murray et al., 2012). Whereas the major precipitating factors underlying drug- and chemical-induced fibrosis have been gleaned from animal models, the key initiating and series of adaptive events that perpetuate this response, especially in humans, are still not well understood. Regardless of etiology, progressive fibrotic liver injury is orchestrated by complex intercellular interactions among hepatocytes (HCs), endothelial cells (ECs), hepatic stellate cells (HSCs), Kupffer cells (KCs), and recruited inflammatory cells (Bataller and Brenner, 2005).

Animal models of chronic liver injury with fibrosis partially recapitulate the human condition, but may fail to provide robust human translation due to species differences in metabolism, injury response, and capacity/mechanisms of repair and regeneration (Liu et al., 2013). Cell culture has been used as a surrogate to dissect the mechanistic details underlying HC dysfunction and fibrogenic outcome. However, conventional two-dimensional (2D), cell-

[1] This Chapter previously appeared as an article in the journal of Toxicological Sciences. The original citation is as follows: Norona, L., *et al. Toxicological Sciences* (2016) 154(2): 354-367.

based hepatic model systems do not reliably recapitulate liver structure, function, and its inherent multicellular architecture (LeCluyse et al., 2012). This is largely due to the absence of non-parenchymal cells (NPCs) relevant to liver injury and the fibrogenic response. HSCs are recognized key effectors in the development and progression of hepatic fibrosis (Puche et al., 2013). However, they also help to define the molecular and structural microenvironment of the parenchymal compartment and space of Disse via the production of soluble and insoluble cues, including growth factors, inflammatory cytokines, and deposition of extracellular matrix (ECM) (Friedman, 2008). These microenvironments mediate requisite gene expression patterns for metabolic homeostasis, cellular differentiation, and maturation (Guillouzo et al., 1993, Rogiers V., 1993) and modulate the liver's response to both acute and chronic injury. These observations suggest that current *in vitro* models used to evaluate potential fibrogenic agents lack fundamental cellular components that may moderate or exacerbate hepatocellular injury, an event strongly associated with the initiation of fibrogenesis (Canbay et al., 2004). Furthermore, the appearance and progression of basic fibrogenic features such as inflammation, tissue remodeling, collagen accumulation, and compensatory hepatocellular regeneration are best detected and interpreted in the context of a three-dimensional (3D) tissue environment. As such, these components are required in order to fully understand quantitative and temporal relationships underlying complex processes, such as fibrosis arising from chronic liver injury.

The recent availability of bioprinted human liver tissue models that incorporate both parenchymal (*i.e.*, HCs) and NPCs (*i.e.*, HSCs and ECs) in a 3D context has created the opportunity to examine progressive liver injury in response to known pro-fibrotic modulators and compounds (Nguyen et al., 2016). In this study, we utilized this novel model system to

establish conditions for monitoring tissue responses after treatment with fibrogenic agents, including transforming growth factor-β1 (TGF-β1), and prototype fibrogenic compounds methotrexate (MTX), and thioacetamide (TAA). Significant concentration- and time-dependent elevations of lactate dehydrogenase (LDH) were observed for both MTX and TAA and were accompanied by the acquisition of a fibrogenic phenotype as supported by tissue remodeling, NPC migration/activation, histologic evidence of collagen deposition, transient elevations in proinflammatory, immunomodulatory, and chemotactic cytokines, and the expression of *ACTA2* and *COL1A1*. In comparison, treatment with TGF-β1, a known pro-fibrogenic cytokine, yielded moderate fibrotic change in the tissue with little evidence of hepatocellular damage. Taken together, these data demonstrate the utility of novel 3D bioprinted tissues to further evaluate compound-induced liver fibrosis in a more defined and systematic fashion.

2.2 Materials and Methods

2.2.1 Tissue Production

Three-dimensional bioprinted liver tissues were manufactured by Organovo (San Diego, CA) using primary cryopreserved human HCs (Life Technologies, Carlsbad, CA), HSCs (ScienCell, Carlsbad, CA), and human umbilical vein ECs (Becton Dickinson, Tewksbury, MA), using patented protocols (U.S. Patents 8,241,905 B2; 8,852,932; 9,222,932 B2; 9,222,932 B2) as described previously (Forgacs et al., 2012, Forgacs et al., 2014, Murphy et al., 2015, Nguyen et al., 2016, Shepherd et al., 2015). Each commercial cell supplier provides assurances that the cells come from tissues collected in compliance with applicable laws and provided based on informed consent by the donors. Briefly, HSCs and

ECs were cultured prior to tissue fabrication and cryopreserved HCs were thawed and prepared for use according to the manufacturer's instructions. Separate bio-inks comprising parenchymal cells (100% cellular paste, generated via compaction) or NPCs ($150e^6$ cells/mL formulated in NovoGel® 2.0 Hydrogel) were prepared and loaded into separate heads of the NovoGen Bioprinter™ platform (Organovo, San Diego, CA) housed within a standard biosafety cabinet (Forgacs et al., 2012, Forgacs et al., 2014, Jakab et al., 2008, Murphy et al., 2015, Nguyen et al., 2016, Shepherd et al., 2015). An automated computer script was then executed to precisely deposit the bio-inks in a two-compartment planar geometry onto the membranes of standard 24-well 0.4 µm transwell membrane inserts (Corning, Tewksbury, MA) via continuous deposition, with NPCs comprising the border regions of each compartment and HCs filling each compartment such that the cell ratios roughly approximated physiologic ratios and the final tissue thickness was approximately 500 µm (Murphy and Atala, 2014). Following fabrication, the tissues were cultured in William's E supplemented with Primary Hepatocyte Maintenance Supplements (Life Technologies, Carlsbad, CA) and EGM-2 (Lonza, Basel, Switzerland) and maintained in a 37°C incubator under humidified atmospheric conditions with 5% CO_2. Liver tissues were allowed to coalesce into tissue-like structures for a minimum of three days with the daily replacement of medium prior to treatment with compounds.

2.2.2 Compound Exposure

Concentration ranges of MTX (Sigma-Aldrich, St. Louis, MO) and TAA (Sigma-Aldrich, St. Louis, MO) were selected based on plasma C_{max} values of effective doses reported in clinical studies and animal models of fibrotic injury (Chilakapati et al., 2005, Shiozawa et al., 2005) and at an estimated sinusoidal concentration (Ferslew and Brouwer,

2014). For TAA, the plasma C_{max} values were further benchmarked against toxicity studies performed *in vitro* where TAA did not elicit LDH release or evidence of cellular necrosis at concentrations up to 50 mM in cultured primary rat HCs (Hajovsky et al., 2012) to select the final concentration range. TGF-β1 (Miltenyi Biotec Inc., San Diego, CA), a well-recognized potent, pro-fibrogenic cytokine that directly stimulates collagen synthesis in HSCs (Leask and Abraham, 2004), was evaluated at an estimated physiologically relevant concentration (0.1 ng/mL) and at a concentration traditionally employed in *in vitro* model systems (10 ng/mL) as a positive control (Fogel-Petrovic et al., 2007). All dosing solutions were prepared immediately prior to addition to liver tissue constructs. Stock concentrations of MTX prepared in 100% dimethyl sulfoxide (DMSO; Sigma-Aldrich, St. Louis, MO) were diluted in 3D Liver Tissue Medium™ (Organovo, San Diego, CA) to final concentrations of 0.1 and 1.0 µM (final DMSO concentration, 0.1%). A 25 mM dosing solution of TAA was prepared directly in the culture medium and further diluted to prepare a 5.0 mM dosing solution. Lyophilized TGF-β1 was reconstituted in Corning™ USP/EP Certified Sterile WFI-Quality Water (Fisher Scientific, Pittsburgh, PA) according to the product data sheet recommendations and added to the medium to prepare the 0.1 ng/mL and 10 ng/mL dosing solutions. To ensure vehicle consistency across treatment groups, 100% DMSO was spiked into the TAA and TGF-β1 dosing solutions and standard culture medium (vehicle control) such that the final DMSO concentration was 0.1%. Liver tissues were treated daily for either 7 or 14 days starting on the third day post-printing.

2.2.3 Lactate Dehydrogenase Assay

Spent medium samples collected on alternate treatment days were analyzed fresh for LDH activity using a commercially available colorimetric assay (Abcam, Cambridge, MA).

The assay was performed per the manufacturer's instructions using a CLARIOstar® microplate reader (BMG Labtech, Germany) with minor modifications. Briefly, a half area polystyrene high-bind 96-well plate (Sigma-Aldrich, St. Louis, MO) was employed, allowing the volumes of the kit reagents to be reduced by half. Samples were diluted to obtain readings within the linear range of the NADH standard curve corresponding to LDH activity between 1.0 and 100 mU/mL.

2.2.4 Albumin Immunoassay

Spent medium samples from treatment days 1, 7, and 14 (*i.e.*, Tx1, Tx7, and Tx14) were analyzed for albumin content by a plate reader-based sandwich ELISA (Bethyl Laboratories, Montgomery, TX) per the manufacturer's instructions with minor modifications as described above. Samples were tested at different dilutions to obtain readings within the range of the standard curve generated from Human Reference Serum (1.6-1,200 ng/mL; Bethyl Laboratories).

2.2.5 Cytokine Measurements

Spent medium samples from select time points throughout the exposure period were aliquoted and stored at -80°C until further analysis. The levels of cytokines released into the medium were assayed on the MESO QuickPlex™ SQ 120 Instrument using the Meso Scale Discovery (MSD) V-PLEX Human Biomarker kit (MSD, Rockville, MD), per the manufacturer's instructions. MSD Discovery Workbench software (version 4.0) was used to generate a standard curve with a 4-parameter logistic fit and $1/y^2$ weighing (R^2>0.998). Cytokine concentrations in unknown medium samples were then interpolated from the standard curve. Cytokine heat maps exhibiting cytokine concentrations for each treatment relative to time-matched, vehicle-treated control were constructed using the JMP statistical

software package Graph Builder (SAS Institute, Inc., Cary, NC).

2.2.6 Histology

At the conclusion of the study, a subset of bioprinted liver tissues from each treatment group were formalin-fixed in a 2% paraformaldehyde solution (*i.e.*, 2% paraformaldehyde, 10 mM calcium chloride, 50 mM sucrose in phosphate buffered saline) for 24 hours at 4°C and transferred to 70% ethanol for 24 hours. After processing and embedding tissues, blocks were sectioned at a 5.0 µm thickness using a rotary microtome (Jung Biocut 2035; Leica Microsystems, Buffalo Grove, IL). Sections were stained with Gill 3 Formulation Hematoxylin (Ricca Chemical Company, Arlington, TX) and Eosin Y Solution, 1% Aqueous (Electron Microscopy Sciences, Hatfield, PA). Additional slides were developed using Gomori's One-Step trichrome (American MasterTech, Lodi, CA) to evaluate collagen content. Slides were imaged using a Zeiss Axioskop microscope (Zeiss, Jena, Germany) and acquired with a Zeiss ICM-1 camera using Zen Pro software (blue edition).

2.2.7 RNA Isolation and Measurement of Fibrosis-Associated Genes using Quantitative Real-Time PCR

At the conclusion of the study, tissue lysates were prepared for each treatment group by homogenization in TRIzol® Reagent (ThermoFisher Scientific, Wilmington, DE). Total RNA was isolated by performing a phenol chloroform extraction/phase separation facilitated by Phase Lock Gel Heavy (5 PRIME, Inc., Gaithersburg, MD) and column purified using the RNeasy Plus Mini Kit (Qiagen, Valencia, CA) according to the manufacturer's protocol. RNA purity and yield was assessed using the NanoDrop 1000 version 3.5.2 (ThermoFisher Scientific). RNA samples were reverse transcribed with the High Capacity RNA-to-cDNA™ Kit following the manufacturer's instructions (ThermoFisher Scientific). Real-Time qRT-

PCR was performed using TaqMan® Universal PCR Master Mix (ThermoFisher Scientific, Wilmington, DE) and manufacturer recommended "Best Coverage" TaqMan® Gene Expression Assays (ThermoFisher Scientific, Wilmington, DE) for hypoxanthine guanine phosphoribosyltransferase (*HPRT*; housekeeping), α-smooth muscle actin (*ACTA2*) and collagen, type 1, α1 (*COL1A1*), two genes known to be up-regulated during fibrogenesis. Triplicate reactions were carried out using a 7900HT Fast Real-Time PCR System with sample analysis performed using ABI PRISM Sequence Detection System software version 2.4 (ThermoFisher Scientific). Relative quantities (RQ) were calculated for each gene of interest by normalizing to *HPRT* and are represented as fold change relative to vehicle-treated control for each set of treatments (n = 2).

2.2.8 Immunostaining

Deparaffinized, formalin-fixed normal native and untreated bioprinted liver tissue sections harvested 60 hours post-printing were subject to heat-mediated antigen retrieval in 1X citrate buffer solution, pH 6.0 (Diagnostic BioSystems, Pleasanton, CA) and immunolabeled using primary antibodies against E-cadherin (ab1416 [1:100], Abcam) and vimentin (ab8978 [1:100], Abcam) to highlight the formation of cellular junctions and distribution of NPCs within the tissues. Additional tissue sections were incubated with primary antibodies against albumin (A6684 [1:500], Sigma), CD31 (ab76533 [1:250], Abcam), desmin (ab15200 [1:200], Abcam), and α-smooth muscle actin (α-SMA; ab7817 [1:200], Abcam) to demarcate the compartmentalized architecture of bioprinted liver and activation status of HSCs in a 3D context. A subset of bioprinted liver sections obtained from tissues exhibiting prominent features of fibrotic change with trichrome staining compared to vehicle-treated control tissues (*i.e.*, 1.0 μM MTX and 25 mM TAA) were immunolabeled for

collagen I (ab34710 [1:500], Abcam), collagen IV (ab6586 [1:200], Abcam), vimentin, and α-SMA to examine the prevalence and distribution of collagen subtypes and migration/activation of NPCs throughout the constructs. Vehicle-treated control tissue was used to assess non-specific antibody staining. A secondary antibody control was also performed on successive bioprinted liver tissue sections as a procedural control (Appendix 1, Figure A1.1). ImageJ software (Schneider et al., 2012) was used to quantitatively measure the percent area covered by immunoreactive collagens I and IV in three fields of view from representative tissue sections.

2.2.9 Statistical Analysis

Unless otherwise noted, results are expressed as the mean of 4-5 replicates ± standard deviation (SD). Replicates refer to the same lot of bioprinted livers from a particular batch or print. The bioprinting process affords high reproducibility from each batch of bioprinted tissues. Statistical significance of treatment-induced differences relative to vehicle-treated control was determined using a two-way or one-way analysis of variance (ANOVA) where appropriate, with post hoc Dunnett's multiple comparisons test using GraphPad Prism version 6.0 (Graph Pad Software, Inc., La Jolla, CA). A *p-value* < 0.05 was considered statistically significant. Outliers were identified using Grubbs' test to identify samples that fell one SD outside of the mean of the data ($\alpha = 0.05$) using GraphPad Prism version 6.0 (Graph Pad Software).

2.3 Results

2.3.1 Bioprinted Constructs Exhibit Key Features of Native Liver

Bioprinting is the automated fabrication of multicellular tissue that mimics the three-

dimensional (3D) architecture and complexity of native tissue via the spatially defined deposition of cells in a proprietary bio-ink (Figure 2.1A, B). Culturing cells in this 3D context facilitates the formation of parenchymal tissue architecture and polarization of epithelial cell membranes as evidenced by E-cadherin staining between parenchymal cells that resembles *in vivo* tissue density and localization (Figure 2.1C, D). The punctate patterning and distribution of mesenchymal marker vimentin is preserved in 3D bioprinted liver and facilitates key heterotypic cell-cell interactions critical for supporting phenotypic features of uninjured liver (Figure 2.1E, F), and sustained viability for at least 4 weeks post-printing (Nguyen et al., 2016). Tissues comprising cryopreserved primary HCs, HSCs, and ECs were fabricated reproducibly on the membranes of standard 24-well culture inserts, thus enabling the use of this system to conduct routine *in vitro* toxicity testing (Figure 2.2A). During the initial 3-day culture period, bioprinted cells coalesce and remodel to form a tissue-like construct with the retention of parenchymal (HC) and non-parenchymal (NPC) compartments. These compartments are illustrated with the hepatocellular marker albumin and the NPC markers CD31 and vimentin which stain ECs and HSCs, respectively (Figure 2.2B). A proportion of vimentin-positive HSCs were observed both within the NPC compartment and scattered throughout the parenchymal compartment making key heterotypic contacts with HCs.

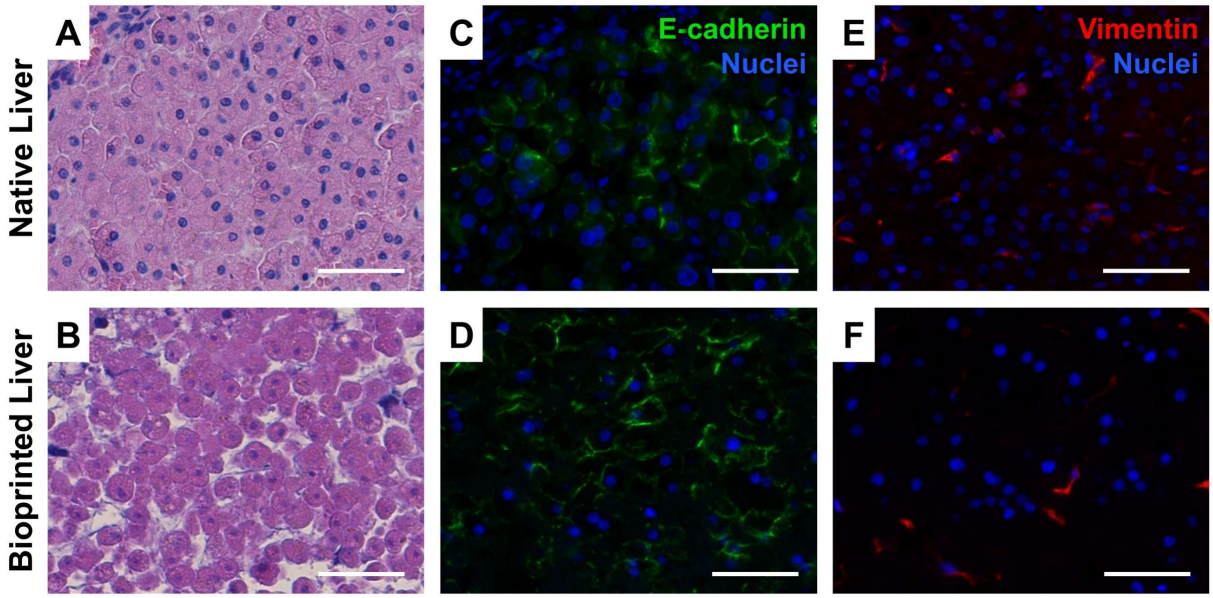

Figure 2.1 *3D bioprinted tissue recapitulates the tissue-like density and architecture of normal liver.* (A) Transverse cross-sections of native human liver and (B) bioprinted human liver tissue stained with H&E. (C and D) Formation of hepatocellular junctions is shown with E-cadherin and the mesenchymal marker (E and F) vimentin is used to highlight distribution patterns within the parenchyma analogous to native liver. Scale bar = 50 µm.

2.3.2 Hepatic Stellate Cells Exhibit a Quiescent-Like Phenotype in a Three-Dimensional Context

Hepatic stellate cells (HSCs) and their activation state within the center of the tissue construct were tracked in 3D culture by staining for desmin, an intermediate filament present in HSCs (Puche et al., 2013, Schmitt-Graff et al., 1991) and α-SMA, a marker of activated HSCs (Friedman, 2008). Prior to incorporation in 3D bioprinted tissues, HSCs were propagated through multiple population doublings and serial passages in 2D culture. HSCs typically reside in a quiescent state in uninjured liver but undergo activation in response to injury or 2D culture (*i.e.*, culture activation on collagen or plastic surfaces) as demonstrated by increased expression levels of activation markers, such as α-SMA (Carpino et al., 2005, Friedman, 2008). When cultured in a 3D context, HSCs embedded within the tissue architecture exhibited a more quiescent-like phenotype as illustrated by the retention of desmin and lack of α-SMA positivity (Figure 2.2C, merge; white arrows). While a majority of the HSCs embodied in the tissue are desmin(+), activated desmin(+)/α-SMA(+) HSCs were noted mainly at the periphery of the tissue (*i.e.*, the apical capsular region and basolateral edge of the tissue in contact with the culture medium and transwell membrane), consistent with a typical culture-activated phenotype (data not shown) and previously reported observations (Nguyen et al., 2016).

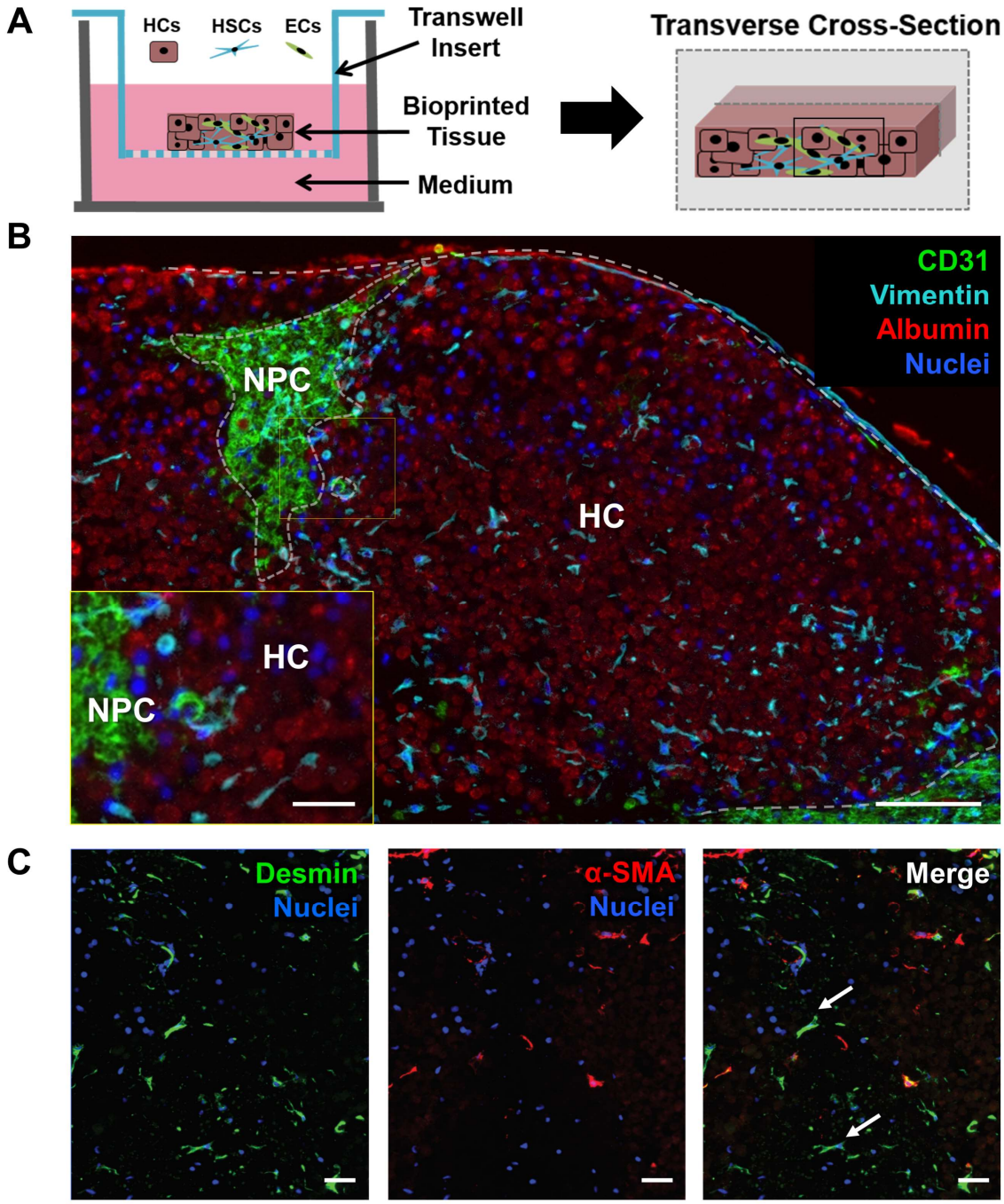

Figure 2.2 *3D bioprinted tissue exhibits a compartmentalized architecture and maintains hepatic stellate cells in a quiescent-like phenotype.* (A) Illustration of a transverse cross-section of bioprinted tissue on a transwell insert comprising hepatocytes (HCs) and compartmentalized endothelial cells (ECs) and hepatic stellate cells (HSCs). (B) The organization of non-parenchymal cells (NPCs) is depicted with CD31 and vimentin staining to mark ECs and HSCs, respectively. Albumin is used to denote the HC compartment. Scale bar = 100 µm, inset scale bar = 25 µm. (C) HSC activation status was examined using desmin (generic marker) and α-SMA (activation marker). Quiescent HSCs are denoted with white arrows. Scale bar = 50 µm

2.3.3 Effects of Fibrogenic Agents on Markers of Hepatocellular Injury and Function

Drug- or chemical-induced fibrosis is a complex and progressive process that usually occurs as a result of chronic exposure to low levels of compounds. To evaluate the culture model as a platform for studying drug- and chemical-induced fibrosis, bioprinted tissues were exposed to known fibrogenic agents, MTX and TAA, for up to 14 days. MTX is a folate antagonist effectively used to manage inflammatory disorders (*i.e.*, rheumatoid arthritis, psoriasis) at low doses for extended periods of time. However, it is known to cause elevations in alanine aminotransferase (ALT) and fibrosis in a subset of patients over prolonged treatment periods (Lindsay et al., 2009, Maybury et al., 2014). TAA is a prototypical fibrogenic agent extensively used in rodent models to study the development of liver injury and fibrosis (Starkel and Leclercq, 2011).

During the course of the study, the tissues remained intact macroscopically, with a marked dose- and treatment-dependent reduction in tissue size noted for 1.0 μM MTX and TAA-treated groups by treatment day 14 (Tx14; Fig 2.3A). LDH release was measured in the culture medium to assess the impact of repeated exposure on tissue viability. During the initial 7-day exposure period, LDH release for MTX- and TGF-β1-treated groups remained consistent with vehicle control levels (Figure 2.3B). Within the same time period, elevations in LDH were observed for 25 mM TAA beginning at Tx3 (Figure 2.3C). At later treatment time points (>Tx9), both 0.1 μM and 1.0 μM MTX-treated groups exhibited a time-dependent 2-3-fold increase in LDH release relative to vehicle control (****$p<0.0001$). TAA exhibited similar trends at the lower concentration beginning on Tx5. However, LDH release measured from the 25 mM TAA-treated group exhibited a monophasic increase that peaked around Tx5 (****$p<0.0001$) and then declined again by Tx11. These results were further

supported by parallel trends in ALT release at similar time points during the exposure period (Appendix 1, Figure A2.2). By Tx4, elevations in ALT were noted for the 1.0 μM MTX- and 5.0 mM TAA-treated groups and sustained for the remainder of the treatment time course. A similar monophasic increase in ALT release was noted for 25 mM TAA, peaking around Tx4.

Albumin output was measured at time points defined by the LDH results (*i.e.*, prior to elevations in LDH, mid-way through the treatment period, and time points at which statistically significant elevations in LDH were observed) during the exposure period as a measure of hepatocellular function (Figure 2.3D). Albumin output (ng/mL/million cells) for most of the treatment groups remained within vehicle-treated control levels during the treatment time course with the exception of the 0.1 ng/mL and 10 ng/mL TGF-β1 (Tx14 increased; *$p<0.05$ and *****$p<0.0001$, respectively) and the 25 mM TAA (Tx7 and Tx14 decreased; ****$p<0.0001$) treatment groups. The measured depreciation in albumin output for 25 mM TAA at Tx7 and Tx14 complements the LDH and ALT results (Figure 2.3C and Appendix 2, Figure A2.2B, respectively) further suggesting a perturbation in tissue function as a result of hepatocellular injury. Because TAA requires CYP2E1-mediated bioactivation to elicit hepatotoxicity, the expression of *CYP2E1* was verified in untreated bioprinted tissues spanning the timeframe of exposure used in the current studies (Appendix 2, Figure A2.3).

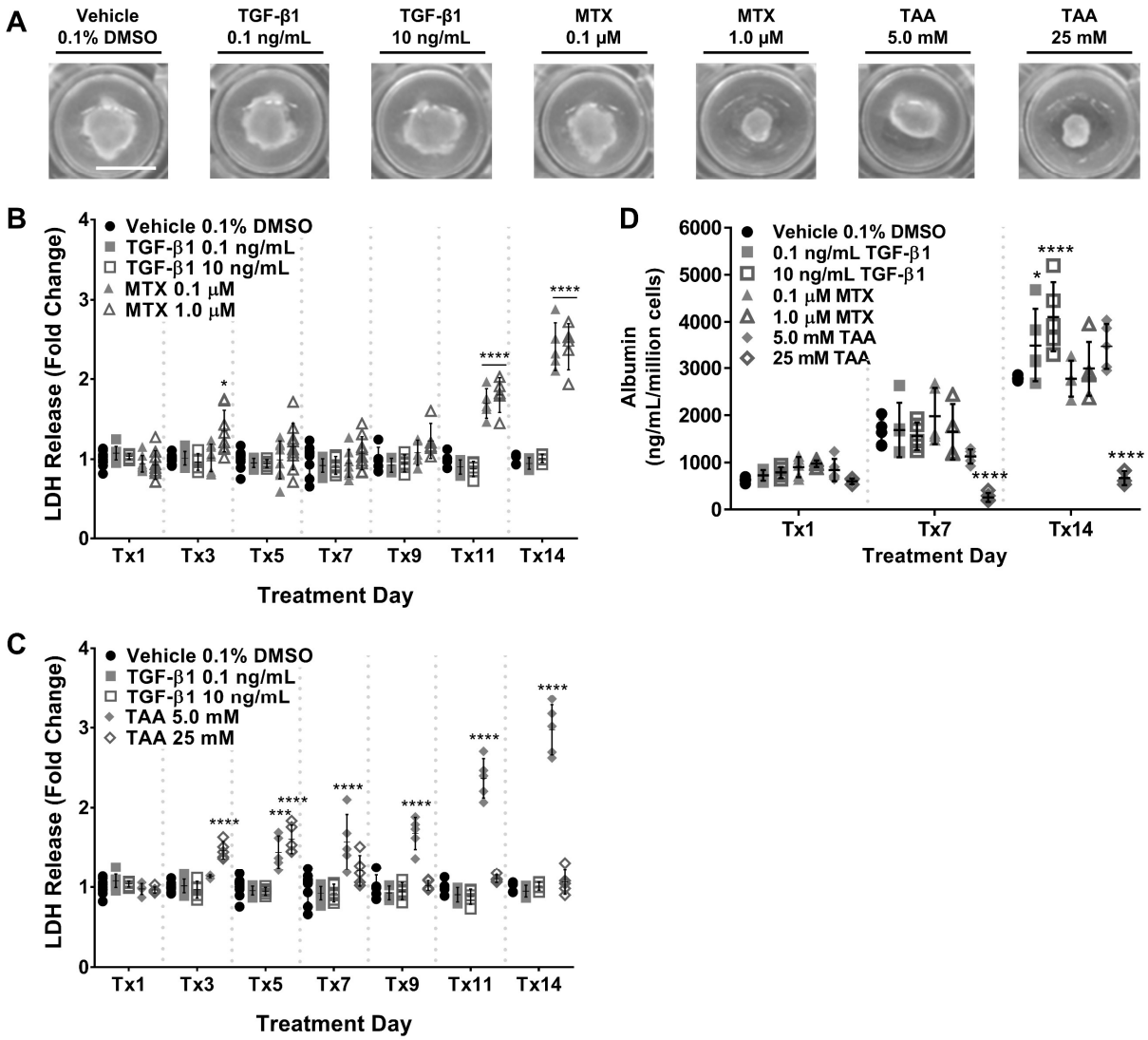

Figure 2.3 *Impact of fibrotic agents on biochemical markers of liver tissue viability and functionality.* (A) Gross images of tissues following 14 days of treatment. Scale bar = 2.5 mm. (B and C) LDH release during an extended 14-day treatment with MTX, TAA, and TGF-β1 (n = 9 for Tx1–Tx7, n = 5 for Tx9–Tx14). (D) Albumin production as a measure of hepatocellular function is depicted at key time points during the treatment period (n = 5). Significance was determined using a two-way ANOVA with post hoc Dunnett's multiple comparisons test (*p<0.05, **p<0.01, ***p<0.001, ****p<0.0001).

2.3.4 Evidence of Collagen Deposition in Tissues Treated with Fibrogenic Agents

For complex disease processes such as fibrosis that lack early and informative biomarkers, histological assessment remains the gold standard for detecting and evaluating the progression of fibrotic injury (Barker et al., 2011, Sebastiani and Alberti, 2006). In order to assess the effects of compound treatment, a subset of tissues from each treatment group were examined histologically. Transverse cross-sections of formalin-fixed, paraffin embedded tissues were stained with hematoxylin and eosin (H&E) to evaluate overall cell and tissue morphology (Figure 2.4). Distinct compartments were evident within the tissue constructs with delineation of HC and NPC compartments (Figure 2.4B). Treatment with 1.0 μM MTX (Figure 2.4G) and TAA at both concentrations (Figs. 2.4D and 2.4E) resulted in a compact and rounded mass of cells compared to the vehicle-treated group (*i.e.*, approximate 50% reduction in tissue size) suggesting possible cell death and tissue degeneration (which was also supported by the biochemical data), ECM deposition, and enhanced contraction of tissue architecture. Invasion of NPCs into the HC compartment was observed for all tissues exposed to fibrogenic agents. For both TGF-β1-treated groups (Figure 4B and 4C), the basal surface of the tissue in contact with the transwell membrane exhibited concentration-dependent differences in the thickness of scar-like tissue (white arrows). This phenomenon was also observed for the MTX- (Figure 2.4F and 2.4G) and TAA-treated (Figure 2.4D and 2.4E) groups with a more extensive replacement of the tissue with fibrous-scarring.

Gomori's trichrome stain (Figure 2.4) revealed stark differences between vehicle-, TGF-β1-, MTX-, and TAA-treated tissues. In the vehicle-treated control, there was faint evidence of collagen deposition (blue) throughout the construct (Figure 2.4A). TGF-β1 treatment caused diffuse areas of collagen deposition localized to the NPC compartment

(Figure 2.4B; outlined), a dose-dependent thickening of the basolateral edge of the tissue (Figs. 2.4B and 2.4C; indicated with white arrows), and a generally preserved HC mass, a histological outcome mirrored in the LDH data (Figure 2.3). MTX (0.1 μM) caused mild hepatocellular damage and evidence of pericellular fibrosis (Figure 2.4F; PF; inset 150% enlarged) that progressed with 1.0 μM MTX treatment to include areas of nodular fibrosis (NF) and a compacted mass of cells separated by fibrotic septae bisecting the hepatocellular compartment (Figure 2.4G; yellow arrows). Treatment with TAA diminished the parenchymal compartment in the tissues in a concentration-dependent manner by 14 days, with entrapment of remaining HCs (Figure 2.4D and 2.4E; EH) and replacement of the parenchymal compartment with extensive whorls of scar-like tissue. Preliminary analysis of two fibrosis-associated genes, *ACTA2* and *COL1A1* in MTX-treated tissues exhibited a 2-3-fold increase in expression relative to vehicle-treated control by Tx14 concordant with histological findings (Figure 2.4H).

Cross-sections of tissues from treatment groups that exhibited pronounced evidence of collagen deposition as evidenced by Gomori's trichrome staining were further examined immunohistochemically for the prevalence of collagens I and IV and the distribution and activation of HSCs within the tissue using vimentin and α-SMA (Figure 2.5). Relative to vehicle-treated control, collagen production (Figure 2.5A and 2.5B) was visually upregulated in tissues treated with 1.0 μM MTX and 25 mM TAA with both collagen subtypes most prevalent in the 25 mM TAA-treated tissue. The average percent area of collagen in the 25 mM TAA-treated group compared to vehicle-treated control was 25.8% versus 7.53% for collagen I and 29.8% versus 2.12% for collagen IV (Figure 2.5A versus 2.5B), respectively.

While collagen I and collagen IV exhibit similar patterns at first glance, closer

examination shows distinguishing patterns in the localization of greatest staining intensity. Collagen I, positive areas were localized to the apical face (*i.e.*, capsular region) of the tissue (Figure 2.5A; white arrow) and at the basolateral edge of the tissue in contact with the transwell membrane (Figure 2.5A; yellow arrow). In addition, collagen I staining was prominent in the septae traversing the parenchymal compartment, thicker ECM fibers present within the tissue constructs (outlined), and in areas of nodular fibrosis (NF) concordant with collagen positive areas in Gomori's trichrome-stained sections (blue staining; Figure 2.4). In comparison, collagen IV positive areas were mainly localized to the immediate periphery of cells in the HC compartment with little to no staining of fibrillar collagen (Figure 2.5B; corresponding areas of collagen I- versus collagen IV-stained sections are outlined). Similar to collagen I, collagen IV was also prominent in nodular areas of collagen deposition, particularly in the NPC compartment.

The distribution and patterning of vimentin in the tissue constructs mirrors the results obtained from collagen immunohistochemistry (IHC) and varies with treatment and the degree of fibrotic injury (Figure 2.5C). In the vehicle-treated group, vimentin positivity appears as small punctate spindle shaped areas with the greatest prevalence in the non-parenchymal compartment and even distribution throughout the parenchymal compartment (white arrows). Following 14 days of treatment, vimentin transitions to a more extensive and diffuse patterning throughout the tissue constructs (series of yellow arrows) compared to vehicle-treated control, particularly in areas corresponding to nodular areas of collagen deposition (NF). In addition to measuring the distribution of NPCs within the tissue constructs, the activation of HSCs in bioprinted liver was also assessed by staining for α-SMA (Figure 2.5D). Activated α-SMA(+) HSCs were mainly noted at the periphery of the

tissue in the vehicle-treated control (white arrow) with the minimal activation of HSCs within the center of the tissue construct. Treatment with fibrogenic agents resulted in an increase in SMA(+) HSCs in the center of the tissue (white arrows) and altered distribution of the cells corresponding to areas of collagen deposition. Overall, these histological features were consistent with the upregulation of *ACTA2* and *COL1A1* relative to vehicle-treated controls at Tx7 and Tx14 (Figure 2.4H and Appendix 2, Table A2.1).

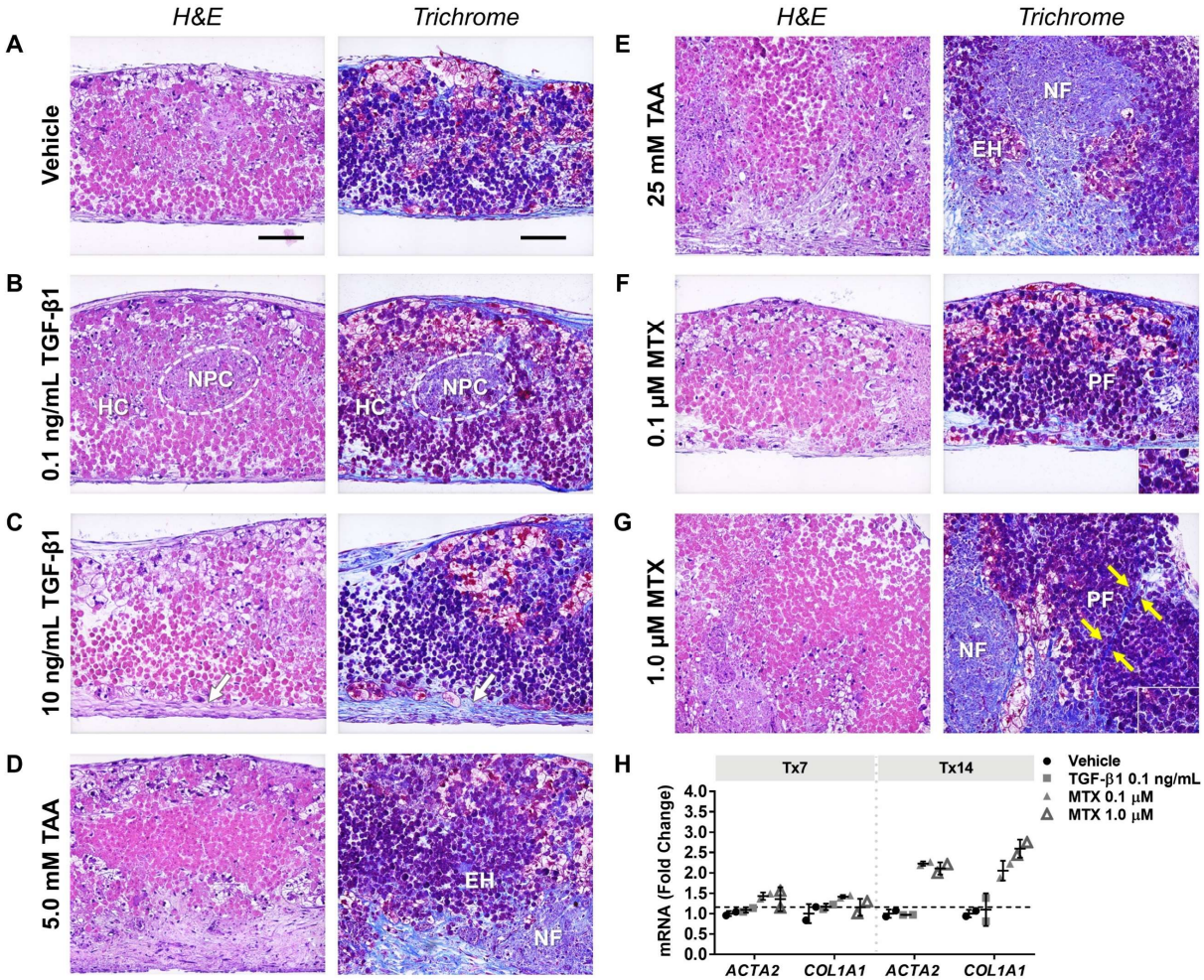

Figure 2.4 *H&E and trichrome staining reveals key features consistent with clinical fibrosis in bioprinted tissues following 14 days of treatment with select fibrogenic agents.* Representative sections of bioprinted liver treated with (A) 0.1% DMSO vehicle, (B) 0.1 and (C) 10 ng/mL TGF-β1, (F) 0.1 and (G) 1.0 μM MTX, and (D) 5.0 and (E) 25mM TAA. (B and C). A circle is used to delineate the non-parenchymal (NPC) from the parenchymal (HC) compartments and white arrows denote the basolateral edge of the tissue in contact with the transwell membrane. Collagen deposition was visualized (blue) in successive sections of bioprinted tissue stained with Gomori's trichrome. Entrapped hepatocytes (EH), nodular areas of collagen deposition (NF), pericellular fibrosis (PF; F and G inset, 150% enlarged), (G) yellow arrows denote bridging fibrosis. Scale bar = 100 μm. (F) Expression of fibrosis-associated genes at Tx7 and Tx14 in MTX-treated tissue.

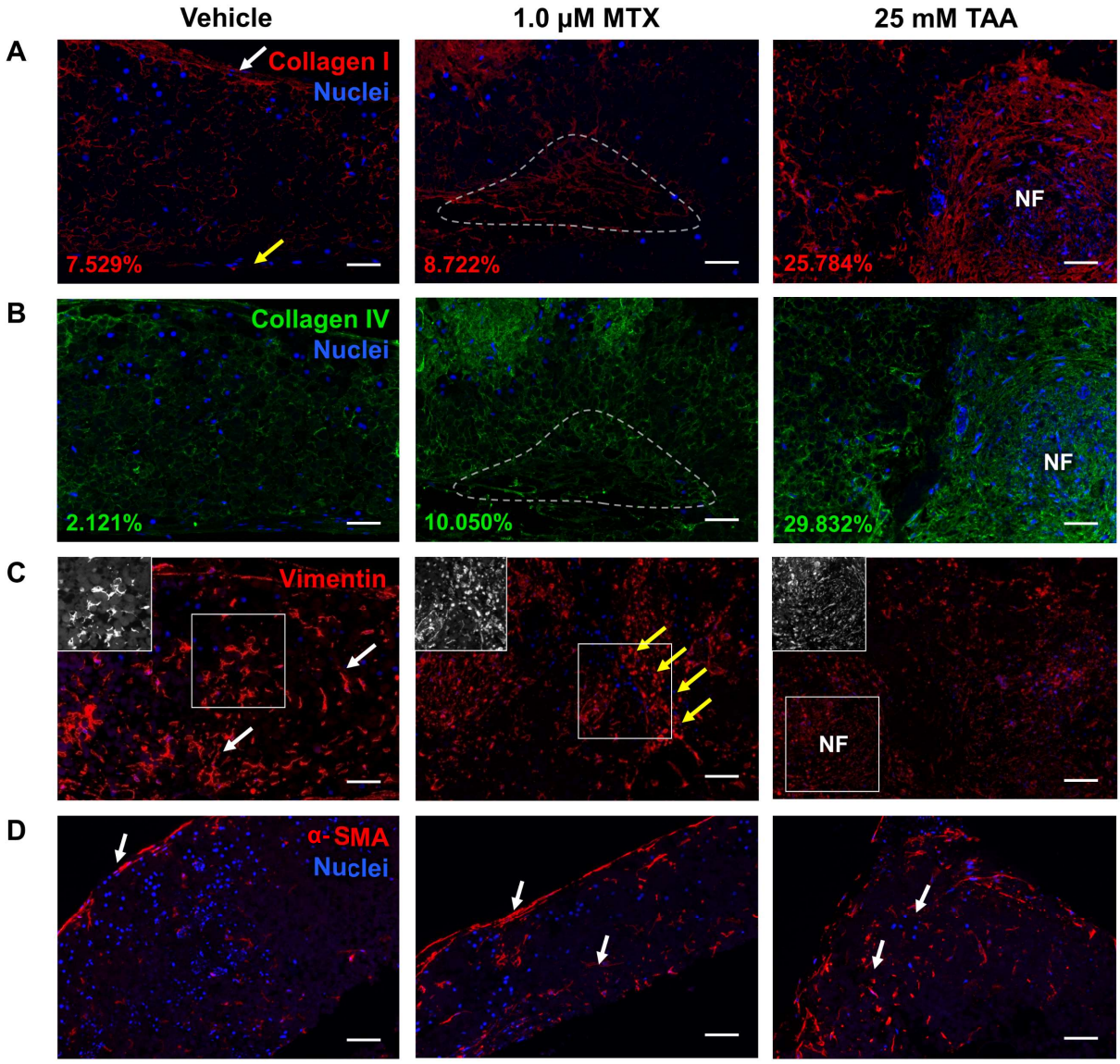

Figure 2.5 *Increased deposition of collagens I and IV and expression of vimentin and α-SMA in tissues exhibiting pronounced fibrogenic change.* Tissues treated with 0.1% DMSO vehicle, 1.0 μM MTX, and 25 mM TAA were further assessed immunohistochemically for (A) collagen I, (B) collagen IV, (C) vimentin, and (D) α-SMA. White and yellow arrows denote the apical and basolateral edges of the tissue, respectively. Areas of fibrillar ECM deposition are outlined in successive collagen I- and collagen IV-stained sections. Nodular areas of collagen deposition (NF). The percent area covered by collagens I and IV is depicted in the bottom left-hand corner of the photomicrographs. (C) Punctate areas of vimentin positivity in control tissue (white arrows) and diffuse patterning in treated tissue (yellow arrows). The black and white inset accentuates the shift in vimentin patterning observed with treatment. (D) α-SMA(+) HSCs were mainly noted at the periphery of the tissue in the vehicle-treated control (white arrows). Increased α-SMA(+) HSCs in the center of treated tissues and altered distribution of the cells corresponding to areas of collagen deposition (white arrows). Scale bar = 25 μm.

2.3.5 Cytokine Profiles are Indicative of a Fibrogenic State

Because inflammation is closely tied to fibrogenesis (Pellicoro et al., 2014), the abundance of pro- and anti-inflammatory cytokines (pg/mL) released into the culture medium from treated tissues throughout the exposure period (*i.e.*, alternate treatment days) was measured. A general decrease in cytokines starting at Tx1 is apparent for all treatment groups including vehicle-treated control (Appendix 2, Figure A2.4). By Tx7, the initial spike in cytokine production subsides (Appendix 2, Figure A2.4) and treatment-dependent differences become perceptible.

In order to assess treatment-dependent effects over time, the fold change in cytokine levels relative to time-matched vehicle-treated control was determined (Figure 2.6). A subset of cytokines depicted in Figure 2.6A changed consistently across replicates and illustrate treatment- and concentration-dependent effects over the course of the 14-day exposure period. Other cytokines detected from the cytokine panel exhibited similar trends although they were admittedly variable. During the initial treatment period (Tx1 and Tx3), deviations in the prevalence of specific cytokines from vehicle-treated control are not readily apparent with the exception of IL-13, an important inflammatory mediator, in treated tissues (Figure 2.6A; decreased). Starting at Tx7, elevations in proinflammatory IL-6 were evident for 1.0 μM MTX and both TAA-treated groups with slight elevations observed for 0.1 μM MTX starting at Tx9. IL-6 regulates acute phase response proteins in response to injury (Choi et al., 1994) and in part, coincides with the biochemical data for MTX and TAA (Figure 2.3 and Appendix 2, Figure A2.2). Furthermore, a more general decrease in cytokines observed starting at Tx7 with 25 mM TAA treatment, was concordant with the timeframe of LDH and ALT release (Figure 2.3C and Appendix 2, Figure A2.2B), and decreased albumin

production at Tx7 and Tx14 (Figure 2.3D) suggesting tissue damage and perturbation of hepatocellular function. In comparison, the trends in cytokines observed with MTX and TAA treatment were not evident for TGF-β1-treated tissues. This difference in profiles is not entirely unexpected, considering the apparent absence of hepatocellular damage seen with TGF-β1 treatment (Figure 2.3) and the different mechanisms of action of cytokine- versus xenobiotic-induced liver fibrosis.

After the initial assessment of selected cytokines, additional cytokine profiling was performed at Tx7 and Tx14 (Figure 2.6B; cytokines exhibiting consistent changes across replicates are depicted). Measurement of cytokine levels at these time points showed treatment- and time-dependent differences in acute phase response, immunomodulatory, angiogenic, and chemotactic cytokines. A Log2(Fold Change) of 2 or -2 was considered statistically significant. IL-6 was significantly increased at Tx7 and Tx14 for 1.0 μM MTX and both TAA treatment groups consistent with initial temporal observations from Figure 2.6A. Fms-related tyrosine kinase-1 (Flt-1), involved in cell proliferation, differentiation, and monocyte activation/recruitment (Motomura et al., 2005), is statistically increased at Tx7 for 25 mM TAA-treated tissues and then returns to vehicle-treated levels by Tx14. Monocyte chemotactic protein-1 (MCP-1), involved in facilitating macrophage/monocyte infiltration to perpetuate an adaptive response to continued insult (Baeck et al., 2012), increases at Tx7 for 1.0 μM MTX and 5.0 mM TAA treatment and continues to increase by Tx14 with the exception of 25 mM TAA. The abundance of eotaxin, a mediator of inflammatory cell infiltration and recruitment, was significantly increased in the culture medium of tissues treated with 10 ng/mL TGF-β1 suggesting a possible direct-acting stimulation of eotaxin expression in the absence of overt hepatocellular injury (Matsukura et al., 2010).

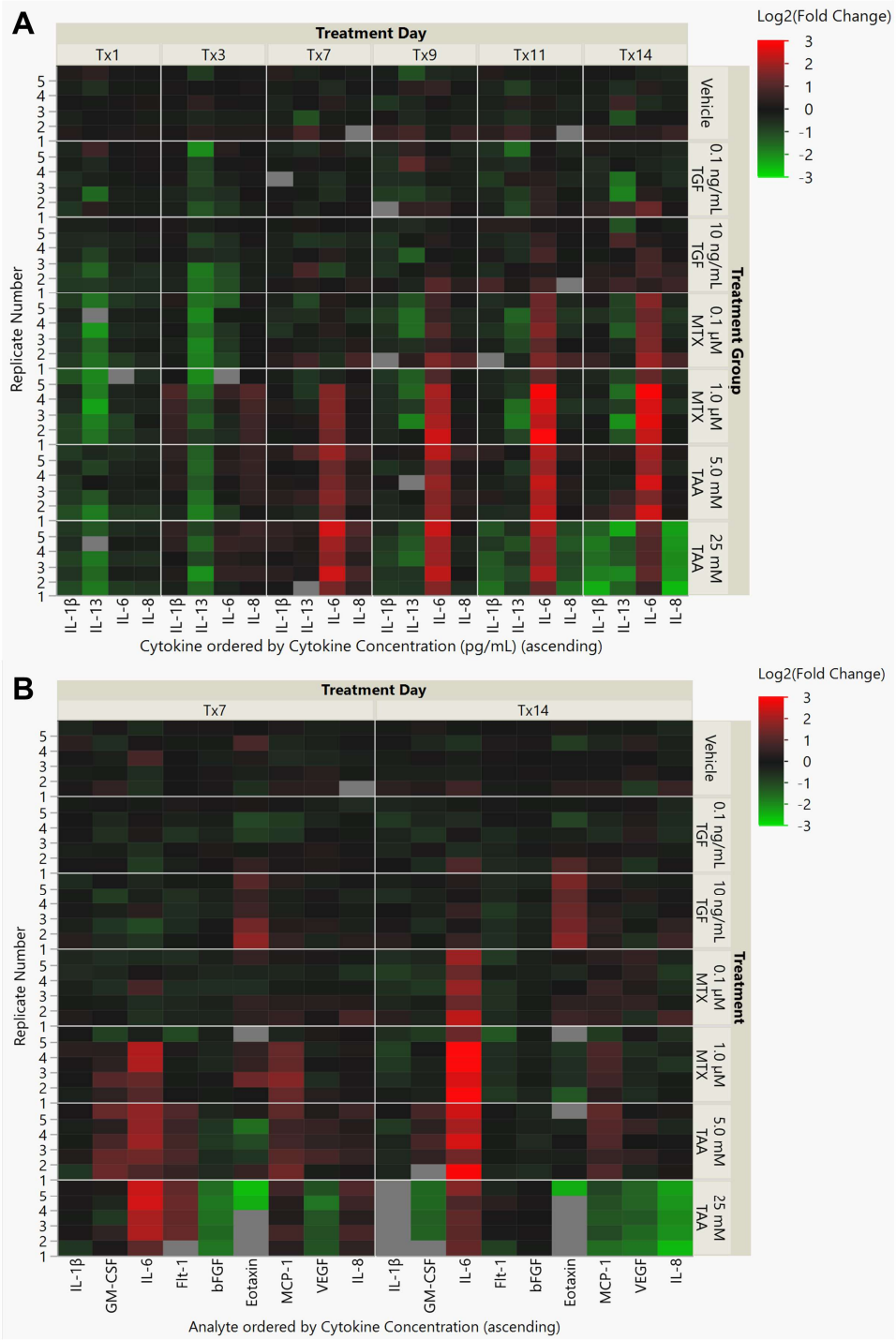

Figure 2.6 *Subset of cytokines exhibiting treatment-dependent differences over time and at select treatment time points.* (A) The upregulation (red) and downregulation (green) of proinflammatory, immunoregulatory, and chemotactic cytokines relative to vehicle-treated control was represented in a heat map. (B) Samples collected at mid (Tx7) and late (Tx14) treatment time points were profiled for additional cytokines and chemokines. Values outside the range of the standard curve or excluded via Grubb's outlier analysis are shaded grey.

2.4 Discussion

Recently, liver fibrosis secondary to compound-induced liver injury has become an interest to the Joint Research Centre (JRC) and other regulatory organizations focused on adverse outcomes (Ankley et al., 2010). Because fibrosis develops over time from a sequence of complex and cumulative interactions between HCs and NPCs, it has proven challenging to model using standard *in vitro* and preclinical *in vivo* models. The development of an effective Adverse Outcome Pathway framework depends on the employment of models that overcome these translational challenges and provide a test bed that is multicellular, compatible with chronic exposure testing regimens, and able to reveal a full spectrum of relevant outcomes from initiation through progression, including biochemical, genomic, and histologic endpoints (Van de Bovenkamp et al., 2007). Here we evaluated the potential of a novel bioprinted *in vitro* tissue model of human liver to model compound-induced fibrosis. This approach represents a significant innovation in the study of progressive liver injury and *in vitro* toxicity testing, as it addresses many of the shortcomings associated with traditional models.

The constitutive activation of HSC monocultures has been a significant barrier in the *in vitro* assessment of potential fibrogenic agents, as compound-related effects are confounded by the culture-activated HSC phenotype. Whereas there have been some recent advances in the study of hepatic fibrosis *in vitro* using precision cut liver slices (PCLS) or spheroids (Leite et al., 2016, Thiele et al., 2015, Van de Bovenkamp et al., 2007, Westra et al., 2016), there still exist limitations in the application of these platforms to understand the progression of events underlying fibrogenesis. PCLS have a short life span *ex vivo* (generally <1 week) and develop early onset fibrogenic changes, irrespective of treatment, which may

confound the interpretation of a causal relationship after compound exposure (Westra et al., 2016). As such, chronic exposure studies aimed at modeling progressive fibrogenic features over weeks to months have not been feasible with PCLS. Finally, whereas the fixed configuration of the cells comprising each slice preserves the normal tissue architecture initially, the ability to tease apart the roles of the different cell types is severely limited. Bioprinting is an efficient and reproducible means of establishing key architectural relationships between cells and preserving tissue-level functions over prolonged periods of time (Nguyen et al., 2016). The 3D nature and substantial biomass of the model enable histological assessment of treated liver tissues, which remains the diagnostic gold standard for the accurate detection and staging of fibrosis (Sebastiani and Alberti, 2006). The unique compartmentalized architecture of bioprinted tissues compared to other 3D models, such as spheroids (Leite et al., 2016), facilitates the temporal assessment of progression by revealing specific patterns of collagen deposition that are analogous to patterns described in human biopsy samples.

Importantly, the incorporation of HSCs into 3D bioprinted tissue re-establishes a quiescent-like phenotype and uniquely enables the model to be used in the assessment of compound effects on early fibrogenic processes -- something that has not been feasible to date using conventional approaches. This phenomenon is consistent with the outcome of elegant fate-mapping studies in mice that demonstrated a subset of HSCs are able to revert to a quiescent-like phenotype (Kisseleva et al., 2012) during the resolution of fibrotic injury. HSCs that have been previously activated exhibit a primed phenotype with rapid and robust patterns of reactivation in response to subsequent injury (Kisseleva et al., 2012, Taghdouini et al., 2015). This observation could explain the accelerated fibrogenic features observed in

the current study, compared to the clinical setting in which fibrosis can take months or even years to develop. Regardless of whether the desmin(+)/α-SMA(-) HSCs represent quiescent or inactivated HSCs, the results presented herein demonstrate their clear capacity to mount a measurable and progressive response to fibrogenic insults.

Following 14 days of exposure, the extent of LDH release and time to peak release was compound-, concentration-, and time-dependent. The monophasic increase in LDH release and subsequent return to vehicle-treated levels for 25 mM TAA most likely reflects the outcome of prior hepatocellular damage, as supported by the corresponding loss of albumin production and decrease in ALT release. By contrast, TGF-β1 treatment did not elicit elevations in LDH release during the entire exposure period. TGF-β1 is a well-established pro-fibrogenic mediator, directly triggering the activation of HSCs and synthesis of ECM (Leask and Abraham, 2004). Albumin production was not significantly perturbed with the exception of the TGF-β1 (increased production) and the 25 mM TAA (decreased production) treatment groups. While previous studies have reported TGF-β1 inhibits albumin RNA and protein synthesis in primary HCs, it should be noted that these studies were conducted in HC monocultures (Busso et al., 1990). We hypothesize the lack of concordance may reflect TGF-β1-induced secretion of ECM proteins and other factors by the NPC compartment that further support HC function in the absence of overt injury. Taken together, these data demonstrate that the exposure conditions described herein are able to produce the mild/moderate HC injury associated with low-concentration, chronic exposure, which sets the stage for the development and detection of more complex adverse outcomes such as fibrosis.

Histological assessment of treated tissues revealed the initiation and progression of

fibrogenic processes in response to insult. The degree of collagen deposition in treated tissues correlated with biochemical evidence of hepatocellular damage, with 1.0 µM MTX and 5.0 and 25 mM TAA-treated tissues exhibiting a disrupted architecture with prevalent collagen deposits that progressed to a scar-like matrix and displaced the HC compartment over time. Interestingly, patterns of collagen deposition and tissue injury observed in the MTX- and TAA-treated groups were analogous to those reported in clinical biopsy samples of MTX-induced fibrosis and preclinical animal models of TAA exposure (Müller et al., 1988, Osuga et al., 2015), which suggests the model may serve as a translational tool for mechanistic and interventional studies involving fibrogenic agents and modulators. Changes in *ACTA2* and *COL1A1* expression, further confirmed the progression- and concentration-dependent nature of the fibrogenic response, particularly in MTX-treated tissues. The treatment-induced mobilization of NPCs and activation of HSCs within the tissue were consistent with findings from published clinical studies of progressive fibrosis (Attallah et al., 2007, Veidal et al., 2011). While future studies will expand the genomic, proteomic, and histologic characteristics of the model during progressive fibrotic injury, these initial observations provide encouraging evidence that the model has translational utility.

Interestingly, compound-dependent fibrogenic responses were elicited in the absence of liver resident macrophages. While inflammation typically precedes or accompanies liver fibrosis and is recognized as a driver of fibrogenesis (Czaja, 2014, Pellicoro et al., 2014), the precise role of KCs in mediating this process remains elusive. This is largely due to the inability to target specific macrophage subpopulations (Tacke and Zimmermann, 2014), a question which can be addressed using this model. We anticipate that KCs will play an important tolerogenic role in attenuating the tissue response during early exposure to pro-

fibrogenic agents (Ju and Pohl, 2005). We sought to validate the established 3D liver model, which consists of two key NPC constituents, namely ECs and HSCs, but also is amenable to modifications in cellular composition. These studies lay the foundation for the future assessment of the role of KCs and other cell types relevant to the response (*i.e.*, sinusoidal endothelial cells) in exacerbating or remediating tissue injury and impact on fibrogenic outcome.

Cytokine profiles differed between early and late time points of exposure to fibrogenic agents, which likely reflects the modulatory role(s) of specific cytokines that mark liver injury and influence fibrogenic outcomes in response to insult. The induction of proinflammatory cytokines during early exposure (Tx1-Tx7) mimics some features of the classic wound-healing response (Pellicoro et al., 2014), with a surge in the production of proinflammatory cytokines that drive tissue remodeling and regeneration and may aid in the formation of a cohesive tissue-like mass after bioprinting. It is likely that both the HSC and EC components of the bioprinted tissues contributed to the elevations of IL-6 and IL-8, which enhance EC survival, proliferation, angiogenesis, and recruitment of inflammatory cells during wound healing (Qazi et al., 2011). IL-1 is also rapidly released in response to tissue damage (Gieling et al., 2009) and could explain the transient increase in IL-1β early in the exposure period.

When cytokines approached steady-state levels in vehicle-treated tissues (10 days post-printing) treatment-dependent spikes in proinflammatory cytokines were detected. Increased chemotactic cytokines, such as MCP-1, at later time points for some treatment groups suggest an adaptive shift in response to persistent tissue stress/injury that results in recruitment of inflammatory cells to the site of damage (Baeck et al., 2012). Observed

differences in the cytokine profiles in TGF-β1- vs. compound-treated tissues is likely due to mechanistic differences between the TGF-β1 response (little to no hepatocellular injury) and compound-induced responses to hepatocellular injury and/or the transient nature of cytokine profiles. The global decline in cytokine production observed at 25 mM TAA by Tx14 was consistent with the decline in viability and functionality for that time point. Significant differences in cytokine levels among treatment groups were not noted during early exposure, likely due to their masking by the observed wound-healing response post-fabrication. Furthermore, cellular interactions and cross-talk that occur during tissue formation could influence susceptibility or magnitude of response to particular insults. Future studies will examine alterations in response profiles in maturing (3- to 5-day old) vs. matured (7- to 10-day old) tissues. Nonetheless, the cytokine data in conjunction with the gene expression and histological data supports the hypothesis that these tissues are actively engaging in fibrogenic processes in response to compound-induced injury.

In summary, the outcomes from these studies support continued development of 3D bioprinted human tissues as *in vitro* surrogates for studying compound-induced liver fibrosis. Future studies will provide new insights into early initiating and adaptive events underlying fibrogenic responses, help identify both common and distinct pathways of compound-induced effects, and improve compound risk assessment. While there exist a number of challenges towards developing effective treatment strategies (*i.e.*, causation, stage of fibrotic injury, co-morbidities), these studies bridge a critical gap that could inform effective therapeutic approaches (*i.e.*, novel biomarkers and interventional strategies) for treatment at early and late stages of fibrogenesis during which different hepatic cell types may be involved and targeted to prevent or reverse liver fibrosis.

2.5 Supplemental Data Description

The levels of fibrogenic markers α-smooth muscle actin (*ACTA2*) and collagen, type 1, α1 (*COL1A1*) measured using RNA isolated from whole tissue constructs is included in Table A2.1. The immunohistochemistry control for the collagen I and IV assessment in Figure 2.5 is available in Figure A2.1. A description of the materials and methods used to measure alanine aminotransferase (ALT) in culture medium samples is provided in Appendix 2. ALT release as a result of compound treatment is represented in Figure A2.2A and A2.2B. In addition, the basal expression of *CYP2E1* in untreated 3D bioprinted liver tissues spanning the treatment period is shown in Figure A2.3. The shift in the abundance of cytokines over time for each treatment group and analyte is reflected in a conditionally formatted heat map in Figure A2.4. Trends are highlighted with abundant cytokines IL-8 and IL-1β in Figure A2.4B and A2.4C, respectively.

2.6 Funding Information

This work was supported by the National Institutes of Health (NIH), Initiative for Maximizing Student Diversity (IMSD) at University of North Carolina at Chapel Hill [R25 GM055336 to L.M.N.], and National Institute of Environmental Health Sciences (NIEHS) Toxicology Training Grant [T32 ES007126 to L.M.N.], and Organovo, Inc. The content is the authors' own and does not reflect the views of the National Institute of Health (NIH). The research described in this article has been reviewed by Organovo, Inc., San Diego, and approved for publication. Approval does not signify that the contents necessarily reflect the views and policies of the Company, nor does the mention of trade names of commercial products constitute endorsement or recommendation for use.

CHAPTER 3 – ROLE OF KUPFFER CELLS IN MODULATING FIBROTIC INJURY IN 3D BIOPRINTED LIVER TISSUES

3.1 Introduction

Crosstalk among hepatocytes (HCs) and resident non-parenchymal cells (NPCs) normally maintains a balance in reparative processes following injury, such as inflammatory cytokine release, response to oxidative stress, and synthesis/change in extracellular matrix (ECM) composition. Fibrosis is marked by an imbalance in these processes and can progress to compromise liver function via changes in the tissue microenvironment, production of various growth factors, inflammatory cytokines, and disruption of normal liver architecture as a result of a change in the distribution and proportion of fibrillar collagens (Puche et al., 2013). The inflammatory response plays an important role in driving these processes, as resident and recruited extrahepatic inflammatory cells are thought to create a more conducive environment via the production of proinflammatory and fibrogenic mediators that further amplify the fibrotic response (Czaja, 2014, Lee and Friedman, 2011).

In uninjured liver, Kupffer cells (KCs) constitute the main population of inflammatory cells in the liver and are important for a number of homeostatic functions (Bilzer et al., 2006, Krenkel and Tacke, 2017). During chronic injury, extrahepatic inflammatory cells are recruited to the site of damage and dramatically shift the population of these cells in the liver (Tacke and Zimmermann, 2014). While studies utilizing transgenic approaches have demonstrated the

general importance of macrophages in not only the initiation of fibrotic injury but also its resolution, the role of KCs during early injury as one of the initial responders remains elusive (Bataller and Brenner, 2005, Duffield et al., 2005). This is largely due to the inability to specifically target subsets of macrophage populations (*i.e.*, resident versus recruited) *in vivo* and the heterogeneity of macrophages during liver injury (Tacke and Zimmermann, 2014). Understanding the role of resident KCs during the early events underlying compound-induced fibrogenesis is critically important to better understand the role of inflammatory processes in the initial response and the development of relevant *in vitro* model systems for compound risk and therapeutic assessment.

Previous work has demonstrated the utility of a 3D bioprinted liver tissue model (ExVive 3D™ Human Liver, Organovo) composed of primary human hepatocytes (HCs), hepatic stellate cells (HSCs), and endothelial cells (ECs) to recapitulate basic fibrogenic features following treatment with prototype fibrogenic agents (Norona et al., 2016). While the base model lacks KCs, the bioprinting process confers a unique advantage by enabling the controlled incorporation of these cells in an automated and precise fashion. Thus, the inclusion of KCs into a model of progressive fibrotic injury would provide a more comprehensive understanding of how injury and fibrogenic events are modulated within a biologically relevant context and provide insight into the effects and responses underlying the initial response to extended compound exposure at an organ level.

The present study sought to understand the role of resident KCs in mediating the injury and fibrogenic response using a previously optimized model of progressive injury leading to fibrosis described in Appendix 2. Expansion to a continuous 28-day exposure to the identified LC20 and LC50 concentrations of fibrogenic and hepatotoxic agents resulted in

mild elevations and sustained lactate dehydrogenase (LDH) release over time. Histological evidence of collagen deposition was evident following the initial 14 days of treatment in the standard model for all fibrogenic and hepatotoxic agents tested (*i.e.*, TGF-β1, methotrexate, and acetaminophen). Incorporation of KCs did not significantly impact LDH profiles at early time points (Tx1-Tx14), however, a narrowing of the general injury window in response to compound exposure (Tx13-Tx15) was observed beyond treatment day 9 (Tx9) in tissues containing KCs (Tx9-Tx19). Assessment of additional markers of tissue function further support mild injury over the treatment timeframe with consistent trends across treatments regardless of tissue composition. The global dampening of inflammatory cytokine profiles in response to treatment in addition to limited collagen deposition at the mid timepoint suggest KCs may limit fibrogenic activity during early exposure to fibrogenic agents, while persistent exposure in the presence of KCs resulted in decreased cellularity regardless of treatment and evidence of collagen deposition at Tx28. Our results suggest KCs may play an important bimodal role during early versus later phases of the response and further demonstrate bioprinted human liver tissues are well-suited to evaluate temporal fibrogenic events *in vitro*.

3.2 Materials and Methods

3.2.1 Tissue Production

Three-dimensional bioprinted liver tissues comprising primary cryopreserved human HCs (Life Technologies, Carlsbad, CA), HSCs (ScienCell, Carlsbad, CA), and human umbilical vein endothelial cells (ECs) (Becton Dickinson, Tewksbury, MA) were manufactured by Organovo (San Diego, CA) with and without the incorporation of primary human KCs (Samsara Sciences, San Diego, CA) using patented protocols (U.S. Patents

8,241,905 B2; 8,852,932; 9,222,932 B2; 9,222,932 B2) as described previously (Forgacs et al., 2012, Forgacs et al., 2014, Murphy et al., 2015, Nguyen et al., 2016, Norona et al., 2016, Shepherd et al., 2015). Due to the nature of the study, separate tissue manufacturing runs were performed per tissue composition to complete the 14- and 28-day exposure studies. Following fabrication, the tissues were cultured in William's E supplemented with Primary Hepatocyte Maintenance Supplements without dexamethasone (Life Technologies, Carlsbad, CA) and EGM-2 (Lonza, Basel, Switzerland) and maintained in a 37°C incubator under humidified atmospheric conditions with 5% CO_2. The removal of dexamethasone from the culture medium did not adversely impact tissue viability, functionality, and response to compound exposure as shown in Appendix 2. Liver constructs were allowed to mature into tissue-like structures for a minimum of six days with the daily replacement of medium prior to the initiation of treatment.

3.2.2 Compound Exposure

LC20 and LC50 concentrations of methotrexate (MTX; Sigma-Aldrich, St. Louis, MO) and acetaminophen (APAP; Sigma-Aldrich, St. Louis, MO) identified based on previous14-day dose response studies were used to conduct long-term exposure studies (Appendix 2). All dosing solutions were prepared immediately prior to addition to liver tissue constructs. Stock concentrations of MTX prepared in 100% dimethyl sulfoxide (DMSO; Sigma-Aldrich, St. Louis, MO) were diluted in 3D Liver Tissue Medium™ without dexamethasone (Organovo, San Diego, CA) to final concentrations of 0.052 µM and 0.209 µM (final DMSO concentration, 0.1%). A stock solution of APAP was prepared directly in the culture medium and further diluted to prepare the 0.151 mM and 0.603 mM dosing solutions. Lyophilized TGF-β1 was reconstituted in Corning™ USP/EP Certified Sterile

WFI-Quality Water (Fisher Scientific, Pittsburgh, PA) according to the product data sheet recommendations and added to the medium to prepare the 0.1 ng/mL and 10 ng/mL dosing solutions. To ensure vehicle consistency across treatment groups, 100% DMSO was spiked into the TGF-β1 and APAP dosing solutions and standard culture medium (vehicle control) such that the final DMSO concentration was 0.1%. Liver tissues were treated daily for either 14 or 28 days starting on the seventh day post-manufacture.

3.2.3 Biochemical Assessment of Tissue Viability and Function

Spent medium samples collected on alternate treatment days were analyzed fresh for lactate dehydrogenase (LDH) activity using a commercially available colorimetric assay (Abcam, Cambridge, MA). Medium samples from treatment days 14 and 28 (*i.e.*, Tx14 and Tx28) were analyzed for albumin content using a plate reader-based sandwich ELISA (Bethyl Laboratories, Montgomery, TX) and urea production using a colorimetric assay (BioVision Incorporated, Milpitas, CA). All samples were diluted where appropriate to obtain values within the range of the standard curve and assays were conducted per the manufacturer's instructions with minor modifications to reduce the volume of sample and kit reagents required by 50% as described previously (Norona et al., 2016).

3.2.4 Histology and Immunohistochemistry

At the conclusion of the study, a subset of bioprinted liver tissues from each treatment group were formalin-fixed, processed, embedded, and sectioned at a 5.0 μm thickness using a rotary microtome (Jung Biocut 2035; Leica Biosystems, Buffalo Grove, IL) as described previously (Norona et al., 2016). Sections were stained with Gomori's One-Step trichrome (American MasterTech, Lodi, CA) to evaluate collagen content. Slides were imaged using the Aperio AT2 Digital Slide Scanner (Leica Biosystems, Buffalo Grove, IL). For

immunohistochemistry, formalin-fixed bioprinted liver tissue sections were deparaffinized and subject to heat-mediated antigen retrieval in Tris/EDTA buffer pH 9.0, blocked, and incubated with primary antibodies overnight at 4°C. The following primary antibodies were used: rabbit anti-desmin-TSA ([1:3350] Abcam, Cambridge, MA), rabbit anti-PCNA ([1:500] Cell Signaling Technology, Danvers, MA), mouse anti-α-SMA ([1:100] Abcam, Cambridge, MA), rabbit anti CD163 ([1:500] Abcam, Cambridge, MA), and mouse anti-albumin ([1:500] Sigma-Aldrich, St. Louis, MO) Vehicle-treated control tissue was used to assess non-specific antibody staining within the tissue constructs. A secondary fluorophore-conjugated antibody control was also performed on successive bioprinted liver tissue sections as a procedural control (Appendix 3, Figure A3.5). Alexa Fluor® 488 or 594 secondary antibodies (ThermoFisher Scientific, Pittsburgh, PA) were used where appropriate. Fluorescence labeling of desmin immunopositive cells was facilitated by Tyramide signal amplification (TSA) with HRP-streptavidin and 1 minute labeling with Alexa Fluor® 488 substrate (ThermoFisher Scientific, Pittsburgh, PA). Slides were washed, dipped in distilled water, mounted with Fluro-Gel II with DAPI and cover slipped (Vector Labs, Burlingame, CA). Slides were visualized and imaged using Zeiss Axioskop microscope (Zeiss, Jena, Germany). Images were acquired with a Zeiss Axiocam IC camera and ZEN 2 (Blue Edition) software version 2.0.

3.2.5 Cytokine Measurements

The levels of cytokines released into the medium on Tx13 and Tx27 were assayed on the MESO QuickPlex™ SQ 120 Instrument using the Meso Scale Discovery (MSD) V-PLEX Human Proinflammatory Panel 1 kit (MSD, Rockville, MD) according to the manufacturer's instructions. Samples and standards were prepared with minor modifications

as described previously (Norona et al., 2016).

3.2.6 RNA Isolation and Quality Assessment

At the conclusion of the study, tissue lysates were prepared for each treatment group by homogenization in TRIzol® Reagent (ThermoFisher Scientific, Waltham, MA) using PreCellys RNase-free microfuge tubes and the Precellys 24 homogenizing instrument (Bertin Corp., Rockville, MD). Total RNA was isolated using the Direct-Zol™ RNA MiniPrep kit per the manufacturer's instructions (Zymo Research, Irvine, CA). RNA purity and yield was assessed using the NanoDrop 1000, version 3.5.2 (ThermoFisher Scientific, Wilmington, DE). RNA integrity for microarray was assessed using the Agilent 2200 Tape Station System (Agilent Technologies, Santa Clara, CA). Isolated samples were of optimal purity (*i.e.*, A260/280 >1.8 and A230/280 > 1.8) and suitable RNA Integrity Number (RIN > 7.5) for subsequent microarray analysis. Samples that did not meet the minimum concentration requirements (*i.e.*, RNA concentration <33 ng/mL) for the Clariom™ S 96-peg microarray with WT PLUS Reagents (ThermoFisher) were concentrated using a Savant SpeedVac Concentrator (ThermoFisher) at a medium heat setting until the volume of RNA eluant was reduced by half.

3.2.7 Statistical Analysis

Unless otherwise noted, results are expressed as the mean of 5-10 replicates ± standard error (SE). Replicates refer to the same lot of bioprinted livers from a particular batch or print. Statistical significance of treatment-induced differences relative to vehicle-treated control was determined using a two-way or one-way analysis of variance (ANOVA) where appropriate, with post hoc Dunnett's multiple comparisons test using GraphPad Prism version 6.0 (Graph Pad Software, Inc., La Jolla, CA). A *p-value* < 0.05 was considered

statistically significant. Outliers were identified using Grubbs' test to identify samples that fell one SD outside of the mean of the data ($\alpha = 0.05$) using GraphPad Prism version 6.0 (Graph Pad Software, Inc.).

3.3 Results

3.3.1 Sustained General Injury Over an Expanded Exposure Supports Mild to Moderate Perturbations in Tissue Viability and Function

LDH activity in spent tissue culture medium was assessed on the day of collection and used as a marker of general tissue injury during the course of treatment (Figure 3.1). In order to examine treatment effects over an extended period of time, the fold change LDH in response to each agent of interest was first compared across the first 14 days of treatment for the 14- and 28-day studies to confirm print-to-print consistency in the observed response (Appendix 3, Figure A3.1A). During the initial treatment period, LDH release gradually declined and approached steady-state levels by treatment day 7 (Tx7) with minor treatment-dependent differences in the rate of decline (Appendix 3, Figure A3.2A). Assessment of the fold change in LDH release relative to time-matched vehicle-treated control remained relatively constant regardless of treatment during this initial exposure period (Appendix 3, Figure A3.2A). Evaluation of LDH fold change past Tx7 shows that the exposure timeframe spans peak LDH release for the highest concentration of each agent tested (Figure 3.1). Exposure to 10 ng/mL TGF-β1 resulted in a 1.5 to 2.0-fold increase in LDH (****$p<0.0001$) that was sustained throughout the exposure period (Figure 3.1A). A 1.5 to 2.0-fold increase in LDH spanned Tx9 to Tx19 for 0.209 μM MTX treated tissues with a gradual decrease in LDH release by Tx27 (Figure 3.1B). A significant increase in LDH release was observed for

0.603 mM APAP from Tx13 to Tx23 with a ~1.5-fold change (Figure 3.1C).

Urea and albumin were also assessed as markers of HC function following repeated exposure to fibrogenic and hepatotoxic agents after 14 and 28 days (Figure 3.2). Treatment with TGF-β1 did not significantly impact urea production at all concentrations tested (Figure 3.2A). However, a significant decrease in albumin output was observed at Tx14 and Tx28 for 10 ng/mL TGF-β1 (Figure 3.2D). While urea production was not significantly altered with MTX treatment, increased albumin was observed at the latest treatment timepoint relative to time-matched, vehicle-treated control (Figure 3.2E). Following treatment with APAP, a dose-dependent decrease in urea production (Figure 3.2C) was measured at Tx14 and Tx28 (****$p<0.0001$) while albumin output was not significantly affected (Figure 3.2F). Albumin output at Tx14 for the standard tissue model was further complemented by immunohistochemical assessment of albumin (Appendix 3, Figure A3.6) following TGF-β1 treatment where albumin positive areas were generally decreased. Regardless of trends in albumin measured in the culture medium, tissues treated with MTX and APAP treatment exhibited an overall decrease in the intensity of albumin staining over time (Appendix 3, Figure 3.6).

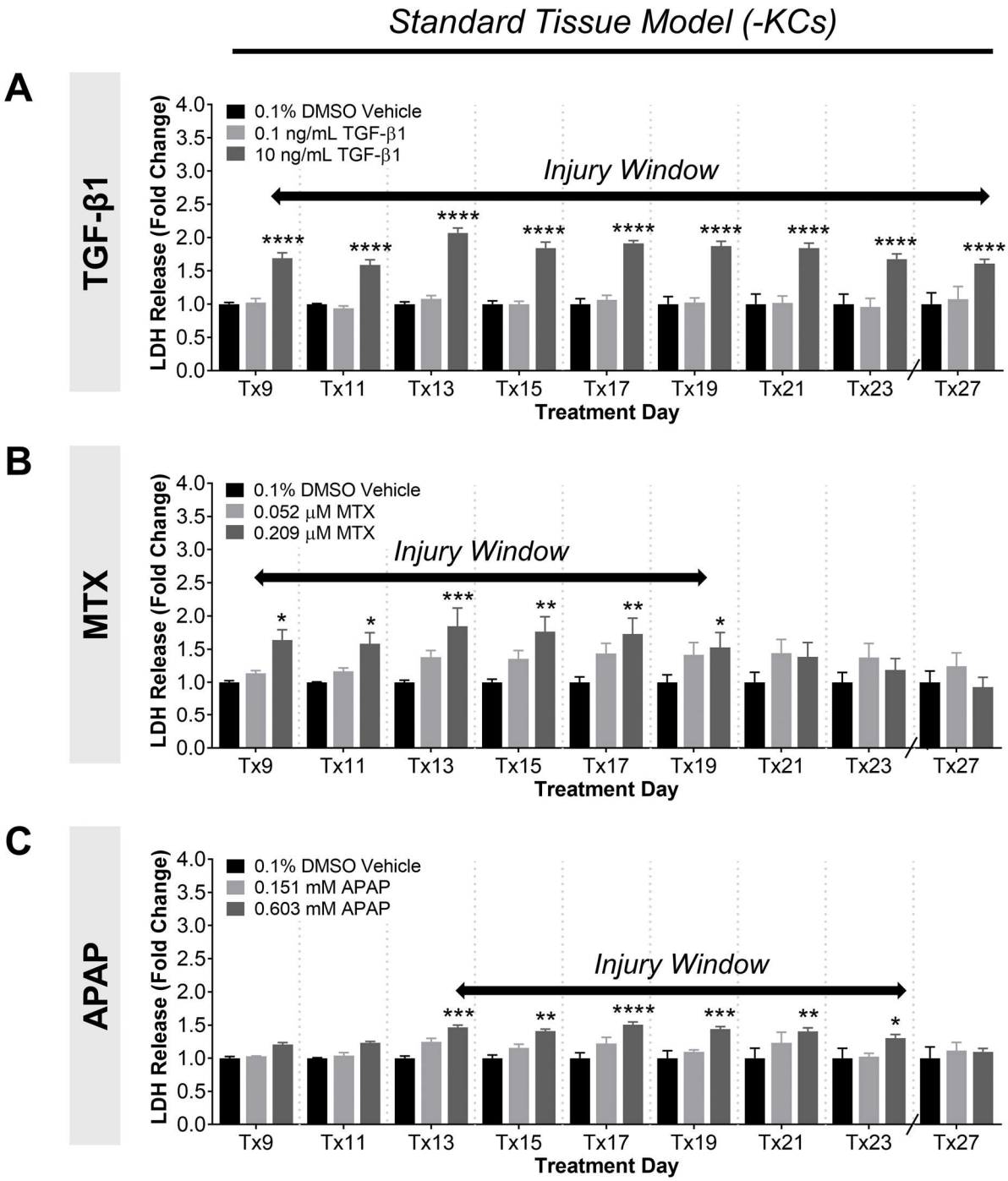

Figure 3.1 *Sustained LDH release following extended compound exposure*. LDH was measured as a nonspecific marker of tissue injury. Significance was determined using a two-way ANOVA with post hoc Dunnett's multiple comparisons test (*p<0.05, **p<0.01, ***p<0.001, ****p<0.0001), n = 5 tissues per treatment group.

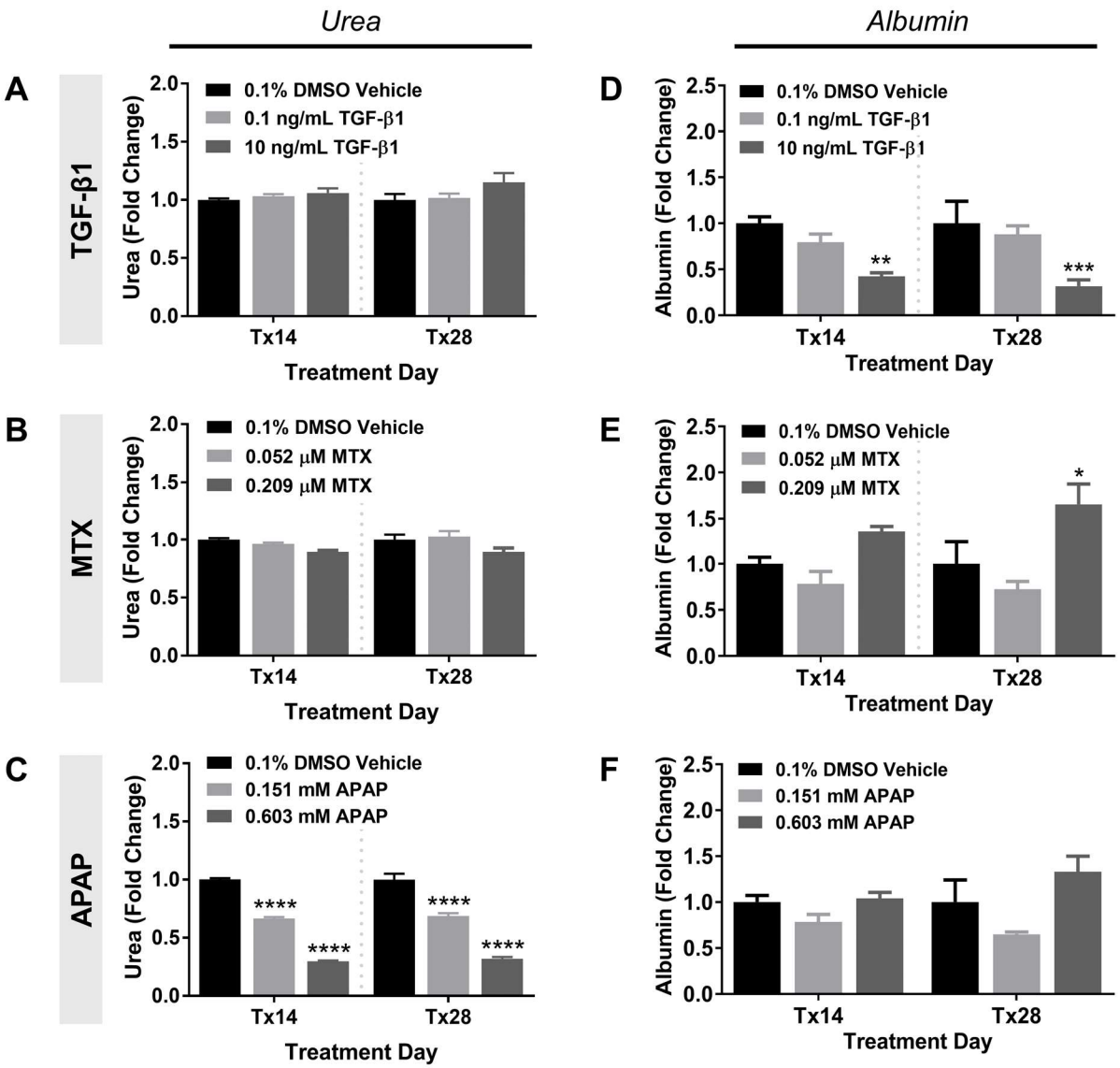

Figure 3.2 *Other markers of tissue functionality suggest mild to moderate injury with compound exposure.* Measurement of urea and albumin production in the standard tissue model (-KCs) is shown. Significance was determined using a two-way ANOVA with post hoc Dunnett's multiple comparisons test (**p*<0.05, ***p*<0.01, ****p*<0.001, *****p*<0.0001), n = 5 tissues per treatment group.

3.3.2 The Incorporation of Kupffer Cells Shortens the General Injury Window Observed in the Standard Model

In order to evaluate the impact of KCs on extended compound exposure, the response across independent tissue prints profiles to each agent of interest was compared across independent tissue manufacturing runs. During this timeframe, the lack of significant differences in the temporal response profiles during this timeframe provided further confidence in the reproducibility of the model (Appendix 3, Figure A3.1B). Similar to the standard tissue model, a gradual decline in LDH release was observed during the first 7 days of treatment regardless of treatment (Appendix 3, Figure A3.2B). The incorporation of KCs into the model as compared to the standard tissue model, did not significantly alter the overall trends in LDH release during the first 14 days of treatment for each agent (Appendix 3, Figure A3.3). Repeated treatment with fibrogenic and hepatotoxic agents resulted in a gradual increase in LDH at the mid treatment timepoint, however, the sustained LDH release observed in the standard model was shortened for the highest concentration of each agent tested (Figure 3.3).

Urea and albumin output at Tx14 and Tx28 exhibited similar temporal trends relative to the standard tissue model (Figure 3.3). Treatment with TGF-β1 did not significantly impact urea production at all concentrations tested (Figure 3.4A). However, a general decrease in albumin output was observed at Tx14 and Tx28 for 10 ng/mL TGF-β1, albeit not significant (Figure 3.4D). By Tx28 the trend in albumin output for 0.1 ng/mL TGF-β1 was increased relative to vehicle-treated control (Figure 3.4D). Similar to the standard tissue model, urea production at Tx28 was decreased with MTX treatment, while a ~4.0-fold increase in albumin production was observed at the latest treatment timepoint relative to

time-matched, vehicle-treated control (Figure 3.4E). APAP treatment in the modified tissue model also resulted in a dose-dependent decrease (****$p<0.0001$) in urea production at Tx14 and Tx28 (Figure 3.4C) and a ~2.0-fold increase in albumin output at Tx14 and Tx28 (Figure 3.4F). Complementary immunohistochemical assessment of albumin was also performed to visualize albumin content within treated tissues (Appendix 3, Figure 3.7). An overall decrease in the intensity of albumin positive areas was observed at Tx14 and Tx28 for tissues treated with 10 ng/mL TGF-β1 while treatment with 0.209 μM MTX and 0.603 mM APAP exhibited temporal trends in albumin staining intensity. Both MTX and APAP treatment resulted in a general decrease in albumin positive areas at Tx14 and comparable intensity to vehicle-treated control at Tx28.

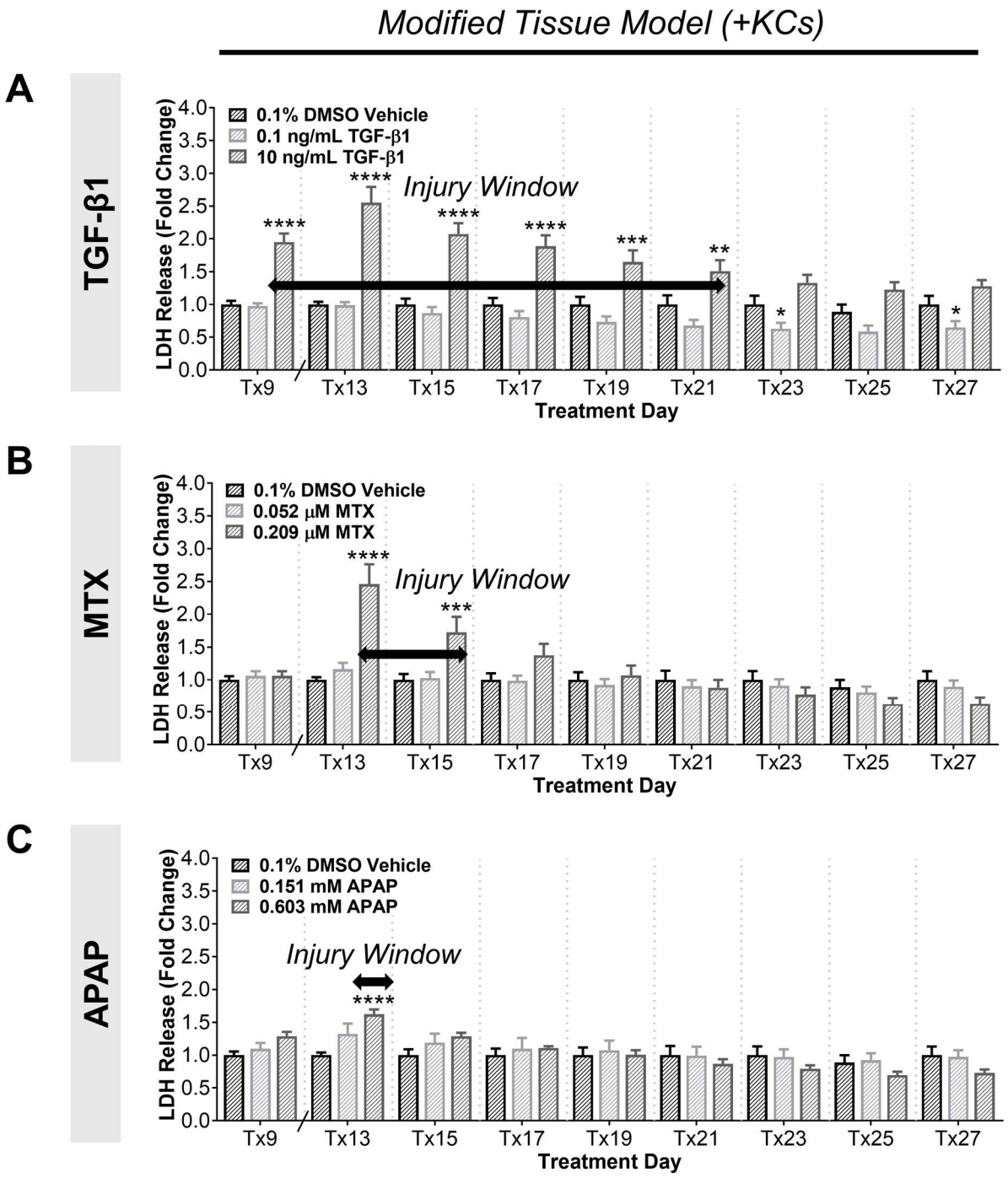

Figure 3.3 *The incorporation of KCs into the model shortens the sustained injury response observed in the standard model*. Significance was determined using a two-way ANOVA with post hoc Dunnett's multiple comparisons test (*$p<0.05$, **$p<0.01$, ***$p<0.001$, ****$p<0.0001$), n = 5-7 tissues per treatment group.

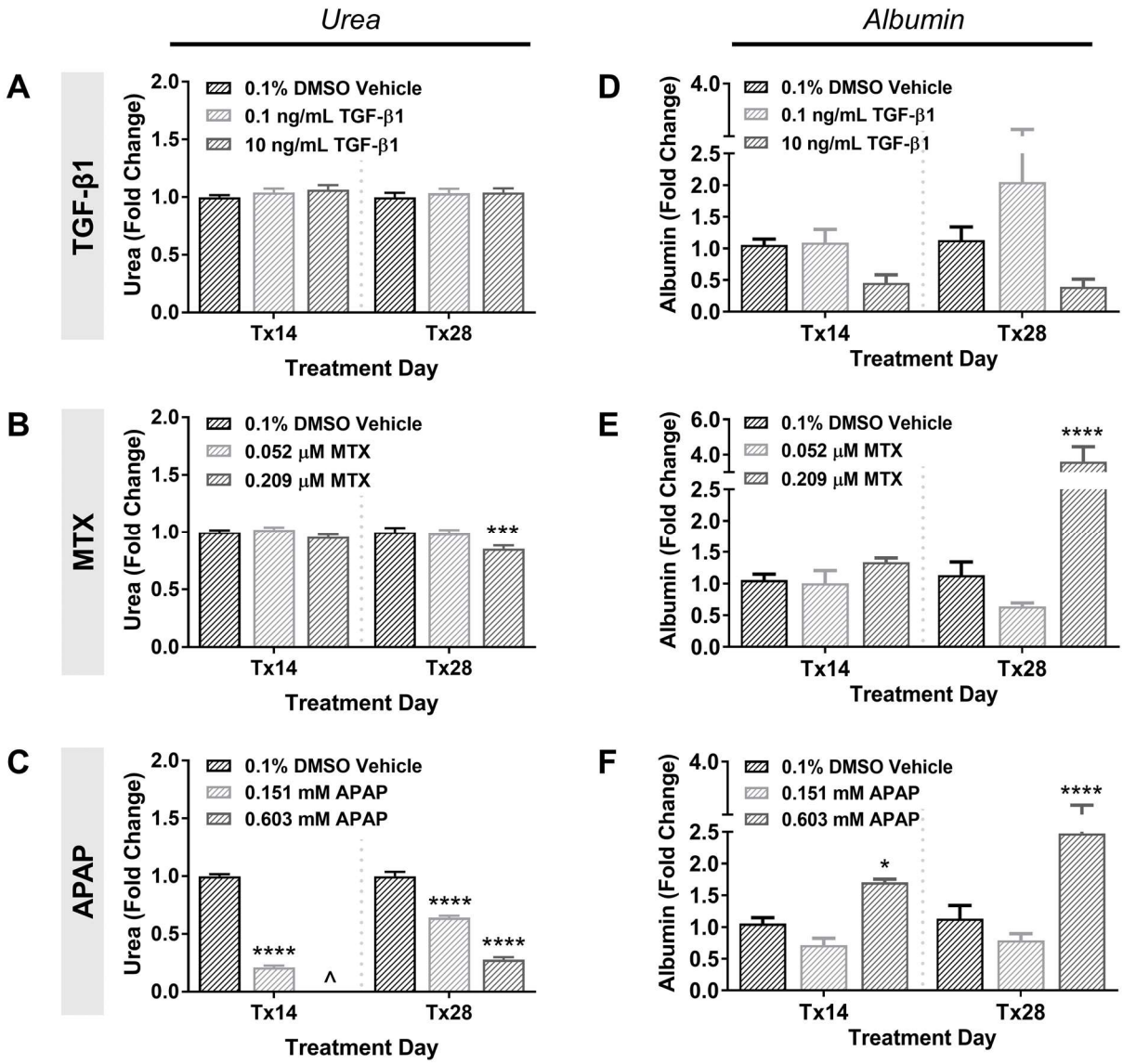

Figure 3.4 *Similar trends in urea and albumin observed for KC-containing tissues.* Significance was determined using a two-way ANOVA with post hoc Dunnett's multiple comparisons test (**p*<0.05, ***p*<0.01, ****p*<0.001, *****p*<0.0001), n = 5-7 tissues per treatment group.

3.3.3 Kupffer Cells May Attenuate Early Fibrogenic Processes in Bioprinted Liver Tissues

Following 14 days of treatment with fibrogenic and hepatotoxic agents, increased collagen deposition (blue) relative to time-matched vehicle-treated control was observed in the standard tissue model without KCs (Figure 3.5). Treatments in which there was an observed shortening of the injury window are depicted. An increase in collagen deposition with TGF-β1 treatment was accompanied by consolidation and encapsulation of the tissue with blue fibrous bands (yellow arrows). Treatment with MTX and APAP resulted in a mild increase in collagen positive areas (blue) within the center of the tissue. Patterns of collagen deposition were mostly diffuse throughout the tissue (white arrows) originating from nodules corresponding to the non-parenchymal compartment. Areas of blue staining (yellow arrows) were also observed indicating organized bands of collagen fibers bridging areas of diffuse collagen staining.

The inclusion of KCs in the tissue model resulted in a general decrease in collagen positive areas at Tx14 with an overall conservation of tissue mass (Figure 3.5). This phenomenon was also consistent with the lower concentrations of agents tested (Appendix 3, Figure A3.4). Similar to the standard model, treatment with 10 ng/mL TGF-β1 resulted in an increase in collagen deposition and encapsulation of the tissue. However, the pattern of collagen deposition within the tissue was more diffuse and mainly restricted to well-circumscribed nodules representing the NPC compartment (white arrows). Treatment with MTX and APAP exhibited a tissue cross-sectional structure that more closely resembled the vehicle-treated control tissue with a decrease in diffuse collagen-positive areas and absence of blue bands of organized collagen fibers observed particularly at the higher concentration of compounds tested (Fig 3.5).

Extended exposure of tissues containing KCs to fibrogenic and hepatotoxic agents resulted in a general decrease in tissue mass compared to the standard tissue model regardless of treatment (Figure 3.6). Similar to the standard model, an increase in collagen deposition within the center of the tissues was observed at Tx28 (Figure 3.6). For the highest concentration of TGF-β1 tested, a decrease in tissue mass was mainly observed for both tissue configurations with increased areas of diffuse collagen positive areas within the center of the tissue (Figure 3.6). Following extended MTX treatment, an increase in diffuse areas of collagen deposition and thicker collagen fibers were evident within the tissue (Figure 3.6). Treatment with APAP for an extended period of time resulted in the appearance of mainly diffuse collagen positive areas at the periphery of the tissue. In addition, the extent of collagen deposition in the modified tissue model with extended APAP treatment was not starkly different relative to vehicle-treated control. Treatment with the lowest concentration of each agent were mostly concordant with trends observed at the latest timepoint (Appendix 3, Figure A3.4).

A panel of proinflammatory cytokines was measured in spent medium samples around the mid (Tx13) and late (Tx27) treatment timepoints to assess the impact of KCs on the inflammatory profile following treatment with select agents. Regardless of tissue composition, a significant effect of time on baseline cytokine abundance is observed (Figure 3.7A and 3.7B). Relative to the standard tissue model, a significant effect of KCs on cytokine abundance at Tx13 (****$p<0.0001$) was evident with a higher abundance measured at baseline for vehicle-treated KC-containing tissues (Figure 3.7C). At the later treatment timepoint tested (Tx27), the presence of KCs did not significantly impact the abundance of cytokines (Figure 3.7D). Assessment of cytokines at mid and late treatment timepoints in the

presence and absence of KCs following treatment suggest that main treatment effects relative to time-matched vehicle-treated control were significant at the mid treatment timepoint (Tx13) for both the standard and modified tissue model (data not shown). Treatments in which a shortening of the general injury window was observed in the modified tissue model were directly compared to assess the impact of KCs at the mid treatment timepoint (Figure 3.8). Incorporation of KCs resulted in a global decrease in proinflammatory cytokine production compared to the standard model at Tx13. Cytokines that were significantly different between tissue compositions following the post hoc test were IFN-γ, IL-10, IL-13, IL-4, TNF-α, and IL-6. While all treatments exhibited similar trends in cytokine production following treatment, the significant difference in levels of IFN-γ measured in the culture medium was unique to APAP-treated tissues with a fold increase measured in the standard model and a fold decrease in the modified tissue model (Figure 3.8C). Because tissues were cultured and exposed to agents for an extended period of time, antibodies directed against CD163, a tissue macrophage marker, were used to confirm the presence of KCs within tissues at both timepoints (Appendix 3, Figure A3.7).

HSC activation status was also assessed in successive sections of tissue using desmin and α-SMA as markers of HSC quiescence and activation, respectively. In the standard tissue model, a majority of the HSCs in the vehicle-treated control exhibited punctate patterning of desmin (white arrows; Figure3.9 A) with few α-SMA positive cells within the center of the construct (yellow arrows). On the apical surface of successive sections, desmin and α-SMA were localized to similar regions of tissue with a majority of cells expressing α-SMA and PCNA within the capsular region (yellow arrow). Treatment with fibrogenic and hepatotoxic agents resulted in an overall decrease in desmin staining within the center of the tissue.

However, dual positive HSCs were still present in the capsular region of the tissue for all treatments. This pattern of staining was consistent across tissue compositions as well (Figure 3.9B). Treatment with fibrogenic and hepatotoxic agents resulted in an overall decrease in desmin staining; however, the punctate patterning observed was almost completely lost (white arrows) when KCs were incorporated into the model.

Following 28 days of exposure, vehicle-treated tissues retained the presence of desmin positive HSCs regardless of tissue composition (Appendix 3, Figure 3.8A and 3.8B). While some desmin positive HSCs (white arrows) were present following treatment of the standard and modified tissue models, the decrease in desmin positive cells throughout the tissue was similar across treatments. Desmin positive cells within treated tissues were mainly distributed in clusters within the tissue but also localized near the apical region. Cells positive for α-SMA were mainly localized to the apical tissue capsule with some PCNA dual positive cells co-localized to this region (cyan arrows). This pattern of staining was relatively similar across treatment groups and tissue compositions (Appendix 3, Figure 3.8A and 3.8B). While there was an overall absence of α-SMA positive cells within the tissues, treatment with TGF-β1 resulted in a slight increase in α-SMA positive HSCs within the center of the tissue constructs (yellow arrows).

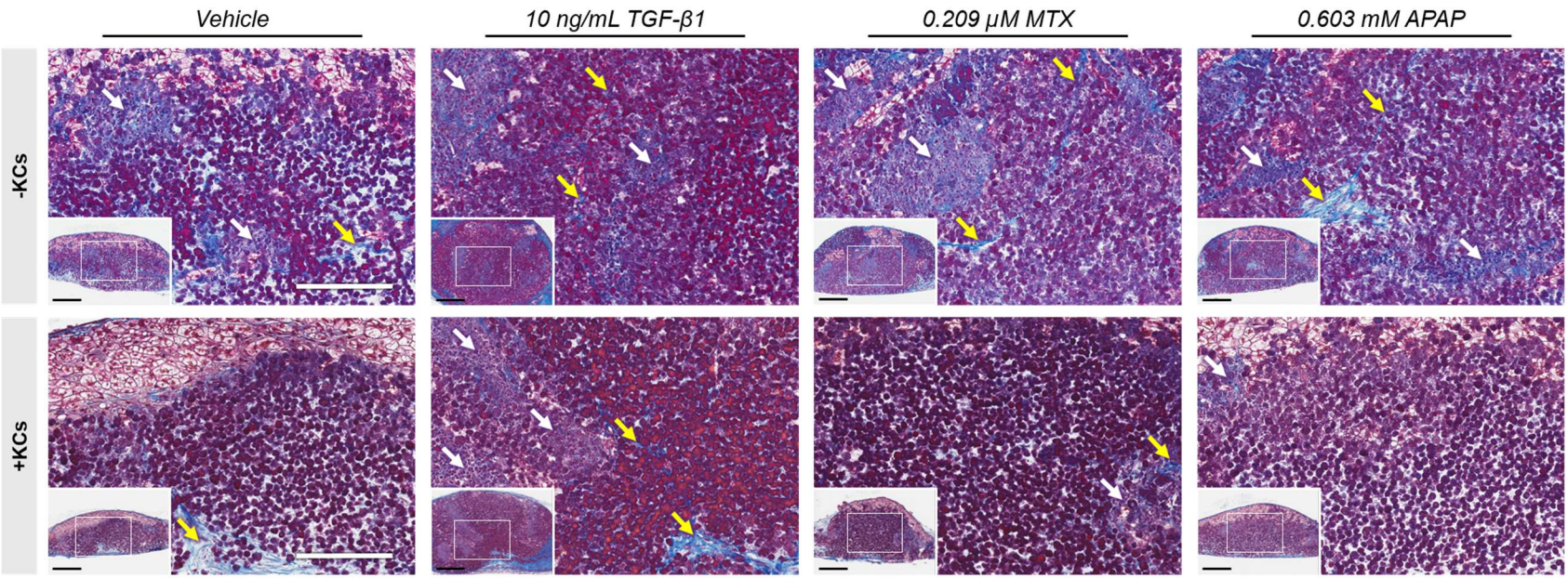

Figure 3.5 *The incorporation of Kupffer cells may limit the extent of collagen deposition in bioprinted liver tissues during early injury*. Representative sections of bioprinted liver treated with select fibrogenic and hepatotoxic agents at treatment day 14. Collagen deposition was visualized (blue) in bioprinted tissue sections stained with Gomori's trichrome. Yellow arrows denote fibrillar areas of collagen deposition and white arrows denote diffuse areas of collagen deposition primarily found within the non-parenchymal compartment. Scale bar = 150 μm, inset scale bar = 300 μm.

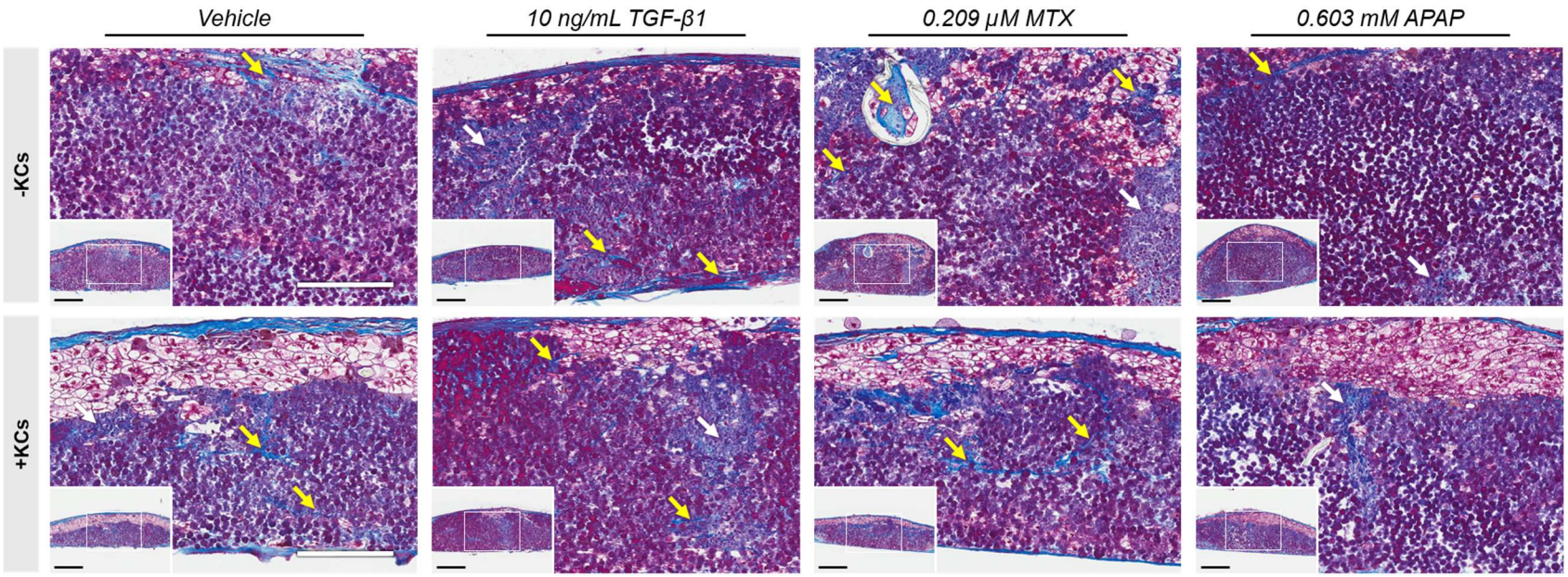

Figure 3.6 *Trichrome-stained tissues sections at treatment day 28.* Representative sections of bioprinted liver treated with select fibrogenic and hepatotoxic agents at treatment day 28. Collagen deposition was visualized (blue) in bioprinted tissue sections stained with Gomori's trichrome. Yellow arrows denote fibrillar areas of collagen deposition and white arrows denote diffuse areas of collagen deposition primarily found within the non-parenchymal compartment. Scale bar = 300 μm, inset scale bar = 75 μm.

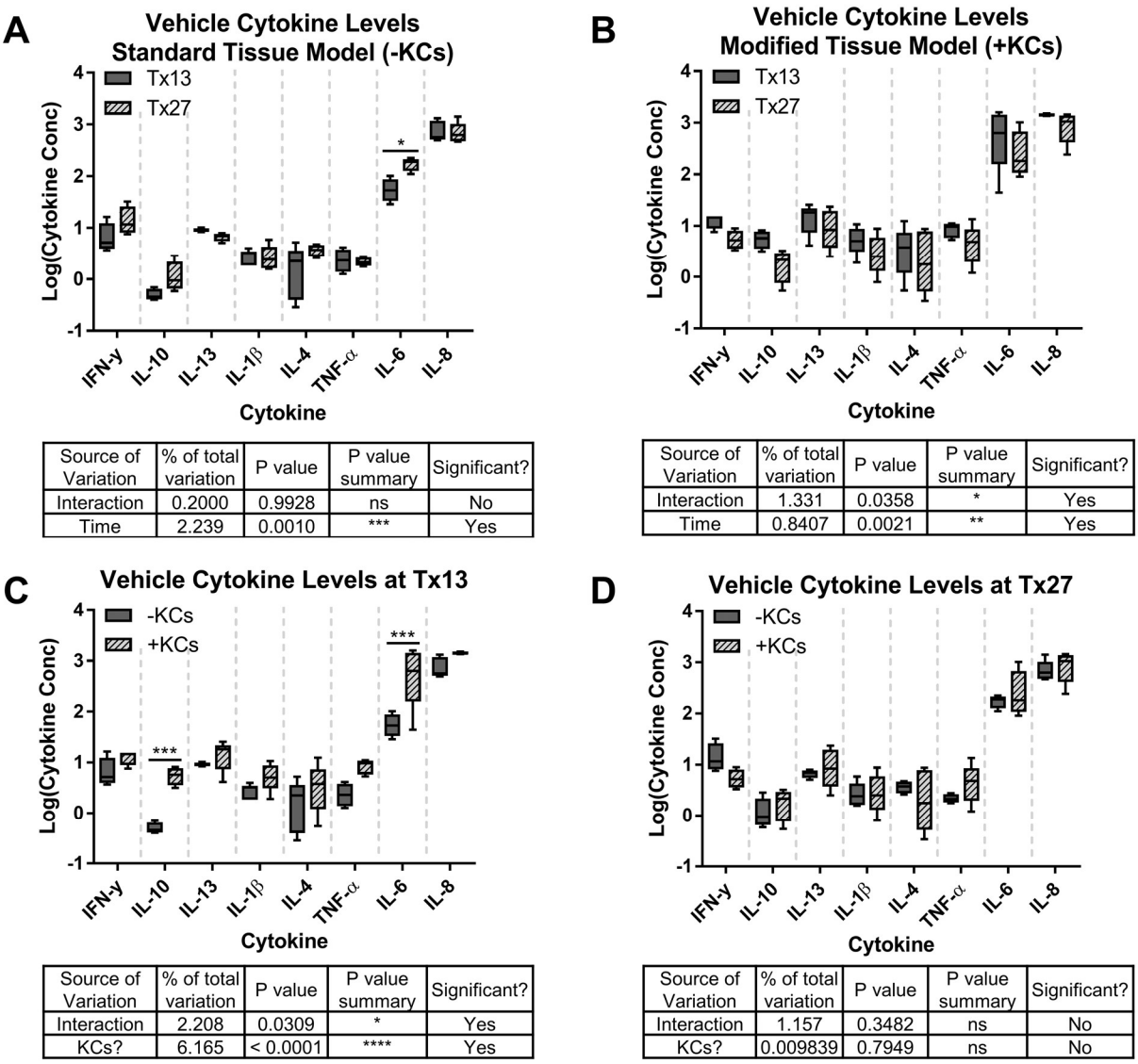

Source of Variation	% of total variation	P value	P value summary	Significant?
Interaction	0.2000	0.9928	ns	No
Time	2.239	0.0010	***	Yes

Source of Variation	% of total variation	P value	P value summary	Significant?
Interaction	1.331	0.0358	*	Yes
Time	0.8407	0.0021	**	Yes

Source of Variation	% of total variation	P value	P value summary	Significant?
Interaction	2.208	0.0309	*	Yes
KCs?	6.165	< 0.0001	****	Yes

Source of Variation	% of total variation	P value	P value summary	Significant?
Interaction	1.157	0.3482	ns	No
KCs?	0.009839	0.7949	ns	No

Figure 3.7 *Baseline cytokine levels across time and tissue compositions.* (A) Comparison of cytokine abundance over time for the standard tissue model without KCs, (B) comparison of cytokine abundance over time in the modified tissue model with KCs, (C) direct comparison of cytokine abundance at treatment day 13 across model compositions, and (D) at treatment day 27. Significance was determined using a two-way ANOVA with post hoc Dunnett's multiple comparisons test (*p<0.05, **p<0.01, ***p<0.001, ****p<0.0001), n = 5 tissues per treatment group.

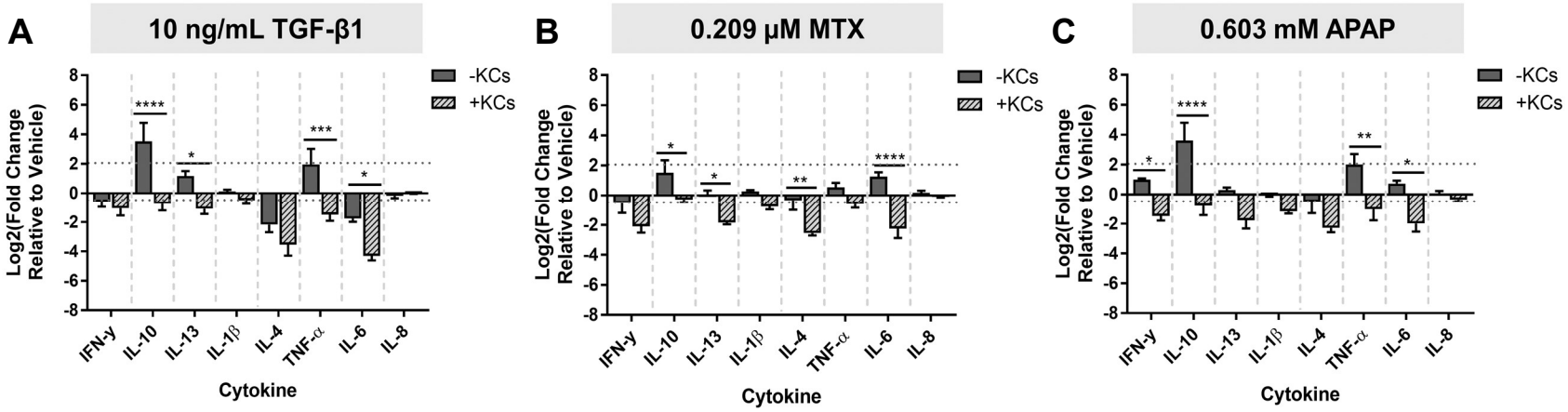

Figure 3.8 *Global dampening of cytokine production observed in the modified tissue model at treatment day 13.* (A) 10 ng/mL TGF-β1, (B) 0.209 μM MTX, (C) 0.603 mM APAP. Select treatment groups represent the concentration of each agent in which the observed injury window was altered with the incorporation of KCs into the model. Significance was determined using a two-way ANOVA with post hoc Dunnett's multiple comparisons test (*$p<0.05$, **$p<0.01$, ***$p<0.001$, ****$p<0.0001$), n = 5 tissues per treatment group.

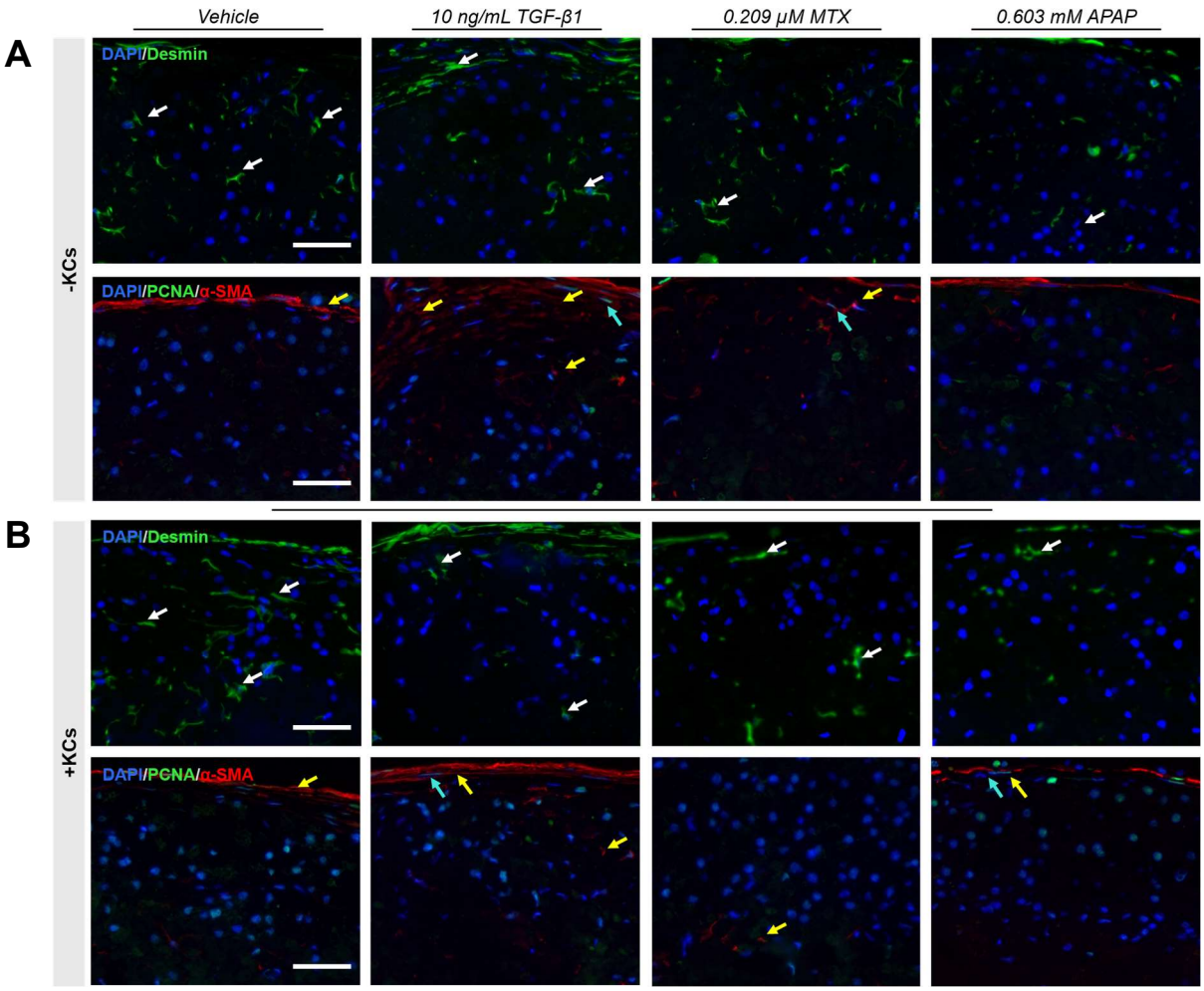

Figure 3.9 *Hepatic stellate cell activation status within treated tissues at treatment day 14.* (A) Standard tissue model. (B) Modified tissue model. White arrows denote desmin positive cells, teal arrows denote proliferating cell nuclear antigen (PCNA) positive cells, and yellow arrows denote α-smooth muscle actin (α-SMA) positive cells. Scale bar = 100 μm, inset scale bar = 50 μm.

3.4 Discussion

The inability to target specific macrophage subpopulations and plasticity of these subsets, particularly during injury, has made it difficult to discern the precise role of KCs in mediating compound-induced liver injury leading to fibrosis (Tacke and Zimmermann, 2014). In order to obtain a resolution of the response at the organ level during early injury, an *in vitro* model that is able to recapitulate basic fibrogenic features and incorporates cell types relevant to the response is warranted (Horvat et al., 2017, Landesmann, 2016). The flexibility of incorporating specific cell types in a tissue relevant context has been a significant innovation in designing these types of platforms with which to understand basic fibrogenic mechanisms but also gain insight into the effects of physiologically relevant exposure scenarios on this outcome (Norona et al., 2016). In this study, we first assessed the impact of extended compound exposure on the injury and fibrogenic response to gain insight into these profiles over time. We then modified the base model by incorporating KCs into the tissues in order to evaluate how resident macrophages modulate tissue response profiles to compound exposure within the same timeframe.

In the standard tissue model, the increase in LDH release as a general marker of tissue viability over time was sustained for at least 11 days for the highest concentration of each compound tested. These elevations in LDH release spanned a 1.5 to 2.5-fold increase relative to time-matched vehicle-treated control indicating mild injury over a majority of the exposure period. Because fibrosis manifests over the course of sustained mild injury and the types of responses observed were in accordance with previous studies, we were confident that the tissues were not overtly destroyed with treatment over the timeframe tested (Appendix 2). Histological assessment following 14 and 28 days of treatment further

confirmed that the tissues remained intact even with extended compound exposure out to 28 days.

Urea and albumin output further support evidence of mild injury over time. While urea production remained largely unchanged with MTX and TGF-β1 treatment, the decrease in urea production observed with APAP treatment is concordant with mitochondrial injury which could potentially perturb the urea cycle given the subcellular localization of enzymes critical to this pathway (Jackson et al., 1986, McGill et al., 2012). Although urea output was significantly perturbed with APAP treatment, the evaluation of other markers of tissue viability and function (*i.e.*, LDH release and albumin output) indicate mild injury. The significant increase in albumin output observed for MTX and general increase following APAP treatment are consistent with previous results and likely reflect adaptive processes (*e.g.*, activation of NPCs and secretion of factors to support the synthesis of albumin) or changes in the release of intratissue albumin (Norona et al., 2016). Decreased albumin output for 10 ng/mL TGF-β1-treated tissues was further complemented by immunohistochemical assessment whereby an overall decrease in albumin staining intensity was observed over time. Interestingly, treatment with MTX and APAP also resulted in a decrease in staining intensity. However, this was not reflective of the albumin detected in the culture medium. These results, in addition to histological evidence of thick fibrous bands encapsulating TGF-β1-treated tissues, suggest alterations in the release of intra-tissue albumin may influence the observed outcomes.

The evaluation of different markers of HC function in the context of mild injury can provide further insight into the stress mechanisms underlying the injury response. In this case, measurement of urea as the primary end product of protein catabolism could indicate a

disruption of metabolic processes within HCs while measurement of albumin may implicate a perturbation of protein synthetic pathways following compound treatment (Mezey, 1982). Nonetheless, the measurement of these markers can be used to benchmark significant perturbations in biochemical indicators of tissue function to further gauge the extent of injury following compound exposure such as in the case of APAP treatment.

Given the unique features of the model and flexibility to incorporate cells in a precise manner, we can begin to evaluate the role of other cells relevant to the response and gain a better understanding of how these cells modulate injury profiles observed in the standard model with repeated compound exposure and the resulting fibrogenic outcome (Nguyen et al., 2016, Norona et al., 2016). Here we describe an evaluation of the role of resident KCs in a model of progressive tissue injury and fibrogenic response. Modification of the standard tissue model via the incorporation of KCs did not significantly alter tissue viability and response to repeated compound exposure during the initial 14 days of treatment. While patterns in urea and albumin were similar across tissue models over time, the magnitude of albumin output at Tx28 for MTX and APAP treatment was on the order of 3.0- to 4.0-fold as compared to the 1.5- to 2.0-fold increase observed for the standard tissue model. In previous studies (Chapter 2) and historical studies conducted at Organovo (data not shown), the significant increase in albumin output tends to precede more substantial tissue damage over an extended exposure. However, the mechanisms regulating this process within these complex tissue models warrant further investigation. Nonetheless, extended treatment with fibrogenic and hepatotoxic agents resulted in a shortening of the general injury profile. These response profiles were accompanied by an overall decrease in collagen deposition at the mid treatment timepoint and further indicate that KCs may attenuate general tissue injury

response and fibrogenic outcome at the onset of early compound-induced tissue injury.

While endpoints such as LDH have been traditionally used as indicators of cytotoxic responses *in vitro*, in the context of more advanced *in vitro* models, it only provides a general understanding of the injury response at a tissue level (Kia et al., 2015). Given the complexity of the fibrogenic response and strong association of HC injury with fibrogenic outcome, there is a need for more specific markers to tease apart the temporal patterns of HC injury and impact on the progression of fibrogenic processes (Rausch, 2006). To this end, we have proposed to measure miR-122, a liver-enriched miRNA, in the culture medium to track the progression of HC injury over the treatment time course. Previous studies have demonstrated the utility of miR-122 as a more sensitive and specific biomarker of HC injury (Kia et al., 2015). Thus, an understanding of the temporal HC response to injury would not only provide additional insight into the role of KCs in modulating the injury and fibrogenic response over the treatment time course but also provide insight into the potential mechanism underlying the measured changes in tissue function.

Following 14 and 28 days of treatment, tissues were stained with Gomori's trichrome to visualize evidence of collagen deposition and assess the impact of KCs on resultant fibrogenic processes. At the mid treatment timepoint, an overall increase in collagen-positive areas was observed in tissues treated with TGF-β1 and MTX. In addition, the global dampening of compound-induced cytokine secretion at Tx13 is consistent with histological outcomes and supports the observed shortening of the general injury window. Cytokines known to drive wound healing were significantly decreased following treatment of the modified tissue model. However, trends in certain cytokines such as IL-10 exhibited disparate trends compared to what was expected (Kong et al., 2012). As an important

immunomodulatory cytokine, IL-10 is thought to play more of an anti-inflammatory role during injury (Sziksz et al., 2015). Because cytokines were measured in the medium at the mid treatment timepoint at the apex of the injury window, it is plausible that transient changes in cytokine production prior to the detection of significant differences in LDH release could have exhibited a more immunomodulatory profile. To this end, archived samples at an earlier timepoint (*e.g.*, Tx7) and could be measured to provide additional support for the trends in cytokine profiles observed at the start of the injury window and provide additional contextual support for the limited collagen deposition detected at the mid treatment timepoint in the modified tissue model.

In addition to prototype fibrogenic agents TGF-β1 and MTX, APAP was selected as a proposed negative control compound as it is known to primarily elicit hepatotoxicity -- an event strongly associated with fibrogenic outcome as proposed in the Adverse Outcome Pathway framework for liver fibrosis (Landesmann, 2016). In the present study, we also sought to gain insight into the fibrogenic potential of extended low concentration APAP exposure to determine whether the fibrogenic potential of a compound is intrinsic or dependent on the context of exposure (*i.e.* extended, low concentration exposure and tissue composition). It is plausible that prolonged low concentration exposure to APAP could result in fibrosis given HCs are a primary target. However, the response is likely to be context-dependent because fibrotic injury due to prolonged APAP exposure has not been frequently described or adequately investigated (Landesmann, 2016).

Interestingly, APAP treatment in the standard tissue model resulted in an increase in collagen deposition at the mid treatment timepoint with primarily diffuse collagen positive areas detected at the later treatment timepoint. While APAP treatment in the modified tissue

model resulted in an attenuation of the fibrogenic response at Tx14, extended exposure resulted in a decrease in tissue cellularity and collagen positive areas at Tx28. Nonetheless, this initial look into the fibrogenic potential of prolonged APAP exposure suggests the context of exposure (*i.e.*, duration of exposure, cell types present) may be particularly important to consider when evaluating the fibrogenic potential of compounds.

In a recent publication, exposure of human hepatic organoids comprising HepaRGs and HSCs demonstrated HSC activation and secretion of pro-collagen as a result of APAP-induced HC injury (Leite et al., 2016). While these findings were confirmed in a rodent model of repeated APAP exposure, the extent of collagen deposition within the livers of mice treated for an extended period of time did not achieve the severity of the response as compared to a prototypical inducer (*i.e.*, CCl_4) and tended to decrease over time (Leite et al., 2016). These findings highlight a need to better understand the mode of action promoting fibrotic liver injury and further suggest there may be a unique series of events downstream of compound-induced HC injury that may be indicative of a compound's fibrogenic potential.

In order to confirm the presence of KCs in the tissues at later treatment timepoints, tissues were immunolabeled with antibodies directed against CD163, a marker of a subset of mature tissue-resident macrophages (Fabriek et al., 2005). CD163-positive macrophages have been illustrated to play an important restorative role during tissue injury and may play an important modulatory role in inflammatory processes as M2 macrophages (Fabriek et al., 2005). While CD68 and CD163 are common markers to detect resident macrophages within tissue sections, phenotypic switching could also occur between the mid and later treatment timepoint leading to the potential bimodal role of KCs at early versus later phases of compound exposure. The ability to discern macrophage polarization (*i.e.*, M1 versus M2

subsets) based on these markers alone remain a challenge (Barros et al., 2013). Given the importance of the microenvironment in regulating these processes, bioprinted liver tissues could provide an important insight into the phenotypic heterogeneity of KCs isolated from perfused liver and their role in modulating injury and fibrogenesis.

Regardless of treatment, KCs were mainly localized to the apical region of the tissue in close association with ballooning, degenerating HCs and the fibrous capsule. Thus, the results confirm the presence of KCs at later timepoints and suggest that these cells migrate to damaged regions of the tissue. Interestingly, at the later timepoint, a decrease in cellularity is observed in KC-containing tissues regardless of treatment. The increase in collagen content at the later treatment timepoint could be attributed to the overall collapse of the parenchymal compartment or a perturbation in KC function following extended compound exposure. While the proportion of KCs used for this system were based on physiologically relevant estimates of the KC population in uninjured liver (Jaeschke, 2008), future studies will assess the titration of these cells into tissues to understand how KCs modulate the baseline tissue cellularity over time.

Given that KCs are incorporated into the tissues via bioprinting, this model represents an isolated system in which the recruitment of extrahepatic monocytes is not considered. The discordant trends in LDH release (*i.e.*, shortening of the injury window) and the observed evidence of collagen deposition in the tissues at the latest treatment timepoint suggest that the possible depletion of KCs over time or perturbations in functionality could lead to the observed decrease in cellularity and/or increase in collagen deposition within bioprinted liver tissues following extended compound exposure. In order to gain additional insight into the impact of KCs on the progression of fibrogenic processes at a molecular level, global gene

expression profiling is currently being conducted on samples collected at Tx14 and Tx28. These data will be subsequently used to assess pathway enrichment of processes corresponding to HC/tissue injury, cytokine production, collagen synthesis and deposition to elucidate the impact of KCs on the response.

In summary, our results demonstrate the important modulatory role of KCs in the progression of injury and fibrogenic response, particularly at early treatment timepoints and further demonstrate the utility of the model to begin to assess more complex processes underlying compound-induced fibrotic injury.

3.5 Supplemental Data Description

Print-to-print consistency in the temporal response to treatment with fibrogenic and hepatotoxic agents was evaluated for the standard tissue model (Figure A3.1A) and the modified tissue model (Fig A3.1B) during the first 14 days of treatment. The raw and fold change LDH relative to time-matched vehicle treated control over the extended time course is shown in Figure A3.2 for both models. A direct comparison of the fold change in LDH release during the first 14 days of treatment was made between the standard and modified tissue model and shown in Figure A3.3. Trichrome staining at Tx14 and Tx28 is shown in Figure A3.4 for the concentrations of fibrogenic and hepatotoxic agents in which there was no observed shift in the injury window with the incorporation of KCs. The immunohistochemistry controls for the IHC assessment in Figure 3.8 is available in Figure A3.5. Additional IHC for CD163 and albumin at Tx14 and Tx28 are shown in Figures A3.6 and A3.7, respectively. The activation status of HSCs within treated tissues was assessed with desmin and α-SMA at Tx28 (Figure A3.8).

3.6 Funding Information

This work was supported by the National Institutes of Health (NIH), Initiative for Maximizing Student Diversity (IMSD) at University of North Carolina at Chapel Hill [R25 GM055336 to L.M.N.], and National Institute of Environmental Health Sciences (NIEHS) Toxicology Training Grant [T32 ES007126 to L.M.N.], and Organovo, Inc. The content is the authors' own and does not reflect the views of the NIH.

CHAPTER 4 – ASSESSMENT OF RECOVERY IN A 3D BIOPRINTED FIBROTIC LIVER MODEL

4.1 Introduction

The clinical presentation of chronic liver injury is dependent on a fine balance between the extent of hepatocellular damage and the liver's capacity for repair and regeneration. Normal reparative processes following acute self-limiting injury typically result in the near re-establishment of baseline levels and organization of extracellular matrix (ECM) (Hernandez-Gea and Friedman, 2011). While our understanding of this dynamic wound healing response has evolved over the past two decades with regards to fibrotic liver injury, evidence is mounting that even advanced fibrosis may spontaneously improve or resolve once the underlying insult is removed or corrected (Iredale et al., 1998, Kisseleva et al., 2012, Traber et al., 2013). The current lack of specific biomarkers makes it particularly difficult to infer not only the progression or severity of the fibrotic response *in vivo* but also its resolution. Thus, some of the more recent approaches utilizing three-dimensional (3D) liver tissues to mimic progressive compound-induced fibrogenesis in an *in vitro* context represent a promising approach towards understanding these processes in a systematic and comprehensive manner (Leite et al., 2016, Norona et al., 2016).

The important role of macrophages in both augmenting and attenuating many processes that impact fibrosis and as well as its resolution suggest that Kupffer cells (KCs)

may play an important role in the remediation of fibrotic liver injury as the primary fixed macrophage in the liver (Bilzer et al., 2006, Krenkel and Tacke, 2017). In Chapter 3, we demonstrated the importance of KCs in mediating general tissue injury profiles in bioprinted liver and provide evidence to suggest they may limit the extent of collagen deposition during early compound exposure. Given the importance of KCs in the response, the present studies utilized the modified base model introduced in Chapter 3 to more closely mimic the cellular complexity of native liver and evaluate the capacity of the model to recover following the induction of fibrogenic processes with classified fibrogenic and hepatotoxic agents (Bataller and Brenner, 2005, Duffield et al., 2005). Moreover, this understanding can provide potential insight into effective therapeutic strategies to mitigate the progression of fibrotic injury by tailoring the treatment regime at early or later stages of the response during which different hepatic cell types might be more involved and targeted.

Following 14 days of exposure to the identified LC50 concentrations of fibrogenic and hepatotoxic agents, tissues were designated for either continued exposure or recovery for an additional 14 days. Regardless of end designation, temporal patterns of lactate dehydrogenase (LDH) release were not significantly different across time. Tissues that underwent a recovery phase at Tx14 exhibited a shortening of the general injury window similar to that described in Chapter 3 for the modified tissue model. While persistent exposure in the presence of KCs resulted in decreased cellularity regardless of treatment and evidence of collagen deposition at Tx28 for TGF-β1 and MTX treatment, the loss in tissue mass over time was not substantial for the recovery group. Our results suggest that while the regression of collagen within this model configuration may require a longer timeframe to become apparent, bioprinted liver tissues retain the biochemical capacity to recover

following removal of the underlying etiology. Although results from the standard tissue model are not presented in this chapter, the data provided in Appendix 4 provide additional support for the tissue response to injury and potential for recovery. These results in conjunction with the results presented in Chapter 3 further support the notion that KCs may play an initial protective role during early injury. However, extended exposure could result in increased stimulation or a perturbation in KC function leading to damage during the later phases of the response. Thus, the dynamic nature of this culture platform makes it a novel tool by which to systematically assess injury and recovery to better understand mechanisms driving these responses and further elucidate the role of resident KCs in modulating the response.

4.2 Materials and Methods

4.2.1 Tissue Production

Three-dimensional bioprinted liver tissues comprising primary cryopreserved human HCs (Life Technologies, Carlsbad, CA), HSCs (ScienCell, Carlsbad, CA), human umbilical vein endothelial cells (ECs) (Becton Dickinson, Tewksbury, MA), and primary human KCs (Samsara Sciences, San Diego, CA) were manufactured by Organovo (San Diego, CA) using patented protocols (U.S. Patents 8,241,905 B2; 8,852,932; 9,222,932 B2; 9,222,932 B2) as described previously (Forgacs et al., 2012, Forgacs et al., 2014, Murphy et al., 2015, Nguyen et al., 2016, Norona et al., 2016, Shepherd et al., 2015). Following fabrication, the tissues were maintained for a minimum of six days prior to initiation of compound treatment on post-manufacture Day 7 under standard culture conditions as described in Chapter 3.

4.2.2 Compound Exposure. LC50 concentrations of methotrexate (MTX; Sigma-Aldrich, St.

Louis, MO), acetaminophen (APAP; Sigma-Aldrich, St. Louis, MO), and transforming growth factor β1 (TGF-β1; Miltenyi Biotec Inc., San Diego, CA) were prepared as described previously (Norona et al., 2016). To ensure vehicle consistency across treatment groups, 100% DMSO was spiked into the TGF-β1 and APAP dosing solutions and standard culture medium (vehicle control) such that the final DMSO concentration was 0.1%. Liver tissues were treated for 14 days beginning on the seventh day post-printing and then designated to either a "Continued Exposure" group in which compound treatment was extended or a "Recovery" group in which the tissues were maintained in DMSO-spiked medium for an additional 14 days.

4.2.3 Biochemical Markers of Tissue Viability and Function

Spent medium samples collected on alternate treatment days were analyzed fresh for lactate dehydrogenase (LDH) activity using a commercially available colorimetric assay (Abcam, Cambridge, MA). Spent medium samples from treatment days 14 and 28 (*i.e.*, Tx14 and Tx28) were analyzed for albumin content using a plate reader-based sandwich ELISA (Bethyl Laboratories, Montgomery, TX) and urea production using a colorimetric assay (BioVision Incorporated, Milpitas, CA). All samples were diluted where appropriate to obtain values within the range of the standard curve and assays were conducted per the manufacturer's instructions with minor modifications as described previously (Norona et al., 2016).

4.2.4 Histology and Immunohistochemistry

At the conclusion of the study, a subset of bioprinted liver tissues from each treatment group were formalin-fixed, processed, embedded, and sectioned at a 5.0 μm thickness using a rotary microtome (Jung Biocut 2035; Leica Biosystems, Buffalo Grove, IL) as described

previously (Norona et al., 2016). Sections were stained with Gomori's One-Step trichrome (American MasterTech, Lodi, CA) to evaluate collagen content. Slides were imaged using the Aperio AT2 Digital Slide Scanner (Leica Biosystems, Buffalo Grove, IL). For immunohistochemistry, tissue sections were prepared and incubated with primary antibodies directed against desmin, PCNA, α-SMA, CD163, and albumin and the appropriate secondary antibodies as described in Chapter 3. Vehicle-treated control tissue was used to assess non-specific antibody staining within the tissue constructs and a secondary fluorophore-conjugated antibody control was also performed as a procedural control (Appendix 4, Figure A4.1). Slides were visualized and imaged using Zeiss Axioskop microscope (Zeiss, Jena, Germany). Images were acquired with a Zeiss Axiocam IC camera and ZEN 2 (Blue Edition) software version 2.0.

4.2.5 RNA Isolation and Quality Assessment

At the conclusion of the study, tissue lysates were prepared and total RNA was isolated and assessed for subsequent microarray analysis as described previously (Chapter 3).

4.2.6 Statistical Analysis

Unless otherwise noted, results are expressed as the mean of 5-10 replicates ± standard error (SE). Replicates refer to the same lot of bioprinted livers from a particular batch or print. Statistical significance of treatment-induced differences relative to vehicle-treated control was determined using a one-way or two-way analysis of variance (ANOVA) where appropriate, with post hoc Dunnett's multiple comparisons test using GraphPad Prism version 6.0 (Graph Pad Software, Inc., La Jolla, CA). A *p-value* < 0.05 was considered statistically significant. Outliers were identified using Grubbs' test to identify samples that fell one SD outside of the mean of the data ($\alpha = 0.05$) using GraphPad Prism version 6.0

(Graph Pad Software, Inc., La Jolla, CA).

4.3 Results

4.3.1. Attenuation of General Injury Profile Following Recovery Complements Kupffer Cell-Mediated Responses During Early Injury

LDH activity in spent tissue culture medium was assessed as a marker of general tissue injury during the course of treatment (Figure 4.1). Because the data for the continued exposure was drawn from Chapter 3 as a comparison, print-to-print consistency in the observed response was examined by comparing the LDH response to each agent during the first 14 days of treatment for the recovery print (Print 5) and historical tissue prints (Prints 3 and 4, Appendix 4, Figure A4.1). Assessment of baseline LDH release (raw and fold change) over time for the recovery group (Appendix 4, Figure A4.2) was concordant with historical LDH response profiles during the initial 7 days of treatment (*i.e.*, gradual decrease in raw LDH over time). Tissues that were stratified into the recovery group during the second half of the culture period exhibited an attenuation of the injury window following removal of the etiological agent (Figure 4.1). This general injury response overlapped with the profile obtained from the continued exposure group in the presence of KCs whereby a shortening of the injury window was observed (Figure 4.1). Comparison of tissues designated for either the continued exposure or recovery group revealed no statistically significant difference in the profiles or magnitude of the response over time for each agent of interest.

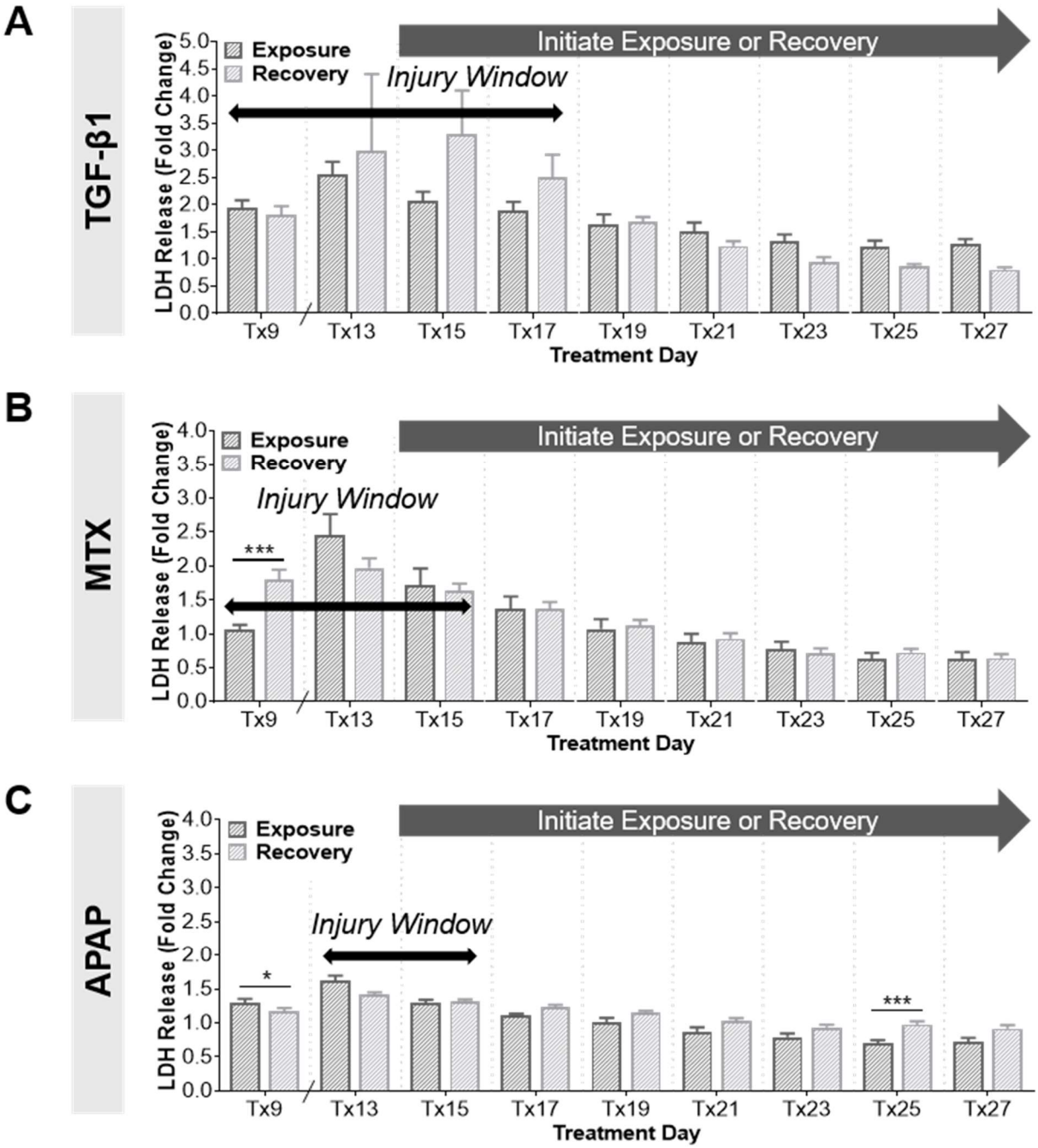

Figure 4.1 *General injury profile over the course of exposure and recovery.* Tissues are grouped by their end designation to either a continued exposure group or a recovery group. Bold dark grey arrow denotes the exposure/recovery period following 14 days of treatment. Data represent the mean ± SEM; n = 7-10. Note: the continued exposure group represents data from the 28-day extended exposure study described in Chapter 3. Significance: Two-way ANOVA with post hoc Dunnett's multiple comparisons test (*p<0.05, **p<0.01, ***p<0.001, ****p<0.0001).

4.3.2 Bioprinted Liver Tissues Retain the Biochemical Capacity to Recover Following Removal of the Underlying Etiology

While the data presented for the exposure/recovery studies is derived from the modified tissue model, trends in biochemical profiles for the standard tissue model (Appendix 4, Figure A4.4) were mainly concordant. As described in Chapter 3, treatment with TGF-β1 did not significantly impact urea at all concentrations tested with continued exposure (Figure 4.2A). However, a decline in albumin output was observed at Tx14 and Tx28 for 10 ng/mL TGF-β1 albeit not statistically significant. Urea production was significantly decreased with MTX treatment and was accompanied by a statistically significant increase in albumin production at Tx28 relative to time-matched vehicle-treated control. Continuous treatment with APAP resulted in a significant decrease in urea production at Tx14 and Tx28 while albumin output at Tx28 was significantly increased.

Following recovery, there was no statistically significant difference in urea production with 10 ng/mL TGF-β1 treatment however, urea was still significantly decreased with 0.209 μM MTX treatment (Figure 4.2B). During the initial 14-days of treatment with 0.603 mM APAP, the significant decrease in urea production was consistent as observed with previous studies. However, following the 14-day recovery period, urea production returned to vehicle-treated levels by recovery day 28 (Rx28). Furthermore, the observed increase in albumin output for both APAP and MTX treatment at the latest timepoint was attenuated in the group of tissues designated for Recovery although measured albumin was still statistically significant relative to vehicle-treated control (Figure 4.2B).

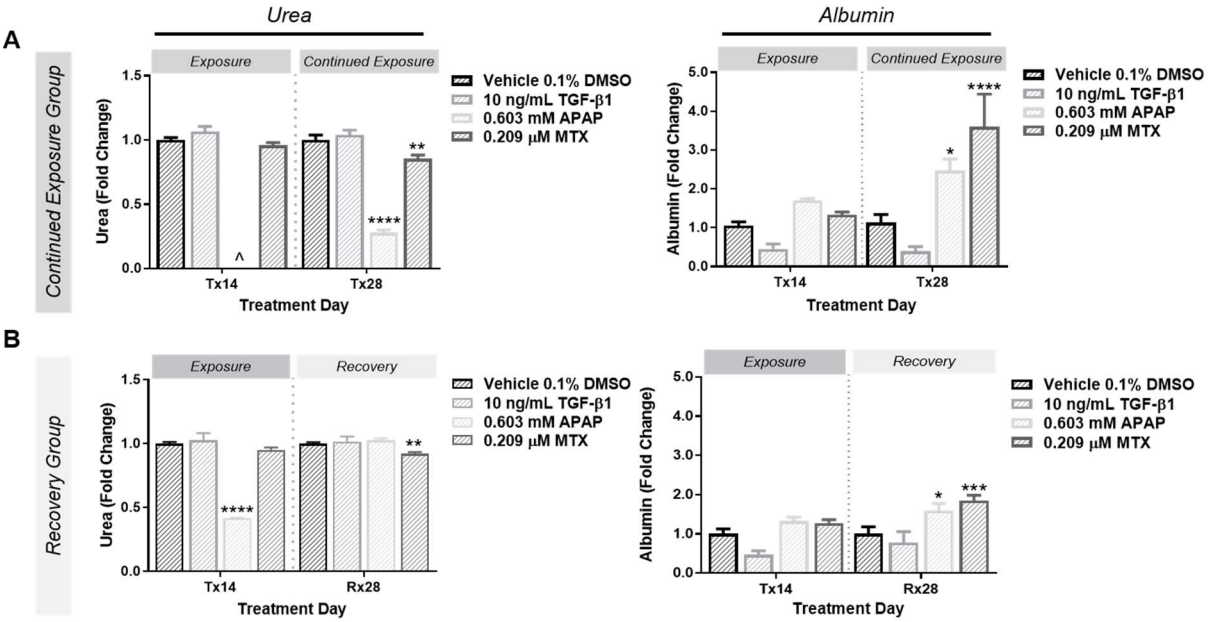

Figure 4.2 *Trends in urea and albumin output suggest recovery.* (A) Assessment of tissues that underwent continued exposure for 28 days. (B) Assessment of tissues that underwent a 14-day exposure followed by 14 days of recovery. Data represent the mean ± SEM; n = 7-10. Note: the continued exposure group represents data from the 28-day extended exposure study described in Chapter 3. Significance: Two-way ANOVA with post hoc Dunnett's multiple comparisons test (*p<0.05, **p<0.01, ***p<0.001, ****p<0.0001).

4.3.3 Impact of Recovery Period on Fibrogenic Cells and Collagen Deposition

Following 28-days of each treatment regimen, tissues were evaluated at a histological level to assess the degree of collagen and impact of the recovery period on collagen deposition within the tissue constructs. Representative sections taken from the center of each treated tissue construct are depicted in Figure 4.3. In the previous chapter, extended exposure of KC-containing tissues to fibrogenic and hepatotoxic agents resulted in an overall decrease in tissue cellularity at Tx28 compared to the standard tissue model. Similar to these outcomes, a decrease in tissue cellularity was still evident for the recovery group. However, treated tissues that underwent a 14-day recovery period displayed a moderate decrease in tissue cellularity by Tx28 (Figure 4.3). While a slight decrease in collagen content was noted in the recovery group, patterns of collagen deposition were mainly different between the continued exposure and recovery group. In the continued exposure group, the decrease in tissue cellularity was accompanied by an increase in fibrillar collagens (bright blue fibers; yellow arrows). Tissues that underwent recovery generally lacked blue collagen fibers. However, diffuse collagen positive areas were mainly localized to regions characteristic of the NPC compartment.

Sections of bioprinted liver were immunolabeled with desmin and α-SMA to assess HSC activation status within the tissues and the presence of KCs at the later treatment/recovery timepoint. Similar to the results in Chapter 3, a decrease in desmin-positive areas were observed following treatment with all agents. However, the localization of α-SMA was mainly limited to the periphery of the tissue. Albumin and CD163 were used to assess the impact of compound treatment on albumin synthesis at a tissue level and to confirm that KCs were still present within tissues at Tx28, respectively.

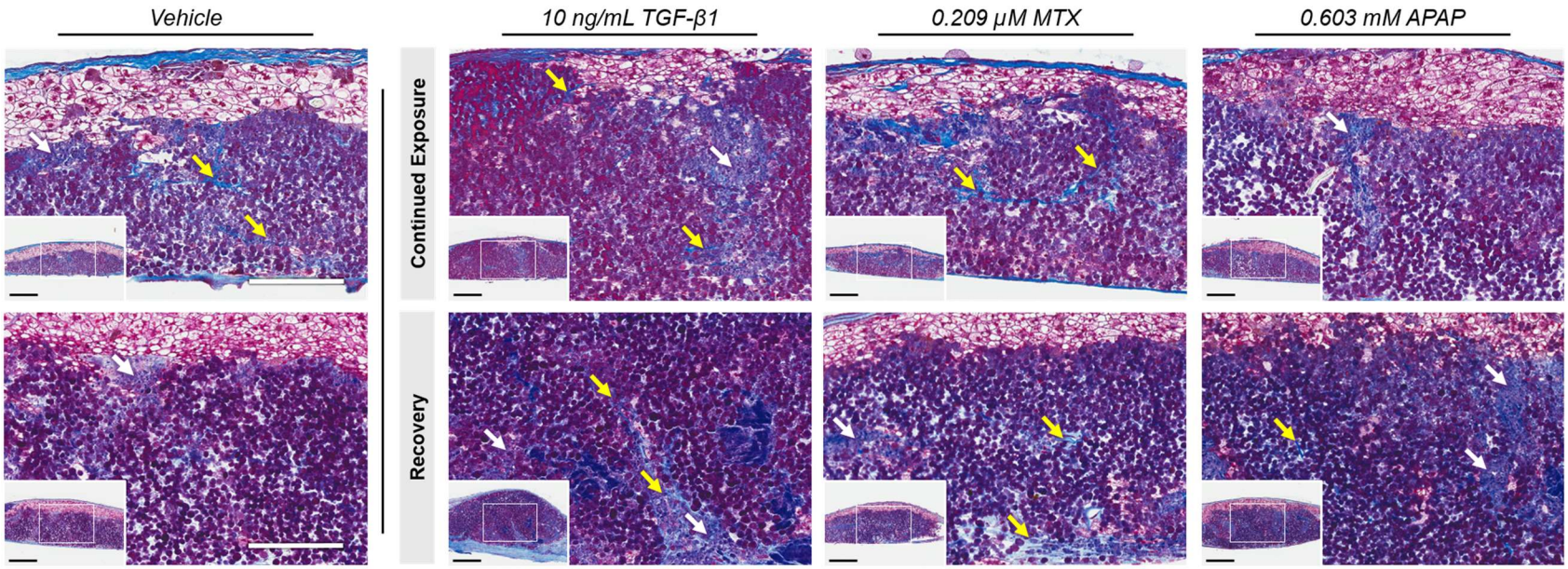

Figure 4.3 *Trichrome-stained tissues sections at the end of the 28-day culture period.* Representative sections of bioprinted liver treated with select fibrogenic and hepatotoxic agents up until treatment day 14 and then stratified into either a continued exposure or recovery group during the latter half of the culture period. Collagen deposition was visualized (blue) in bioprinted tissue sections stained with Gomori's trichrome. Yellow arrows denote fibrillar areas of collagen deposition and white arrows denote diffuse areas of collagen deposition primarily found within the non-parenchymal compartment. Scale bar = 300 μm, inset scale bar = 75 μm.

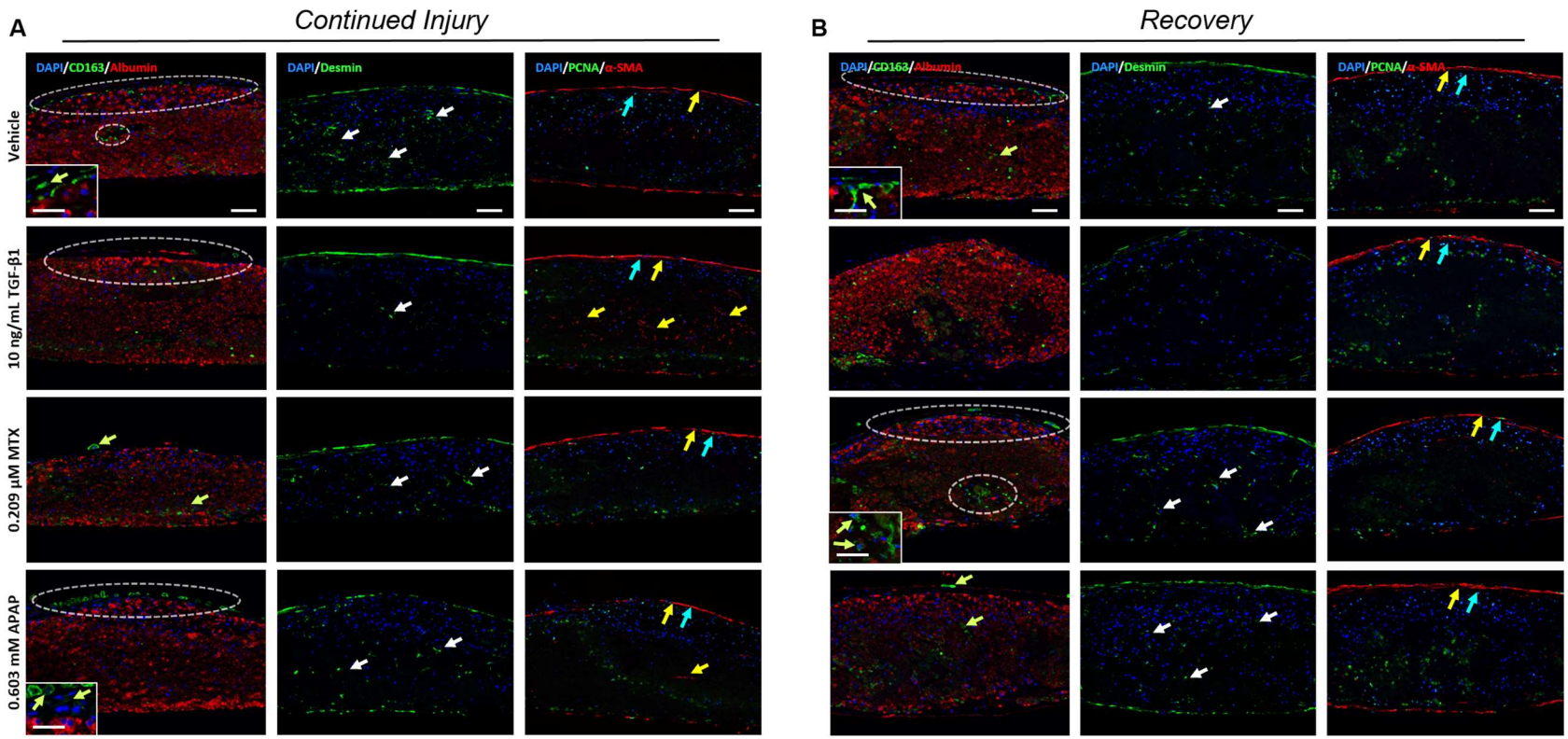

Figure 4.4 *IHC assessment of continued exposure and recovery tissues at treatment day 28.* Dotted lines circumscribe the primary region in which CD163 positive cells were localized. White arrows denote desmin positive cells, teal arrows denote proliferating cell nuclear antigen (PCNA) positive cells, and yellow arrows denote α-smooth muscle actin (α-SMA) positive cells. Scale bar = 100 µm, inset scale bar = 50 µm.

4.4 Discussion

Here we present an exciting approach utilizing novel 3D bioprinted liver tissues composed of primary human HCs, ECs, HSCs, and KCs to model progressive fibrotic injury and regression following removal of the underlying etiology. While studies have demonstrated dual and opposing roles of macrophages in chronically injured liver, the role of resident macrophages or KCs in mediating both the initiation of the response and its recovery have been elusive (Duffield et al., 2005). Given that macrophages are the primary fixed macrophage in the liver and play important homeostatic roles in not only the maintenance of normal liver function but also injury, the present study utilized a modified tissue model in which KCs were admixed at an estimated physiologically relevant ratio and incorporated into bioprinted liver tissues. In the current bioprinted model system, primary HCs don't readily proliferate *in vitro*, and prioritization of compound concentrations for each agent were chosen based on evidence of mild injury that could be monitored over continuous exposure and evidence of collagen deposition within the tissue was selected (Nguyen et al., 2016). Recovery of bioprinted liver tissues was defined as the capacity of the model to return to time-matched, vehicle-treated trends in biochemical indicators of injury and tissue function as well as evidence of collagen of collagen regression.

The collective results obtained for this study provides evidence to support the notion that following 14-day exposure to low concentrations of fibrogenic and hepatotoxic agents, 3D bioprinted liver tissues retain the functional capacity to return to baseline levels of function following compound removal and tissue maintenance for 14-days. Interestingly, for MTX-treated tissues urea did not return to time-matched vehicle-treated levels during the recovery period. This decline over time may be due to the persistent effect of

polyglutaminated metabolites which have been shown to accumulate in the liver with prolonged exposure (Cronstein, 2005).

Furthermore, these data provide additional insight into the role of KCs in attenuating the response to early injury evoked as a consequence of repeated compound exposure. In Chapter 3, we demonstrated that the incorporation of KCs into bioprinted liver tissues resulted in a shorted injury window during continuous 28-day exposure to LC50 concentrations of select fibrogenic and hepatotoxic agents. In the current study, initiation of recovery in the modified tissue model following 14 days of treatment resulted in a comparable shortening of the injury window over the treatment time course. Given the overlap of these response profiles, we infer that KCs may play an important modulatory role during early injury. However, during extended exposure, KCs may be modulating tissue response in other ways that don't necessarily manifest as a perturbation of tissue function.

Given that the regression of collagen deposition in the model was not strikingly different between the continued exposure and recovery group, this could potentially be explained by the amount of time required to observe evidence of regression or recovery or the absence of recruited inflammatory cells. In the present study, the 14-day timeframe in which recovery was assessed may not have been sufficient to observe regression of collagen deposition. Studies in rodent models of spontaneous fibrosis resolution have demonstrated evidence of scar regression by 7 days of recovery and near return to normal tissue architecture and collagen content over the course of 28 days (Iredale et al., 1998). Inhibition or depletion of macrophages during this timeframe has demonstrated an important role of resident and recruited macrophages in facilitating recovery (Tacke and Zimmermann, 2014).

The 3D bioprinted liver model represents an isolated study of compound-induced

liver injury and fibrogenesis and therefore does not take into account the recruitment of inflammatory cells during progressive injury (Pellicoro et al., 2014). The impact of KCs during continued exposure in addition to the patterns of general injury following recovery suggest KCs may attenuate early compound-induced tissue injury as assessed by LDH release alone. Because the general injury profiles are similar across variables (*i.e.*, incorporation of KCs and removal of the etiological agent), an additional marker of injury specific to HCs (*i.e.*, miR-122) is currently being evaluated to provide insight into the role of KCs in mediating injury and recovery from compound exposure.

Immunohistological assessment of CD163 was performed to confirm the presence of KCs in bioprinted tissues following extended exposure to compounds of interest. While KCs appear to be present at later treatment timepoints in both the continued exposure and recovery group, the shortened timeframe of recovery in an intact system could be due to the complementary role of recruited macrophages which may play a restorative role once the underlying etiology is removed or corrected. Indeed, specific targeting of bone marrow-derived monocytes in addition to KCs play has demonstrated that these cells facilitate the reversal of fibrotic liver injury (Duffield et al., 2005). A number of studies have demonstrated a fine balance between the production of ECM and matrix remodeling during hepatic injury and repair which is dependent on MMPs and tissue inhibitor of metalloproteinases (TIMPs) (Arpino et al., 2015). During recovery, both resident and recruited macrophages secrete matrix degrading enzymes such as matrix metalloproteinases (MMPs) and collagenases. In addition, the disappearance of myofibroblasts correlates with a decrease in the production of inhibitors of these enzymes (*i.e.*, TIMPs) thus favoring the degradation of fibrillar collagens and tissue remodeling (Liu et al., 2013). Further studies are

warranted to assess the degree of fibrotic injury and capacity to recover. Additional studies are in progress to understand whether the model exhibits features of recovery on a transcriptional level. Thus, microarray analysis and pathway based approaches will provide more insight into the resolution of fibrogenic processes and provide a summary of enriched pathways underlying the observed response.

The present results demonstrate the utility of bioprinted liver tissues for assessing spontaneous recovery following removal of the underlying etiology. While the regression of collagen in bioprinted liver tissues was not robust, the trends in biochemical markers suggest that the tissues retain some capacity to recover following removal of the etiological agent. Thus, this implicates the utility of this model system to potentially assess recovery in a more biologically relevant context. The development of effective therapeutics for treating fibrotic liver injury have been limited mainly by the lack of understanding of the temporal complexity of the response over time as well as limited insight into fibrogenic processes as they occur at the level of the liver. Thus, the ability to incorporate specific cell types into the model confers a unique advantage in the ability to dissect the roles of different cell types in driving the response or recovery. This understanding could therefore be leveraged to strategize more effective therapeutic approaches to prevent, limit, or drive the regression of fibrogenic processes.

Because fibrosis is a dynamic, progressive, and multifaceted process, there exist a number of challenges (*i.e.*, causation, stage of fibrotic injury, co-morbidities) towards developing effective treatment strategies. Organotypic human-based culture systems that recapitulate key aspects of the fibrogenic response represent more relevant strategies to understand the dynamics of liver fibrosis in a systematic and controlled setting (Norona et al.,

2016). Characterization of the response on a cellular, molecular, and histopathological basis could potentially bridge a critical gap that would not only facilitate the identification of specific biomarkers reflective of the response but also help inform novel and effective therapeutic approaches. More specifically, an understanding of the early initiating and adaptive events underlying the response as well as the cell types involved could help guide specific interventional strategies at early and late stages of fibrogenesis during which different hepatic cell types may be involved and might be targeted to inhibit or reverse fibrotic liver injury.

4.5 Supplemental Data Description

Print-to-print consistency in the temporal response to treatment with fibrogenic and hepatotoxic agents was evaluated across historical prints during the first 14 days of treatment (Figure A4.1). Raw and fold change LDH relative to time-matched vehicle treated control over the extended time course is shown in Figure A4.2 for the continued exposure and recovery group. Urea and albumin output during the exposure and recovery period was assessed following treatment with fibrogenic and hepatotoxic agents (Figure A4.4).

4.6 Funding Information

This work was supported by the National Institutes of Health (NIH), Initiative for Maximizing Student Diversity (IMSD) at University of North Carolina at Chapel Hill [R25 GM055336 to L.M.N.], and National Institute of Environmental Health Sciences (NIEHS) Toxicology Training Grant [T32 ES007126 to L.M.N.], and Organovo, Inc. The content is the authors' own and does not reflect the views of the NIH.

CHAPTER 5 – CONCLUSIONS, PERSPECTIVES, AND FUTURE DIRECTIONS

Advancements towards more organotypic model systems have significantly improved the stability and longevity of liver-like *in vitro* models as well as their predictivity when used as a model for compound-induced liver injury (Godoy et al., 2013). One of the biggest challenges for safety and risk assessment today is to integrate more complex, multicellular *in vitro* models of the liver that represent the architectural and cellular complexities of the organ *in vivo* and balance those with efficiency and throughput of the more traditional model systems historically utilized for toxicity testing (Knudsen et al., 2015). Given the complexities of fibrotic liver injury, there has been a need for sufficiently complex models with which to model basic fibrogenic processes in order to elucidate early mechanisms underlying compound-induced fibrotic liver injury (Horvat et al., 2017, Knudsen et al., 2015, Landesmann, 2016).

Although bioprinted liver tissues do not fully recapitulate every aspect of liver architecture and physiology (*i.e.*, flow, sinusoidal structure, zonation of parenchymal cells), they represent a significant advancement in the study of compound induced fibrogenesis compared to some of the conventional *in vitro* modeling approaches discussed in Chapter 1. The sustained viability and functionality of the model in addition to the ability to precisely incorporate various cell types into patterns that more closely resemble native architectural relationships between cell types enables a comprehensive and integrated approach for

assessing more complex processes in a biologically relevant and systematic way (Nguyen et al., 2016, Norona et al., 2016). However, with these advancements, there exist new challenges in utilizing these types of models to assess complex processes in an *in vitro* system. Some of the main challenges include deconvoluting responses when multiple cell types are present and throughput limitations in obtaining quantitative outcomes that take into account complexities in tissue architecture and composition. Despite these challenges, our studies utilizing bioprinted liver tissues to model compound-induced fibrogenesis demonstrate the importance of sufficiently capturing dynamic cellular interactions/processes that may dictate toxicity outcomes and the context in which the exposures are conducted.

Like any predictive model, the utility of an approach is dependent on the question at hand. As part of this dissertation work, we sought to validate and optimize a model of fibrotic liver injury using 3D bioprinted liver tissues in order to understand early events underlying compound-induced effects on the initiation of the response at a liver level. Given that the base model represents the major cell types involved in the response, we hypothesized that the model would facilitate the detection of robust fibrogenic processes following repeated low concentration exposure to fibrogenic agents. In Chapter 2 we demonstrate advanced fibrogenesis and ability of the model to recapitulate basic fibrogenic features following treatment with classified fibrogenic agents over a span of 14 days -- a process which typically takes months to years to develop. We also demonstrate that the context of exposure is particularly important to consider when conducting these types of studies and that the cytokine milieu post manufacturing influences the progression and extent of fibrogenic processes across tested compounds. In Chapter 3 we describe the impact of KCs in modulating early injury and fibrogenic response and further suggest that these cells may play

a bimodal role in response to extended compound exposure. In Chapter 4 we demonstrate the dynamic nature of the model at a biochemical level and suggest that tissues retain the capacity to recovery following 14-days of compound treatment representing mild injury. Although regression of collagen deposition was not prominent following the recovery period, these results suggest that the tissues retain the biochemical capacity to recover following removal of the underlying etiological agent. Thus, bioprinted liver tissues represent an integrated biological system that can be used to better understand complex mechanisms and series of events underlying compound induced fibrogenesis

5.1 Future Directions

5.1.1 Pathway Analysis and Identification of Molecular Signatures Unique to Fibrogenic Agents

While liver fibrosis represents a common conserved wound healing response across a broad spectrum of liver injuries, there is a need to better understand the molecular mechanisms underlying compound-induced fibrogenesis for risk assessment purposes (Landesmann, 2016). HC injury represents an initiating event in the fibrogenic cascade. However, not all hepatotoxic compounds cause fibrotic liver injury (Horvat et al., 2017). While these types of processes have been difficult to describe in the human population as alluded to earlier, model systems that accurately reflect fibrogenic processes will help fill key knowledge gaps in evaluating the fibrogenic potential of compounds in a systematic manner.

While we generally know about acute/high-dose exposure scenarios, the limitations of conventional models have hindered our understanding of chronic low-dose exposure scenarios. Thus, these novel types of approaches enable the study of compound effects at the

liver level to identify potential gene expression signatures or enrichment of liver-fibrosis relevant pathways that may be unique to fibrogenic agents and reflective of indicators of fibrogenic processes early on. These types of approaches would not only complement predictions of toxicity but could also be used to identify novel biomarkers of the progression of the response over time. Given that the AOP for liver fibrosis is mainly qualitative, there is a need for a better understanding of quantitative relationships between the key events proposed in the pathway and the adverse outcome. As such, a better understanding of the molecular underpinnings of the response as well as an integration of the response at the biochemical, and histological level could potentially aid in the identification of informative biomarkers during injury and recovery to guide compound screening strategies and inform novel therapeutic strategies.

5.1.2 Therapeutic Interventions

Many of the therapies implicated for the treatment of hepatic fibrosis over the past decade (*e.g.*, IL-10, γ-interferon, α-interferon, and peroxisome proliferator-activated receptor-γ ligand, etc.) have failed to show clinical efficacy in humans (Mehal et al., 2011). Moreover, the use of animal models to identify promising targets to remediate fibrotic injury have been largely disappointing due to the heterogeneity of the response across species, limited efficacy, and translational hurdles (Chu et al., 2013, Martignoni et al., 2006). Thus, there is a major need for more human relevant approaches to understand the core cellular and molecular mechanisms underlying the progression and dynamic nature of the fibrogenic response.

When designing effective therapeutics for the treatment of dynamic processes such as fibrosis, it is particularly difficult to specifically target a particular cell type or pathway

during the progression of the response given its dynamic and multifactorial nature (Friedman and Bansal, 2006). Furthermore, the progressive series of events as they occur in humans remain largely unknown due to limited predictive tests and biomarkers to gain insight into the events occurring at the liver level (Gressner et al., 2009). Thus, the use of more complex model systems such as 3D bioprinted liver tissue would enable a significant advancement in understanding the basic mechanisms of injury and series of events leading to the initiation of fibrogenic processes (Leite et al., 2016, Norona et al., 2016). By gaining a better understanding of the dynamic complexities underlying the response, this knowledge base could potentially inform novel therapeutic strategies at particular stages of the disease process during which certain cell types may play more prominent roles. Thus, targeting the right cell type at the right time could prove a useful strategy towards managing and remediating fibrotic injury in patients.

5.1.3 Bridging the *In Vitro* to *In Vivo* Gap

One of the major limitations of human-based model systems for complex processes such as fibrosis is the limitation in translating *in vitro* to *in vivo* outcomes. As toxicity testing has shifted towards human-based *in vitro* models, it becomes increasingly important to verify that novel model systems used to model the pathogenesis of the response recapitulate the disease process in a reliable way (Davila et al., 1998). Because non-invasive measures provide limited predictive value with regards to the progression of fibrotic liver injury in humans, it is particularly difficult to benchmark *in vitro* findings with *in vivo* results (Sebastiani and Alberti, 2006).

The ExVive™ Human Liver model provides a viable test bed for the evaluation of chronic insults in a model that is both human and tissue-like in cellularity and architecture,

and thus affords a unique opportunity to assess the molecular and histological correlation between chronically injured human clinical specimens and model outcomes. While the mechanisms and pathogenesis of liver injury may vary depending on the etiology, the latter stages of progression are likely to share many molecular and histopathological features (Bataller and Brenner, 2005). Thus, banked human liver tissue specimens collected from explanted livers with confirmed chronic injury and fibrosis could potentially be used to verify clinical correlation with fibrotic processes evoked in the current bioprinted model.

While the fibrotic injury modeled in 3D bioprinted liver tissues could be directly compared to human biopsy samples, the dynamic nature of the response, differences in the disease progression, different etiologies, genetic factors, co-morbidities, and sampling heterogeneity could potentially lead to disparate results. Given that the model represents the early events underlying fibrotic injury and that clinical samples typically represent fibrosis that is relatively well-advanced, there is a need bridge this understanding to infer the series of events as they occur in an intact system.

The development of immunodeficient mice with the engraftment of human cells has been a promising approach to study human relevant disease processes, toxicology, and metabolism (Ito et al., 2012). Advancements over the past decade have improved the ability to develop mice with functional humanized immune systems to evaluate human hematopoiesis and immunity. Given the role of the immune system in mediating fibrogenic processes these types of approaches could potentially bridge this gap to provide the means by which advanced *in vitro* models could be validated for mimicking the progression of the response in an intact system (Ito et al., 2012). Furthermore, the utility of mouse genetics could also help mechanistically inform important aspects of the response in a context that

may more reliably recapitulate the human condition.

5.1.4 Induced Pluripotent Stem Cell Models

Induced pluripotent stem cell (iPSC) technology represents a promising tool to complement human relevant toxicity testing and represents a renewable source of cells to use for toxicological screening approaches (Lu et al., 2015). The ability to non-invasively obtain blood samples from normal and diseased individuals and differentiate these cells into various cell types represents a unique approach for building donor-matched models and evaluating compound effects and the roles of specific cell types in driving the response. From a toxicity risk assessment standpoint, it is important to consider additional susceptibility factors (*i.e.*, genetic predisposition, co-morbidities/exposures, diet, etc.) and how they influence adverse outcomes with compound exposure to make a more comprehensive basis for compound risk assessment and decisions regarding exposure limits. In addition, the use of these cells could facilitate the identification of novel therapeutic strategies.

5.2 Remaining Challenges

Regardless of the remaining scientific and technical challenges, certainly we can acknowledge that incorporating basic biological principles of liver tissue architecture, cellular interactions into the design of new cell culture platforms is leading to a new generation of cell culture models that more closely recapitulate the *in vivo* situation. It is clearly evident that histotypic architecture, heterotypic cell interactions, and microenvironmental context affect the phenotype and susceptibility of target cells to xenobiotic exposure, as well as alter the corresponding biological and toxicological responses during compound exposure. Ultimately, the goal is to mimic the human *in vivo* situation as

closely as possible, whether the purpose is to better understand susceptibility under normal or diseased conditions. Moreover, these emerging technologies enable us to ask new questions and distinguish new mechanisms of compound action previously not observed in short-term, 2D monocultures or cell lines. Accordingly, the incorporation of these new *in vitro* technologies into future testing paradigms should provide more relevant, predictions of exposure and multifaceted adverse liver outcomes for human risk assessment.

APPENDIX 1 – SUPPLEMENTAL DATA FOR CHAPTER 2

Supplemental Materials and Methods

Alanine aminotransferase (ALT) release was measured in culture medium sampled on alternate treatment days with a commercially available Human ALT ELISA (Biotang Inc., Lexington, MA) per the manufacturer's instructions using a CLARIOstar® microplate reader (BMG Labtech, Germany). Samples were diluted to obtain readings within the linear range of the ALT standard curve corresponding to an assay range between 1.5 and 400 U/L. The ALT results are presented in Figure A1.2.

Table A1.1 *Time-dependent up-regulation of two fibrosis-associated genes (fold-change relative to vehicle control)*

	Day 7		**Day 14**	
Treatment	*ACTA2*	*COL1A1*	*ACTA2*	*COL1A1*
Vehicle	1.000 ± 0.062	1.000 ± 0.232	1.000 ± 0.103	1.000 ± 0.092
0.1 ng/mL TGF-β1	1.090 ± 0.064	1.165 ± 0.081	0.968 ± 0.002	1.098 ± 0.403
10 ng/mL TGF-β1	-	-	1.717 ± 0.054	1.842 ± 0.053
0.1 μM MTX	1.427 ± 0.092	1.415 ± 0.040	2.227 ± 0.055	2.054 ± 0.243
1.0 μM MTX	1.355 ± 0.291	1.155 ± 0.208	2.107 ± 0.149	2.596 ± 0.223
5.0 mM TAA	-	-	2.056 ± 0.318	1.636 ± 0.292
15 mM TAA	-	-	*	1.086 ± 0.190

Values are the means ± SD (n = 2), shaded values denote a fold-change greater than 2 relative to time-matched vehicle. *Denotes average fold change of 0.0004

Figure A1.1 *Immunostaining results for negative control tissue sections using secondary antibodies alone.* Parallel negative controls omitting primary antibody (conjugated secondary antibodies alone) did not show appreciable non-specific staining or background autofluorescence in the emission channel for the secondary antibody.

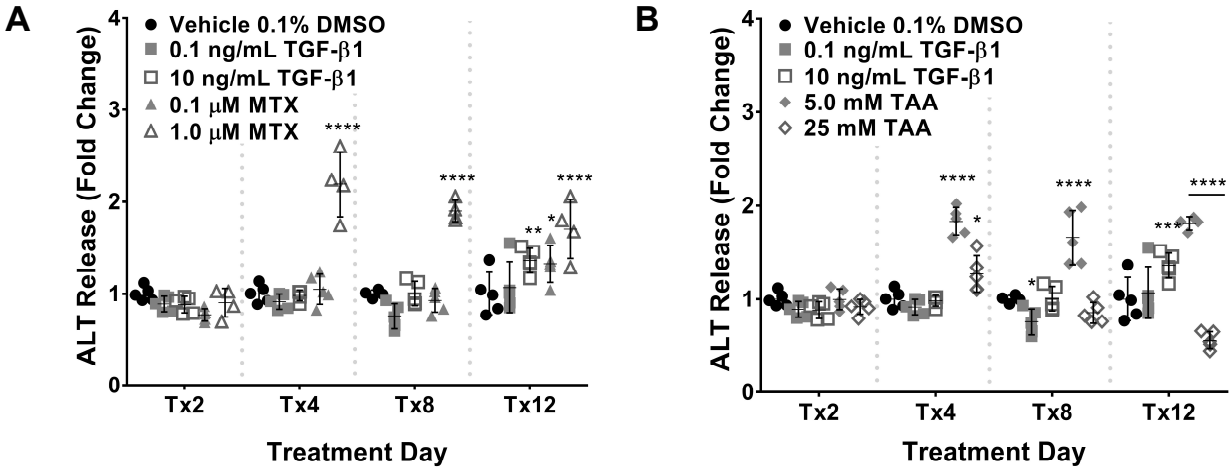

Figure A1.2 *Temporal concordance of ALT release with biochemical markers of tissue injury as a result of compound treatment.* Medium concentrations of ALT in (A) MTX- and (B) TAA-treated liver tissues, represented as the fold change relative to vehicle-treated control at alternate treatment points throughout the treatment period. Significance was determined using a two-way ANOVA with post hoc Dunnett's multiple comparisons test (*$p<0.05$, **$p<0.01$, ***$p<0.001$, ****$p<0.0001$; n = 5).

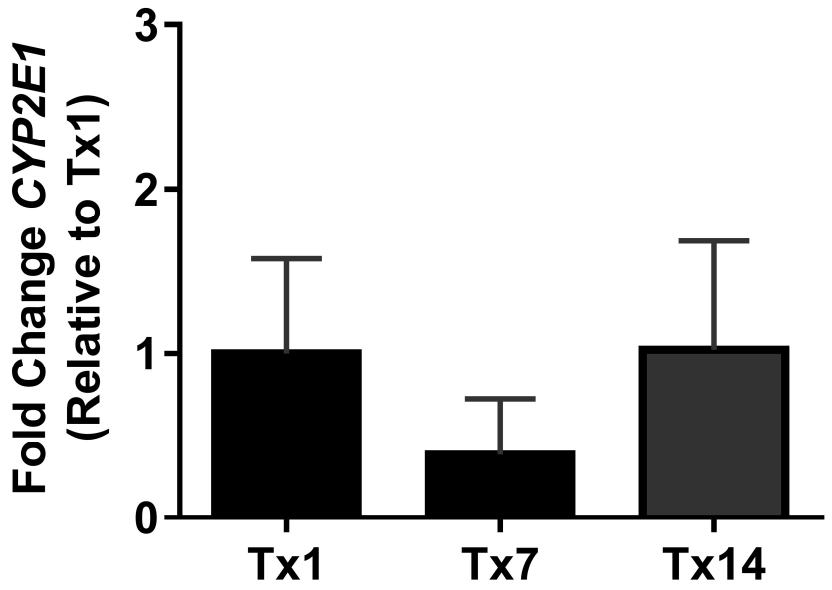

Figure A1.3. *CYP2E1 expression is sustained in untreated bioprinted liver.* The fold change in the relative quantity of *CYP2E1* transcripts (normalized to *GAPDH*) is represented relative to Tx1 at time points spanning the treatment period (average Ct = 24, n = 6).

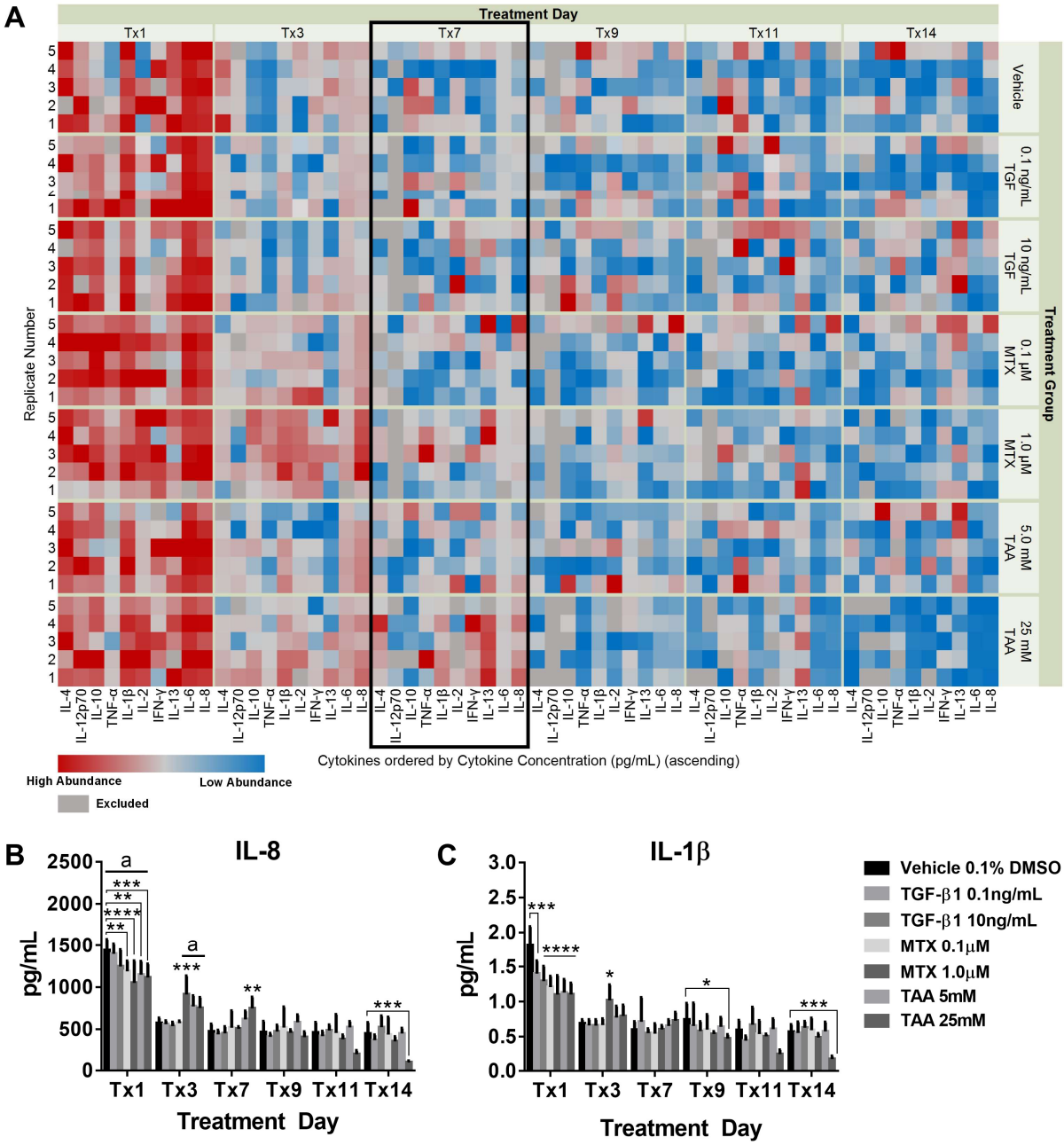

Figure A1.4. *Time- and treatment-dependent changes in the abundance of cytokines released into the culture medium over the treatment time course.* (A) The prevalence of proinflammatory cytokines (pg/mL) declined over time, reaching steady state levels by Tx7 (A; black box). (B) IL-8 and (C) IL-1β exhibited similar trends over time; however, transient elevations were noted for certain treatment groups at early time points (n = 5). Measured abundance of IL-8 (B) extrapolated beyond the standard curve is denoted with (a) and is reflected in the heat map (A). Significance was determined using a two-way ANOVA with post hoc Dunnett's multiple comparisons test (*p<0.05, **p<0.01, ***p<0.001, ****p<0.0001).

APPENDIX 2 – MODEL OPTIMIZATION AND VALIDATION OF TISSUE LOTS

In Chapter 2, we demonstrated the utility of 3D bioprinted liver tissues to recapitulate basic fibrogenic features with robust evidence of collagen deposition over a span of 14 days. In order to resolve the early processes mediating the response, model optimization studies were conducted to adjust the exposure timeframe and validate concentration-dependent patterns of injury/fibrogenic response in two donor lots of bioprinted liver tissue. Given that the cytokine abundance shifts substantially over the first 3-10 days post-manufacture, compound exposure was delayed to post-print day 7 given that cytokine levels decline and reach steady-state levels over this timeframe (Appendix 1, Figure A1.4). Using this modified exposure regimen (Figure A2.1), the tissue injury response to compound exposure was assessed in two independent HC donor tissue lots comprising NPCs derived from the same source. Hepatocyte donor characteristics are provided in Table A2.1.

Tissue constructs were successfully manufactured for each lot as described previously (Norona et al., 2016) and allowed to mature for 6 days based on the surge in cytokine production observed post-manufacture as described in Chapter 2 (Appendix 1, Figure A1.4). Figure A2.1 outlines the modified dosing scheme from manufacture Day 0 through treatment day 14 (Tx14). A repeated 5-point dose response (unless otherwise indicated) was conducted over the course of 14 days to identify concentrations of fibrogenic agents corresponding to different degrees of HC stress/injury (*i.e.*, the lethal concentration 20 [LC20] and lethal concentration 50 [LC50]) that would be used in subsequent extended exposure studies (4 weeks) in the standard and modified tissue models and recovery studies in the modified tissue model presented in Chapters 3 and 4, respectively.

Tissues were dosed daily with either transforming growth factor-β1 (TGF-β1), acetaminophen (APAP), methotrexate (MTX), or thioacetamide (TAA). Because inflammation is closely tied to fibrogenesis, dexamethasone, a synthetic corticosteroid with anti-inflammatory properties, was removed from the culture medium due to the potential interference with KC and HSC cytokine production resulting from treatment (Pellicoro et al., 2014). Studies using 2D co-cultures of HCs and KCs have demonstrated the potent and persistent effect of dexamethasone on hampering cytokine production (Rose et al., 2016). Instead, hydrocortisone remained in the culture medium as a physiologically relevant and less persistent counterpart to support HC function and viability over time. Although the removal of dexamethasone from the medium was not directly compared within a particular lot of tissues, the extended viability of the tissues and consistent response to profiles to compound exposure across donor HC lots, provided confidence in the results obtained for LOT B. The following subsections are organized on a compound basis and describe the dose response results obtained for each lot of tissues.

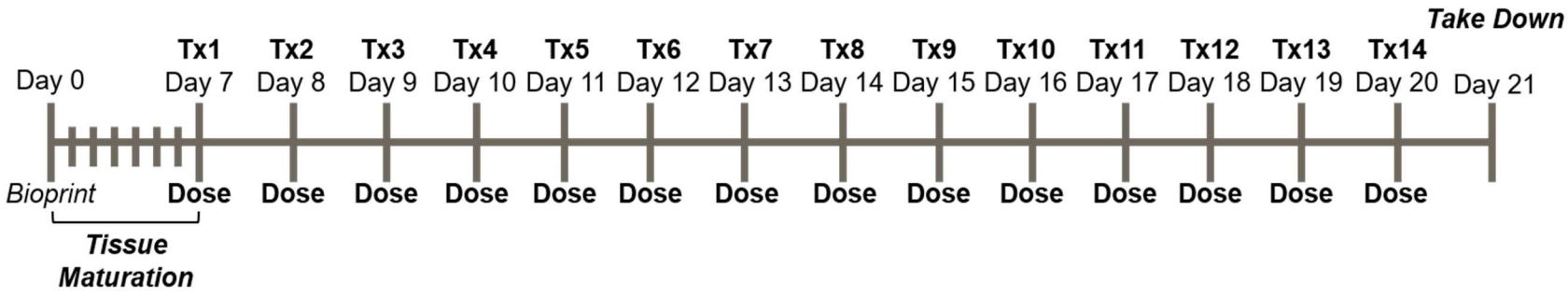

Figure A2.1 *Outline of the modified 14-day exposure timeframe with an extended tissue maturation period.*

Table A2.1 *Hepatocyte donor information for LOT A and LOT B tissues*

Donor Demographics: LOT A		**Donor Demographics: LOT B**	
Donor Number	HMC1015	*Donor Number*	HFC1047
Gender	Male	*Gender*	Female
Age	21	*Age*	29
Race	Caucasian	*Race*	Caucasian
Cause of Death	Hypertension 2nd Intracerebral Hemorrhage	*Cause of Death*	Anoxia Secondary 2nd Drug Intoxication
Smoker	Yes	*Smoker*	Yes
Social History	Alcohol Use, No Drugs or Medication	*Social History*	Alcohol Use, Rare Marijuana Use, Xanax Ingested Daily for 3 Years
Medical History	None	*Medical History*	Jaundice as an Infant. Hypertension (Mostly Compliant with Medication), Medications Taken at Home: Oxycodone, Fentanyl, Xanax, Vicodin, Paxil. Administered in the Hospital: Dextrose, Heparin

Methotrexate

Exposure to methotrexate (MTX) ranging from 0.01-10 μM (5 concentrations) resulted in a gradual increase in LDH release following repeated exposure to each concentration (Figure A2.2). Temporally distinct differences in injury markers corresponding to general tissue injury versus HC-specific injury was observed over the course of 14 days of exposure with a rapid dose-dependent release of the HC-specific injury marker alanine aminotransferase (ALT) during the initial exposure period (~Tx1-Tx3) followed by a delayed and sustained dose-dependent elevation in lactate dehydrogenase (LDH) release (~Tx7-Tx14) out to Tx14 (Figure A2.3). While the magnitude of response differed across HC donor tissues which, could be due to donor HC susceptibility, the consistent dynamic shift in the profile of ALT and LDH release suggest early HC injury precedes general sustained tissue injury over the treatment time course.

Indicators of mild injury were accompanied by a progressive, dose-dependent increase in collagen deposition by Tx14 further implicating the impact of the extent of injury on the magnitude of fibrogenic outcome at a tissue level (Figure A2.4). As compared to previous studies in which dosing was conducted on post-manufacture day 3 (Chapter 2), trends in general injury over time were consistent; however, the delayed initiation of treatment resulted in a markedly attenuated fibrogenic response (Figure A2.4). Furthermore, the differential expression of fibrogenic transcripts (*ACTA2* and *COL1A1*) is likely reflective of the progression of the response within each donor tissue lot. These results suggest that the context of injury (*i.e.*, wound healing response post-manufacturing) may play an important role in driving the progression of fibrotic injury in this model system.

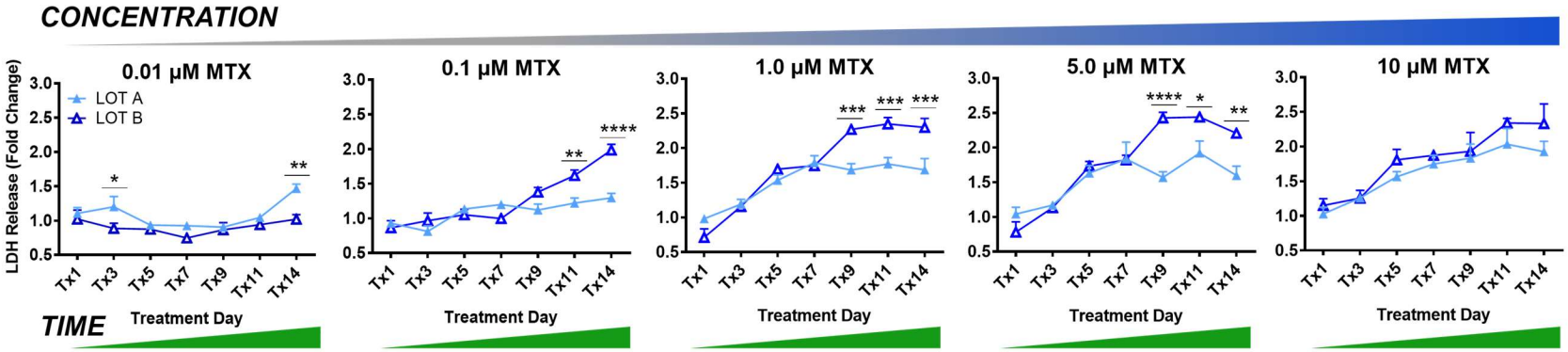

Figure A2.2 *Repeated dose response profiles in two lots of bioprinted tissues over 14 days of treatment.* Treated tissues exhibited similar trends in LDH release with an overall higher magnitude of response observed for LOT B at mid to late timepoints. Data represent the mean ± SEM; n = 5. Significance: Two-way ANOVA with post hoc Dunnett's multiple comparisons test (*$p<0.05$, **$p<0.01$, ***$p<0.001$, ****$p<0.0001$).

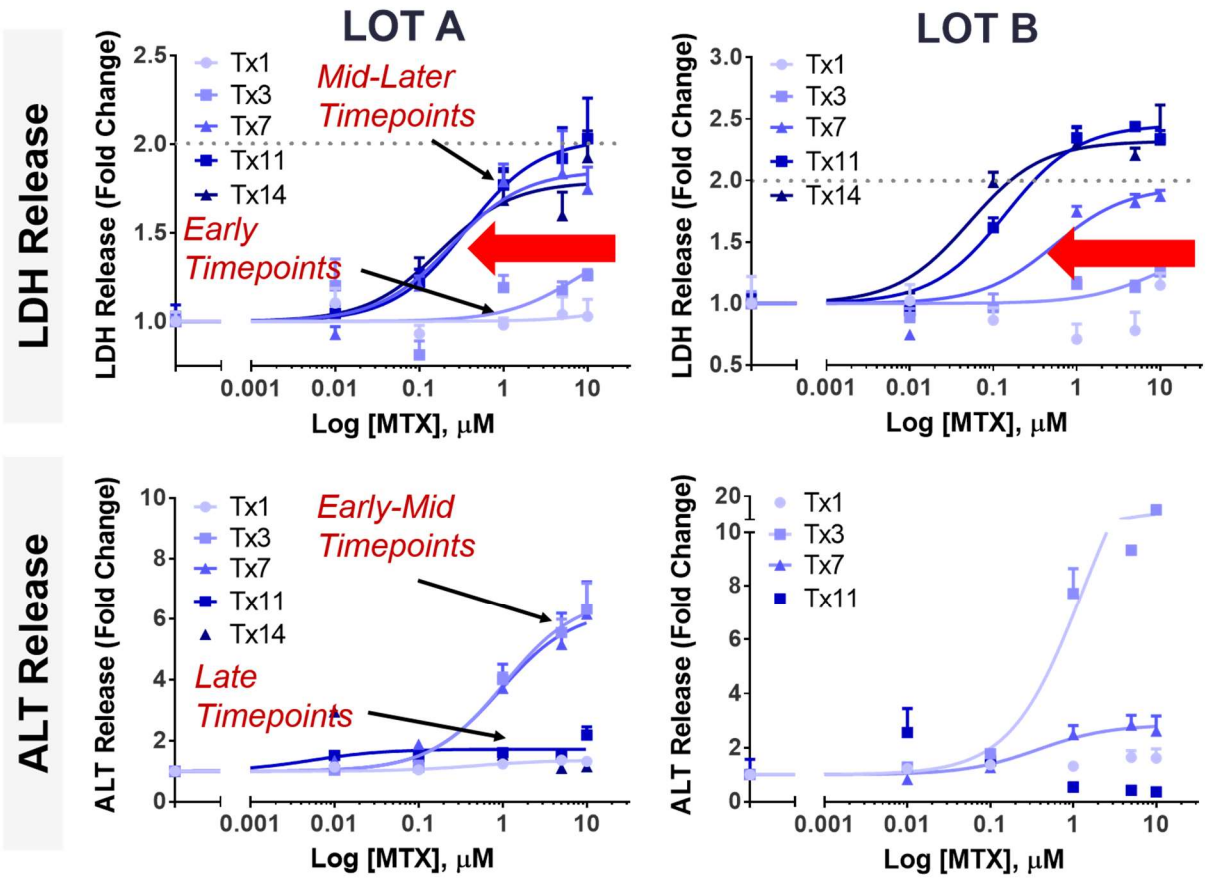

Figure A2.3 *Temporal LDH and ALT dose response profiles for two lots of bioprinted tissue treated with methotrexate.* LDH release (general injury) and ALT (HC specific injury) were measured to understand the dynamics of injury over the course of MTX exposure. A shift in the dose-response profile with repeated compound exposure is denoted by the red arrows. Data represent the mean ± SEM; n = 5. LDH release was used to identify the LC20 (0.052 μM) and LC50 (0.209 μM) concentrations used in Chapters 3 and 4.

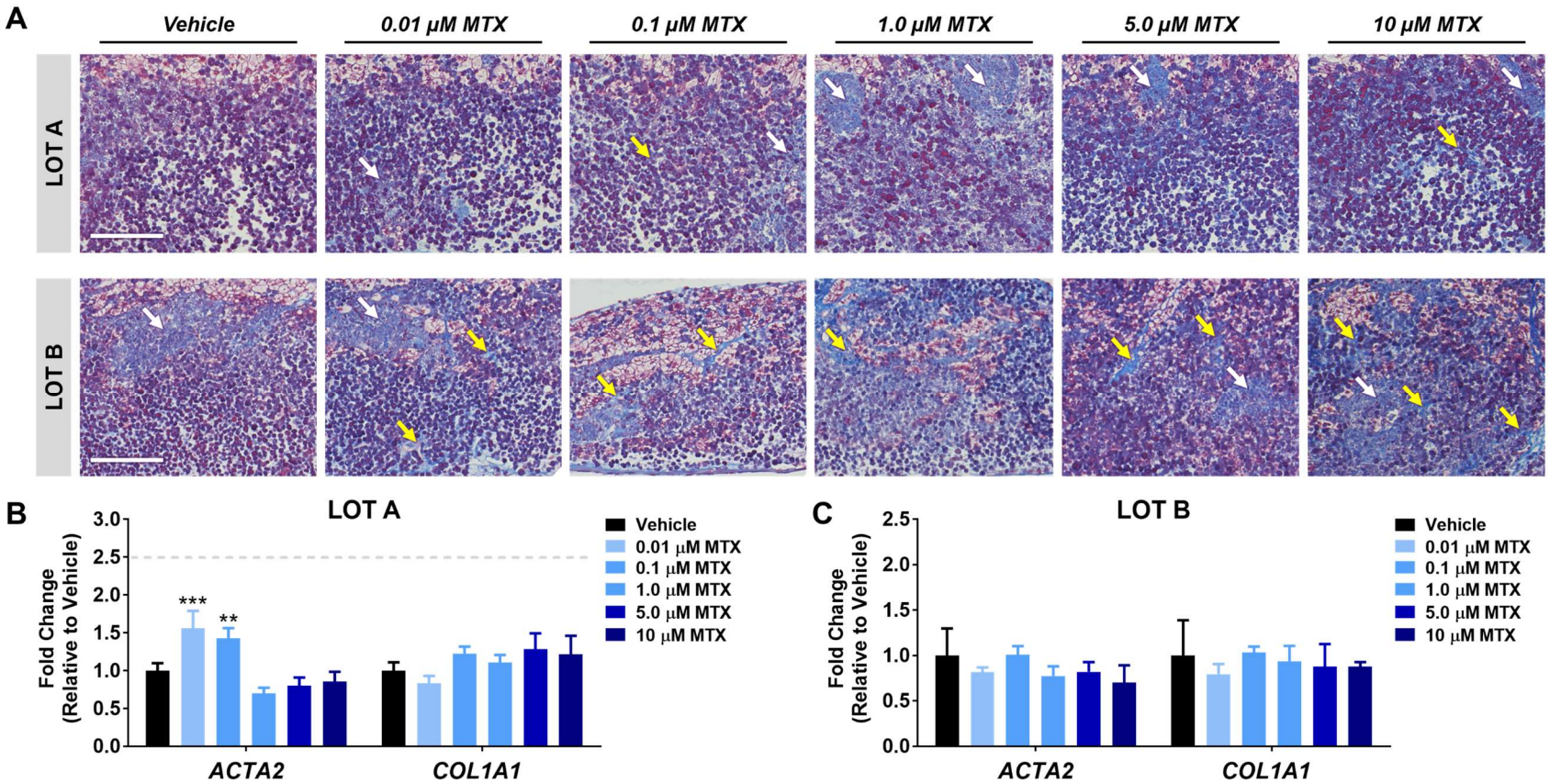

Figure A2.4 *Trichrome-stained tissue sections corresponding to two donor tissue lots exhibit similar patterns of collagen deposition with increasing dose of methotrexate.* (A) Representative sections of bioprinted liver at treatment day 14. Collagen deposition was visualized (blue) in bioprinted tissue sections stained with Gomori's trichrome. Yellow arrows denote fibrillar areas of collagen deposition and white arrows denote diffuse areas of collagen deposition primarily found within the non-parenchymal compartment. Scale bar = 200 μm. (B and C) Relative expression of fibrogenic genes α-smooth muscle actin (*ACTA2*) and collagen 1a1 (*COL1A1*) in tissue LOT A and LOT B, respectively.

Thioacetamide

While the LDH response profiles among MTX-treated tissues were similar to the initial exposure studies described in Chapter 2, thioacetamide (TAA)-treated tissues exhibited an altered general injury profile following the delayed initiation of compound exposure (Figure A2.5). The lack of biochemical indicators injury despite a dose-dependent increase in collagen deposition as evidenced by trichrome staining was consistent across both tissue lots (Figure A2.6). The discordance in tissue injury profiles over time suggest that the context of exposure for certain compounds may influence progressive injury and the extent of fibrotic injury. Thus, these results suggest a longer exposure period may be required to see TAA-induced LDH release and that the context of exposure is important to consider when evaluating the fibrogenic potential of compounds in an *in vitro* setting. Trends in the expression of fibrogenic genes at Tx14 support the temporally regulated expression of *ACTA2* (a major marker of HSC activation) and *COL1A1* (marker of collagen deposition due to HSC activation) (Figure A2.6B and A2.6C). Due to the nature of the response, LC20 and LC50 concentrations of TAA could not be identified therefore, further investigation is warranted to understand how underlying inflammatory processes impact susceptibility to injury and fibrogenic outcome.

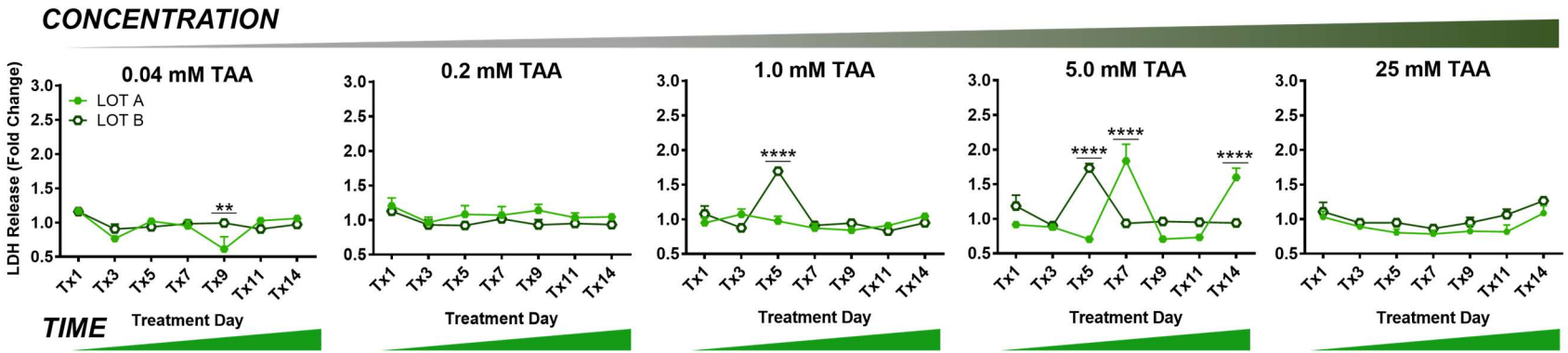

Figure A2.5 *Repeated dose response profiles in two lots of bioprinted tissue over 14 days of treatment with thioacetamide.* Treated tissues exhibited similar trends in LDH release over time with no evidence of dose-dependent effects following repeated exposure. Data represent the mean ± SEM; n = 5. Significance: Two-way ANOVA with post hoc Dunnett's multiple comparisons test (*$p<0.05$, **$p<0.01$, ***$p<0.001$, ****$p<0.0001$).

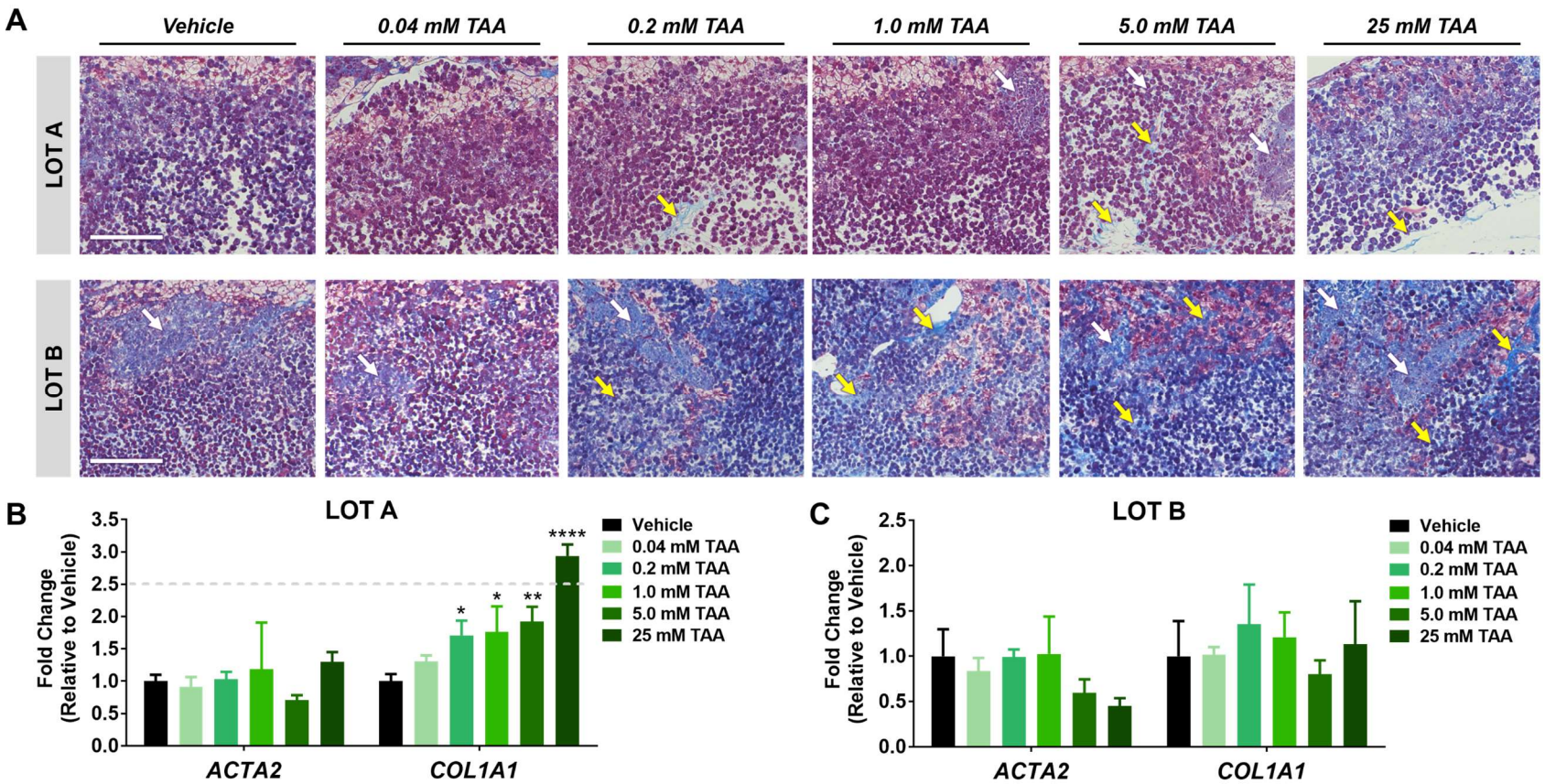

Figure A2.6 *Trichrome-stained tissue sections corresponding to two donor tissue lots treated with thioacetamide.* Representative sections of bioprinted liver at treatment day 14 depict differences in collagen deposition between LOT A and LOT B. Collagen deposition was visualized (blue) in bioprinted tissue sections stained with Gomori's trichrome. Yellow arrows denote fibrillar areas of collagen deposition and while areas denote diffuse areas of collagen deposition primarily found within the non-parenchymal compartment. Scale bar = 200 µm. (B and C) Relative expression of fibrogenic transcripts in tissue LOT A and LOT B, respectively.

Acetaminophen

Interestingly, trends in LDH release were mild for all concentrations of APAP tested (Figure A2.7A). Complementary to the LDH data, a concentration-dependent decrease in tissue ATP content was observed at Tx14 (Figure A2.7B). Histological assessment was not performed on APAP-treated tissues for the purpose of this optimization study since the main goal was to identify concentrations of compounds to be used in subsequent long-term exposure studies. Due to the overall lack of a dose-dependent increase in LDH release following 14 days of repeated APAP treatment, ATP content was used to identify the LC20 (0.052 μM) and LC50 (0.209 μM) concentrations used in Chapters 3 and 4.

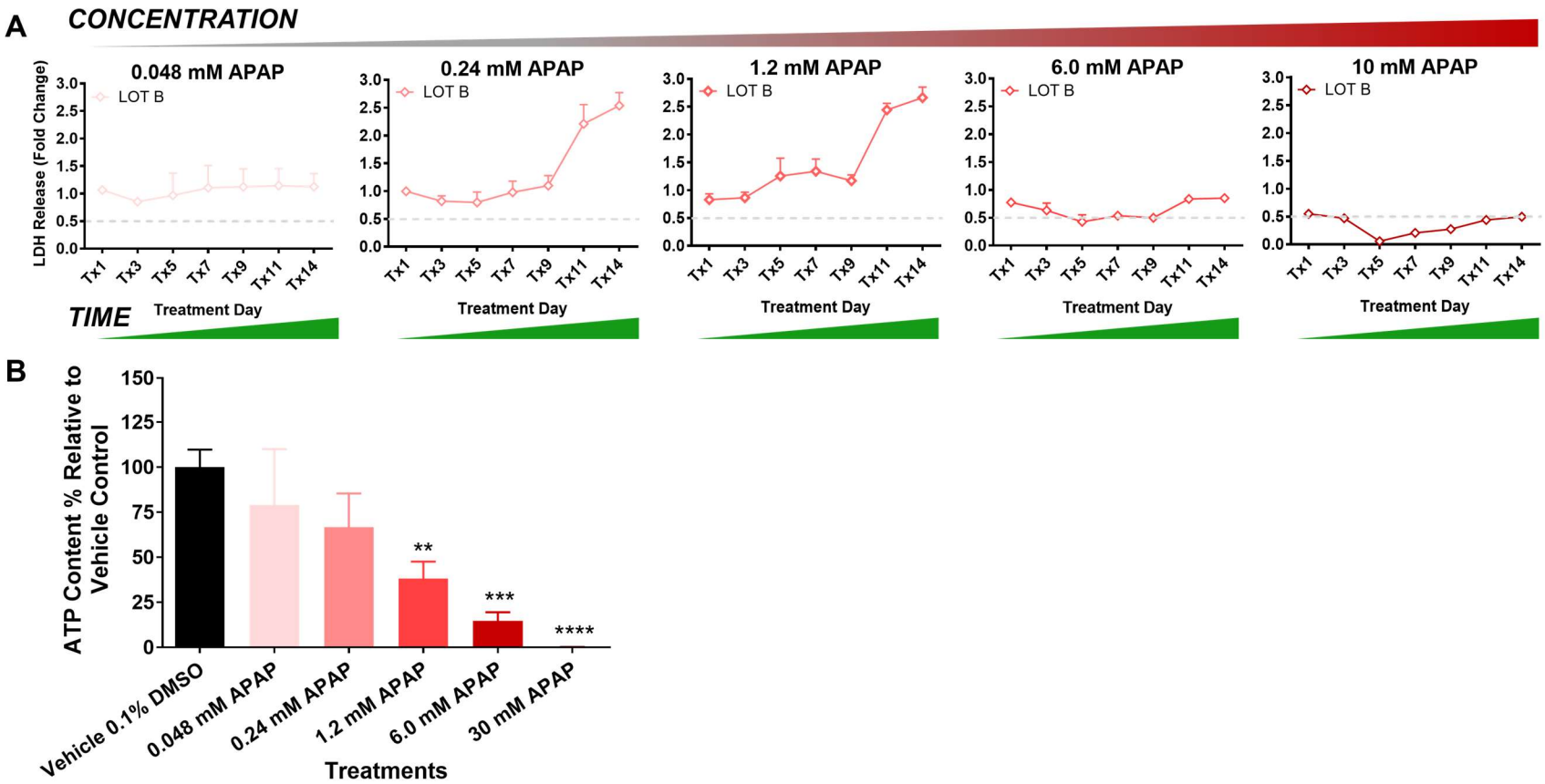

Figure A2.7 *Repeated dose response profiles in tissue LOT B over 14 days of treatment with acetaminophen.* (A) LDH release over time for each concentration tested. (B) ATP content of bioprinted liver tissues at Tx14 following repeated APAP. Data represent the mean ± SEM; n = 5 for LDH; n = 3 for ATP. Significance: Two-way ANOVA with post hoc Dunnett's multiple comparisons test (*p<0.05, **p<0.01, ***p<0.001, ****p<0.0001).

APPENDIX 3 – SUPPLEMENTAL DATA FOR CHAPTER 3

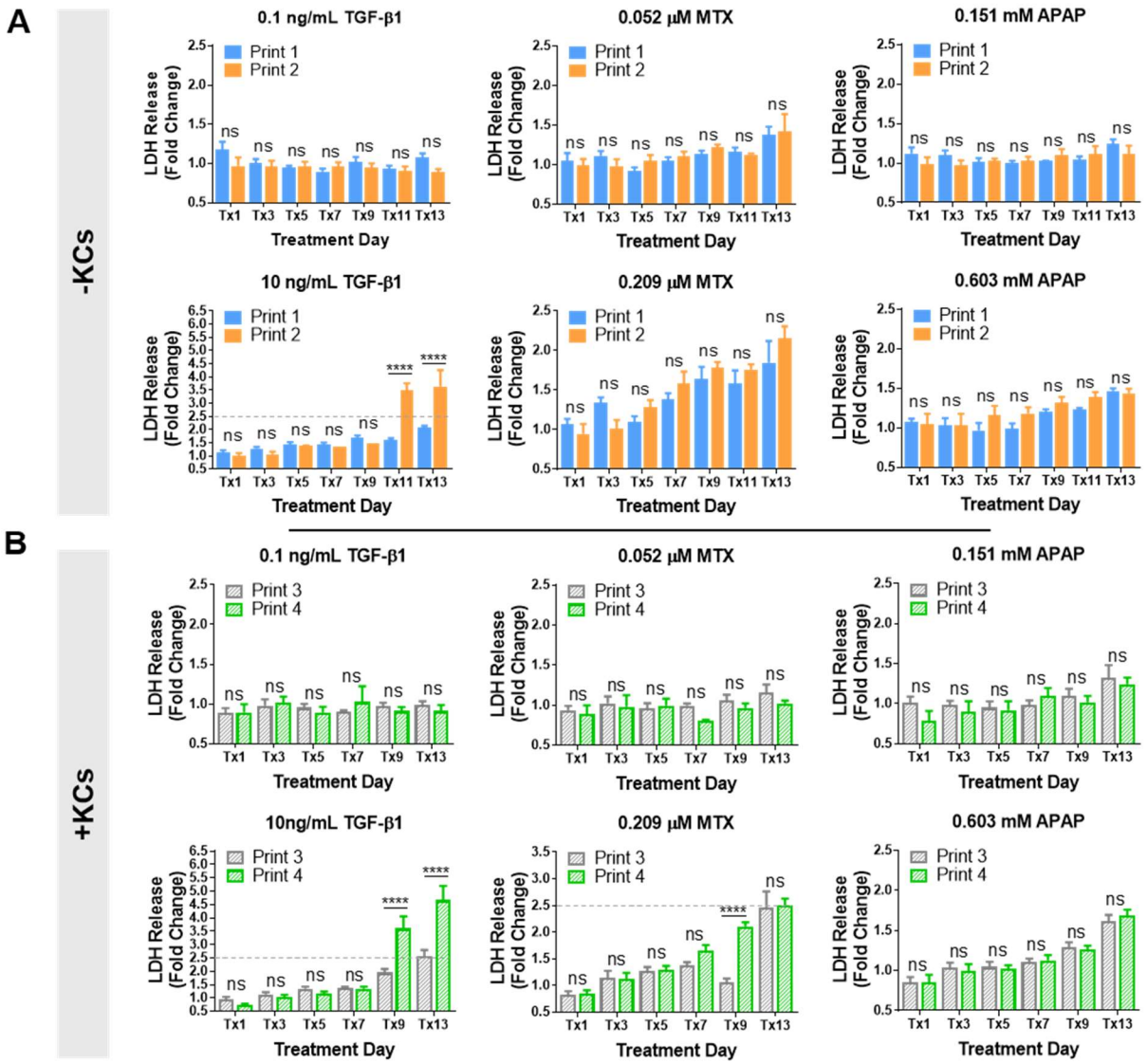

Figure A3.1. *Print-to-print consistency in LDH response profiles regardless of tissue composition*. Data represent the mean ± SEM; n = 5-7. Significance: Two-way ANOVA with post hoc Dunnett's multiple comparisons test (*p<0.05, **p<0.01, ***p<0.001, ****p<0.0001).

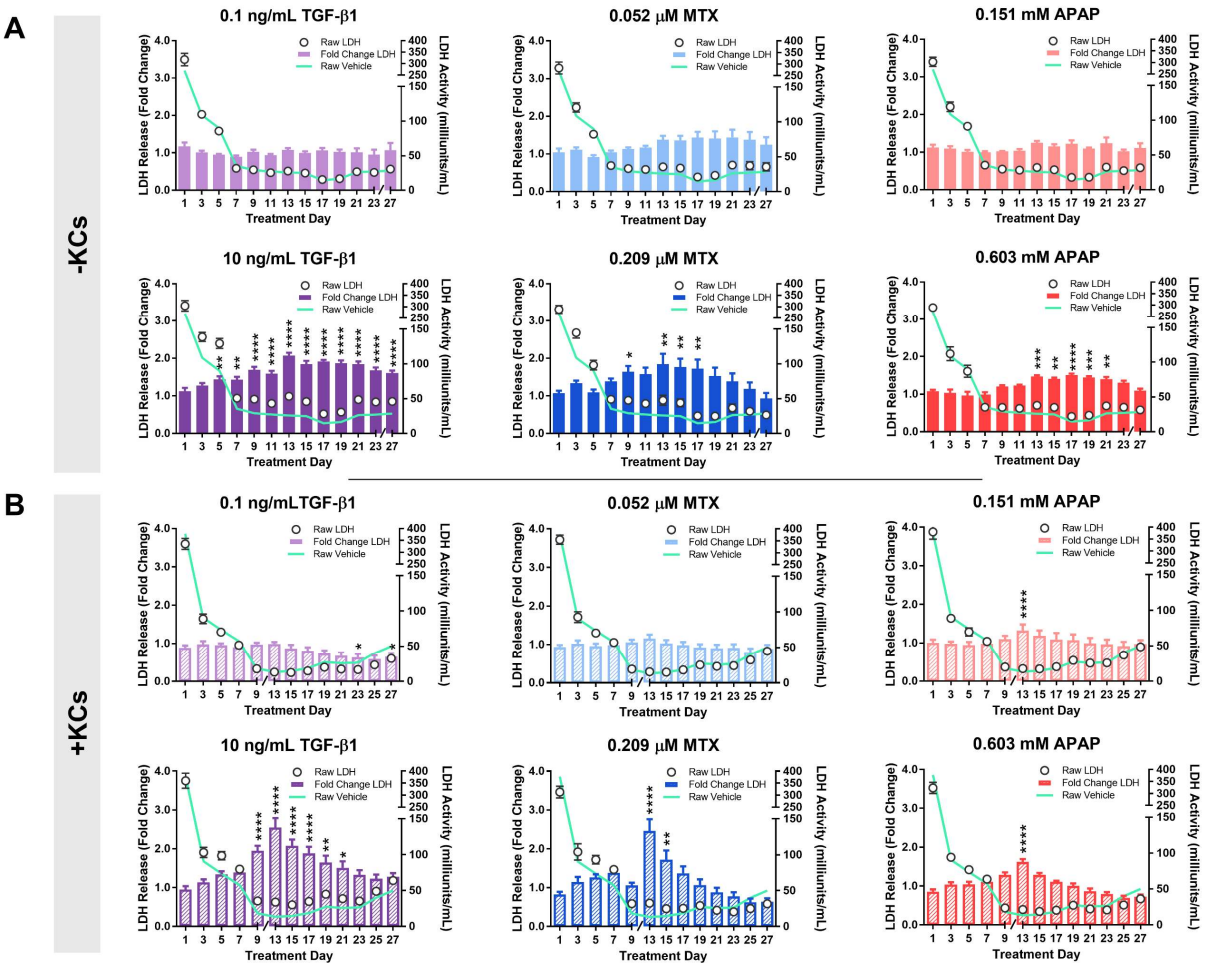

Figure A3.2 *Decrease in raw LDH release during the first 7 days of treatment regardless of tissue composition.* Data represent the mean ± SEM; n = 5-7. Significance: Two-way ANOVA with post hoc Dunnett's multiple comparisons test (*p<0.05, **p<0.01, ***p<0.001, ****p<0.0001).

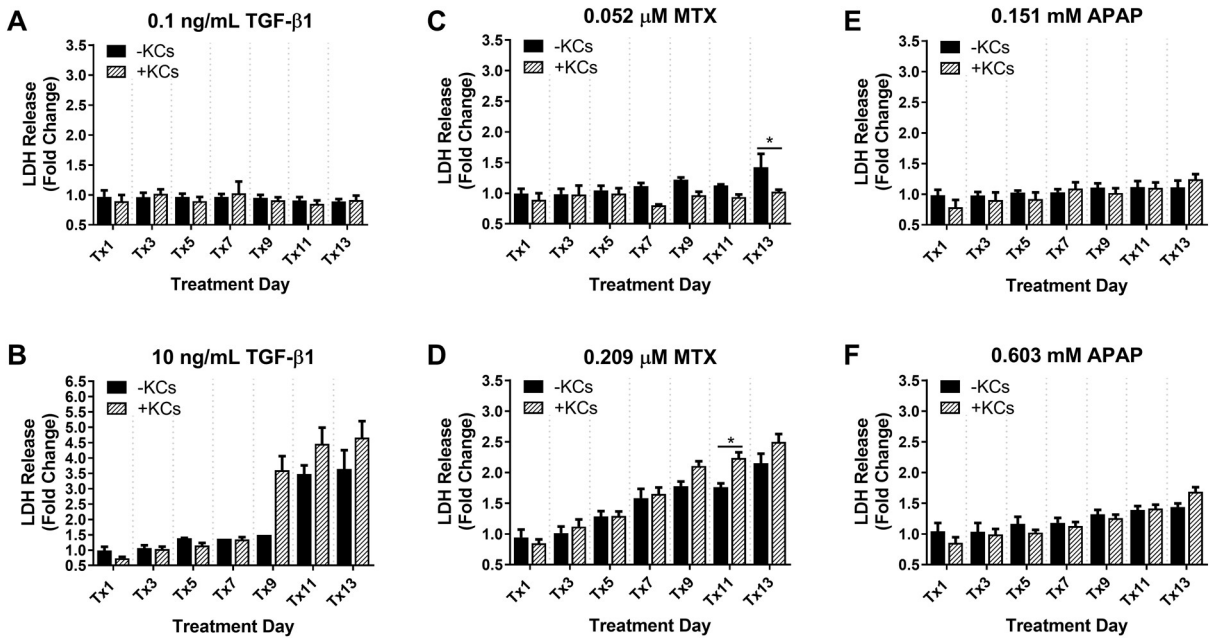

Figure A3.3 *Kupffer cells do not significantly alter the general injury profile during the first 14 days of treatment with fibrogenic and hepatotoxic agents.* Data represent the mean ± SEM; n = 5-7. Significance: Two-way ANOVA with post hoc Dunnett's multiple comparisons test (*p<0.05, **p<0.01, ***p<0.001, ****p<0.0001).

Vehicle
0.1 ng/mL TGF-β1
0.052 μM MTX
0.151 mM APAP
Treatment Day 14
Treatment Day 28
-KCs
+KCs
-KCs
+KCs

Figure A3.4 *Trichrome-stained tissue sections at treatment day 14 and 28 for all other treatment groups.* Representative sections of bioprinted liver treated with select concentrations of fibrogenic and hepatotoxic agents. Collagen deposition was visualized (blue) in bioprinted tissue sections stained with Gomori's trichrome. Yellow arrows denote fibrillar areas of collagen deposition and white arrows denote diffuse areas of collagen deposition primarily found within the non-parenchymal compartment. Scale bar = 300 µm, inset scale bar = 75 µm.

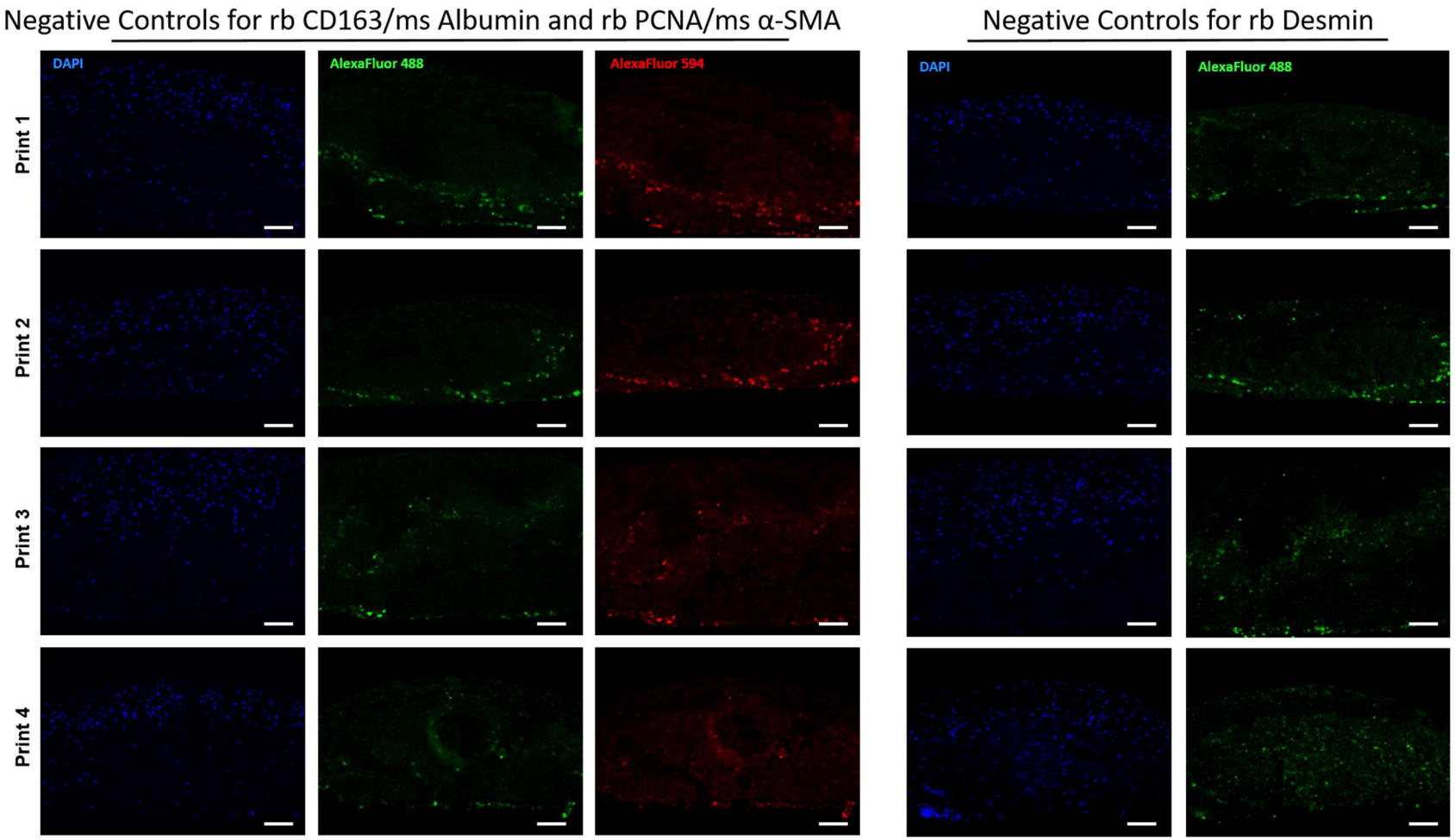

Figure A3.5 *Immunostaining results for negative control vehicle-treated tissue sections using secondary antibodies alone.* Parallel negative controls omitting primary antibody (conjugated secondary antibodies alone) showed some background autofluorescence in the emission channel for the secondary antibodies.

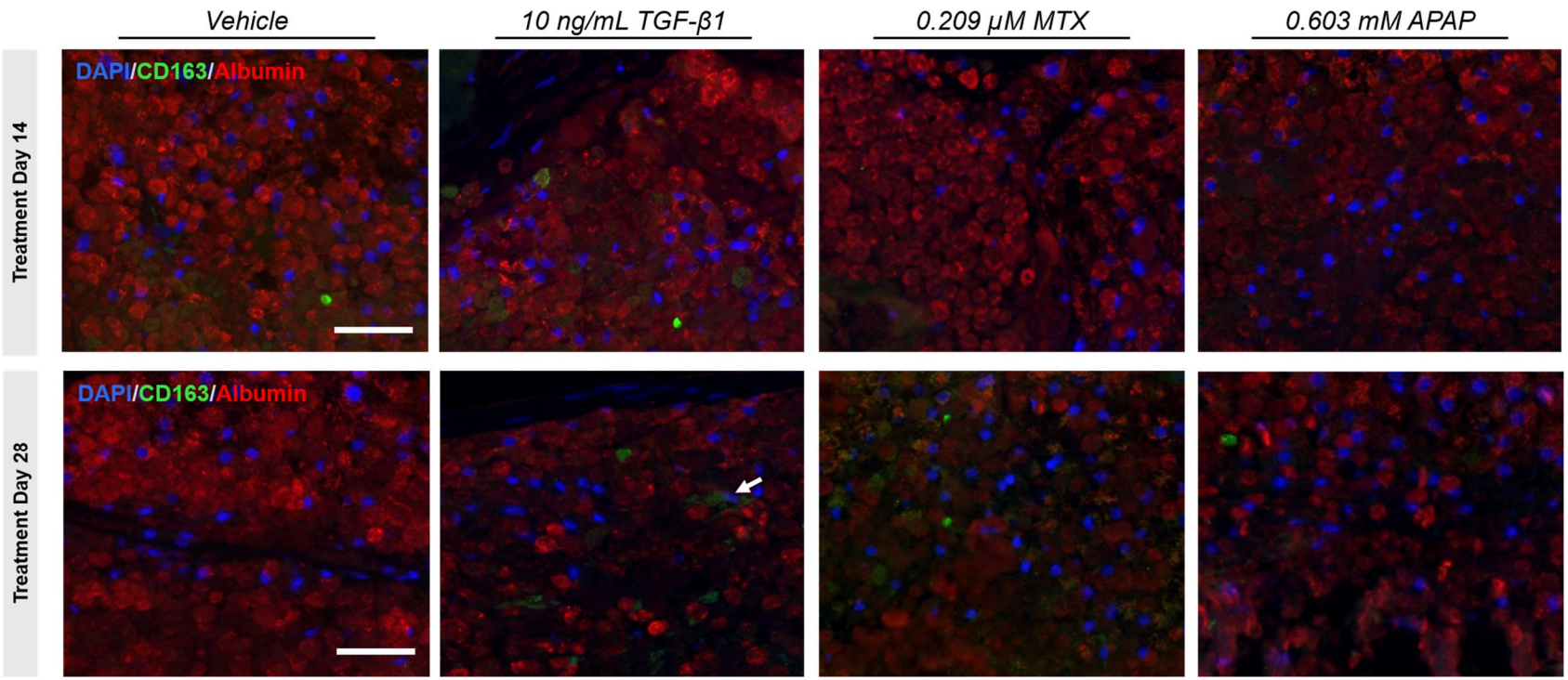

Figure A3.6 *CD163 and albumin staining at treatment day 14 and 28 for the standard tissue model (-KCs).* Mid and apical region of each tissue is shown. Very few CD163 positive cells (white arrows) were detected within the tissues. Scale bar = 50 µm.

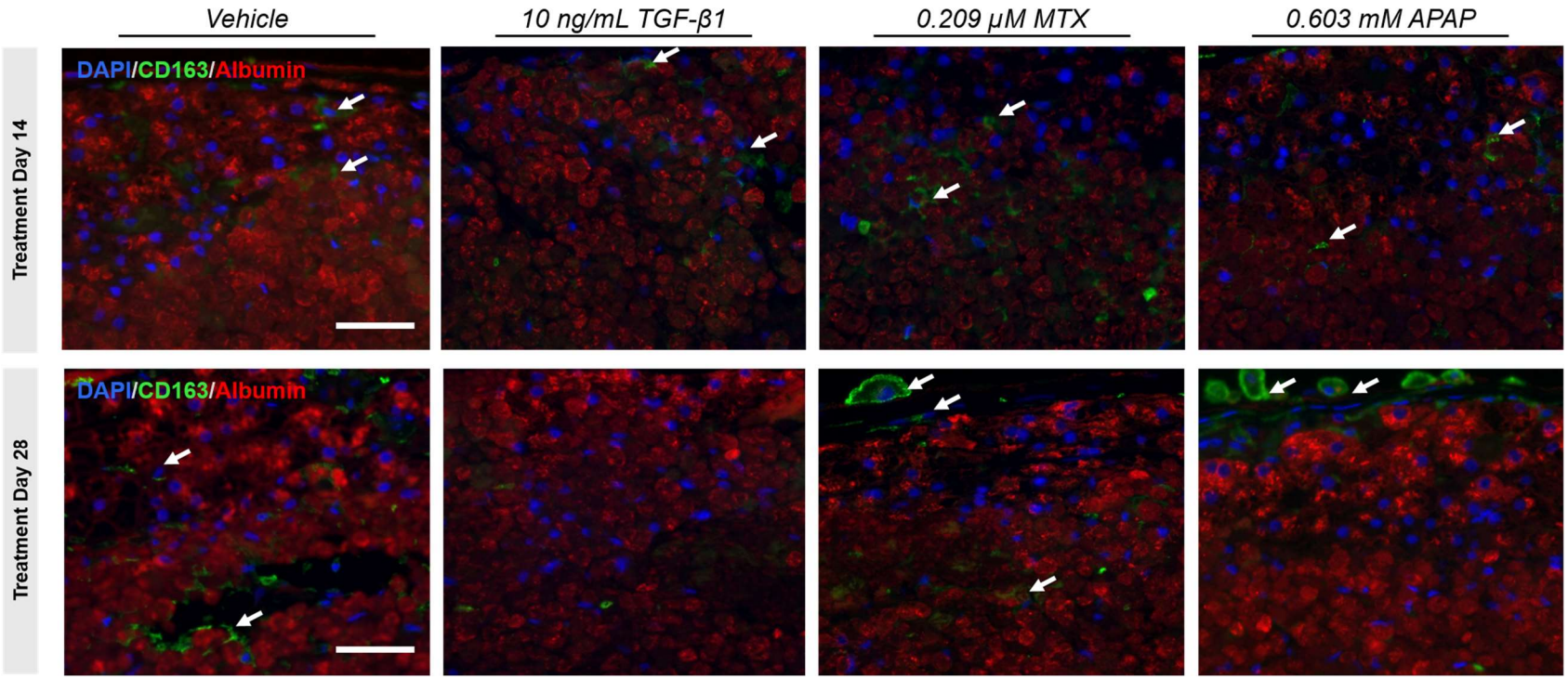

Figure A3.7 *CD163 and albumin staining at treatment day 14 and 28 for the modified tissue model (+KCs).* Mid and apical region of each tissue is shown. CD163-positive cells (white arrows) were localized in the apical region of the tissue in close association with ballooning hepatocytes and the fibrous capsule. Scale bar = 50 μm.

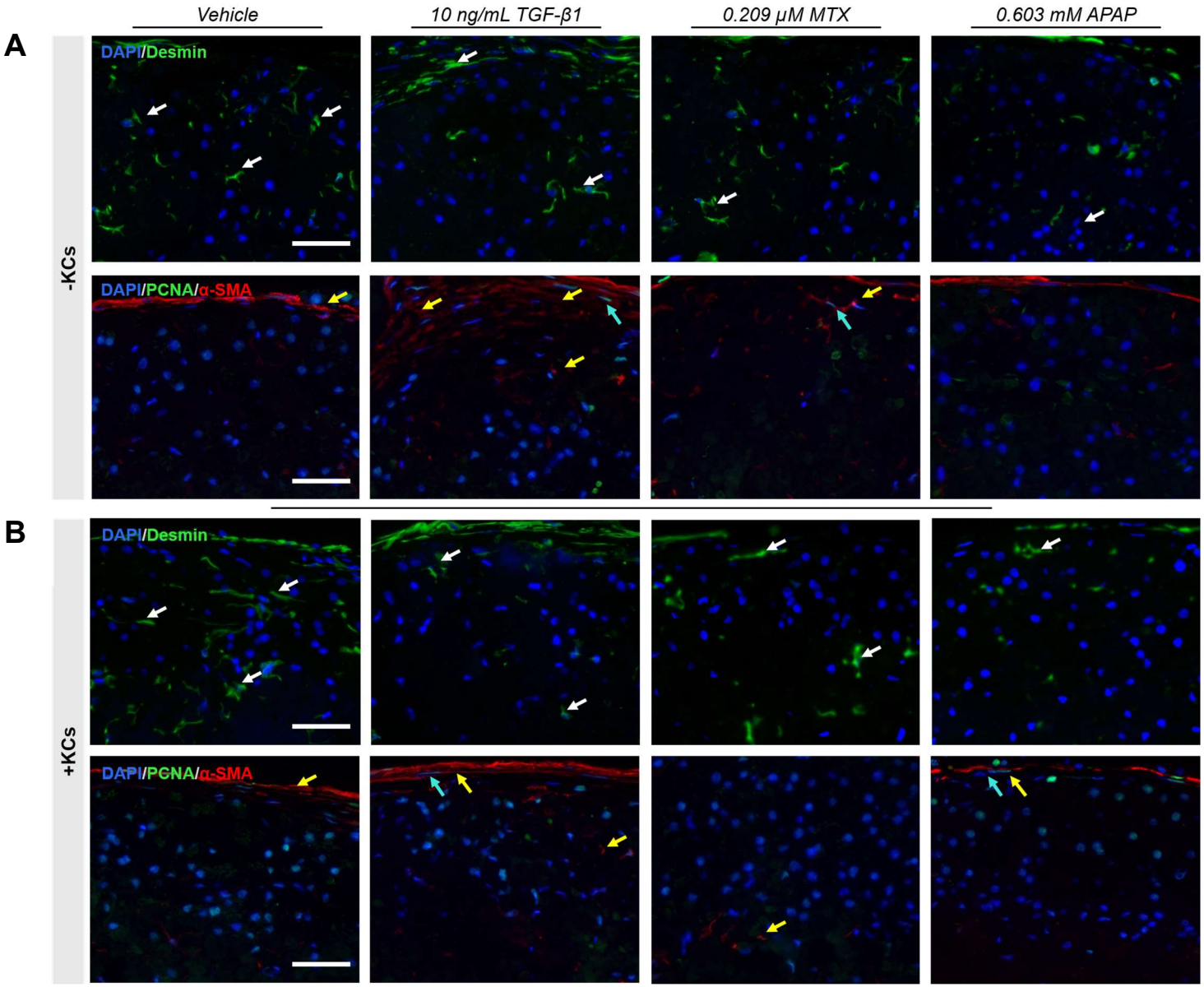
Vehicle
10 ng/mL TGF-β1
0.209 μM MTX
0.603 mM APAP
A
-KCs
DAPI/Desmin
DAPI/PCNA/α-SMA
B
+KCs
DAPI/Desmin
DAPI/PCNA/α-SMA

Figure A3.8 *Hepatic stellate cell activation status within treated tissues at treatment day 28.* White arrows denote desmin positive cells, teal arrows denote proliferating cell nuclear antigen (PCNA) positive cells, and yellow arrows denote α-smooth muscle actin (α-SMA) positive cells. Scale bar = 50 µm.

APPENDIX 4 – SUPPLEMENTAL DATA FOR CHAPTER 4

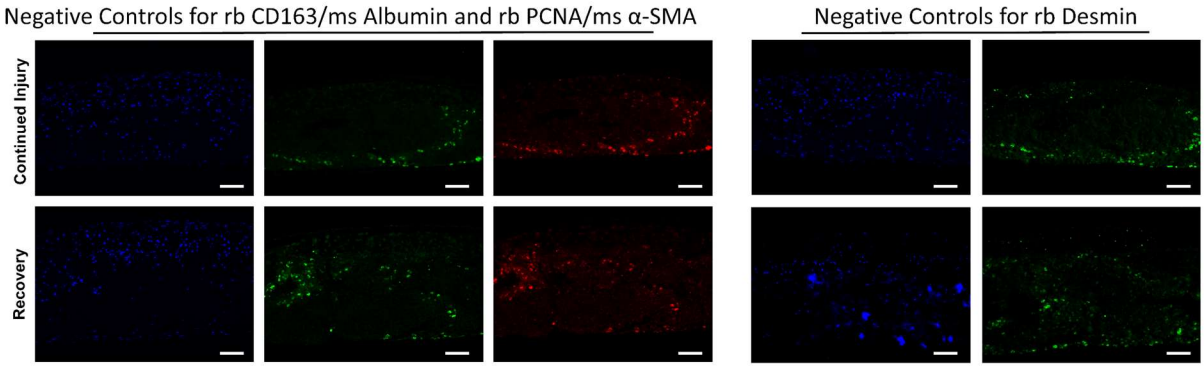

Figure A4.1 *Immunostaining results for negative control vehicle-treated tissue sections using secondary antibodies alone.* Parallel negative controls omitting primary antibody (conjugated secondary antibodies alone) showed some background autofluorescence in the emission channel for the secondary antibodies.

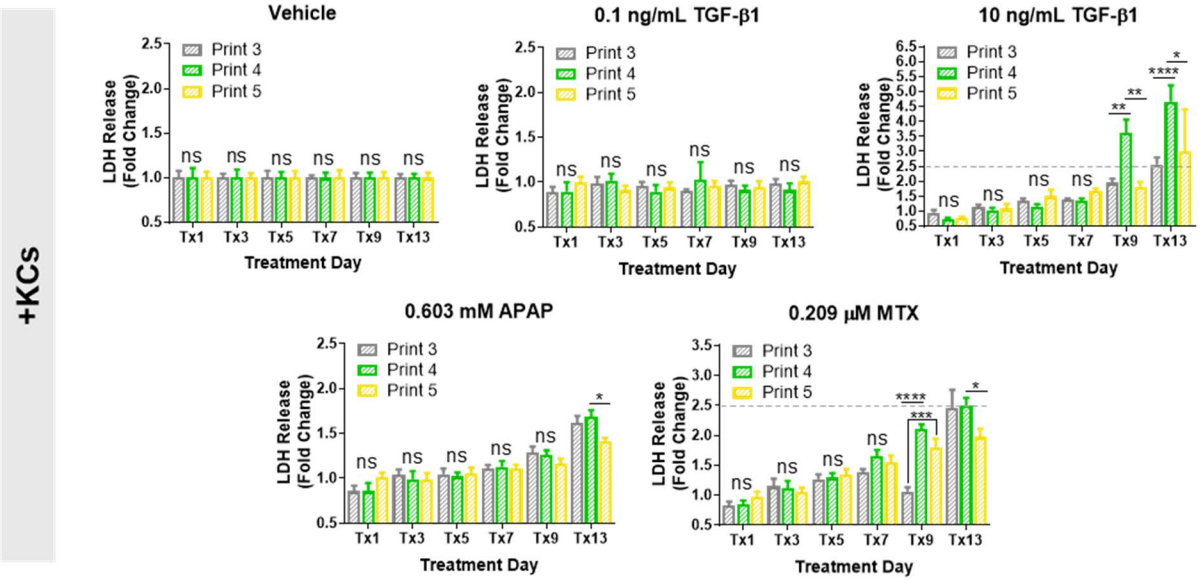

Figure A4.2. *Print-to-print consistency in LDH response profiles with historical prints*. Data represent the mean ± SEM; n = 7-10. Significance: Two-way ANOVA with post hoc Dunnett's multiple comparisons test (*p<0.05, **p<0.01, ***p<0.001, ****p<0.0001).

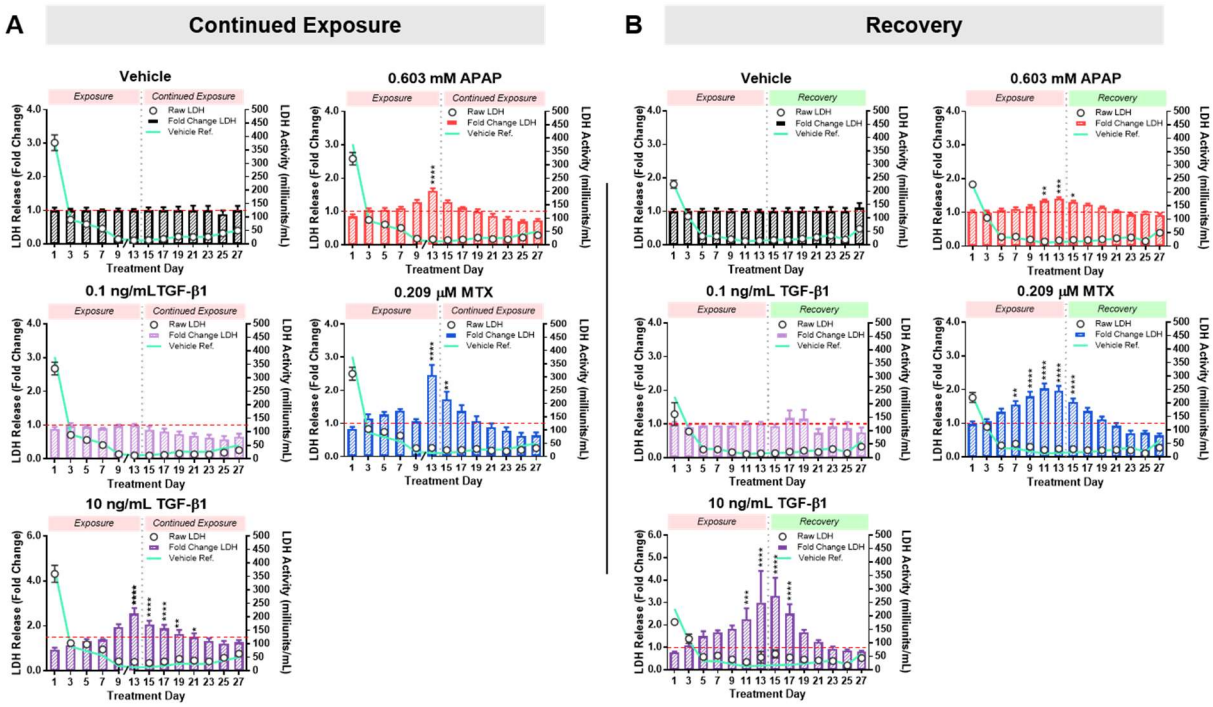

Figure A4.3 *Decrease in raw LDH release during the first 7 days of treatment regardless of tissue composition.* Data represent the mean ± SEM; n = 7-10. Significance: Two-way ANOVA with post hoc Dunnett's multiple comparisons test (*p<0.05, **p<0.01, ***p<0.001, ****p<0.0001).

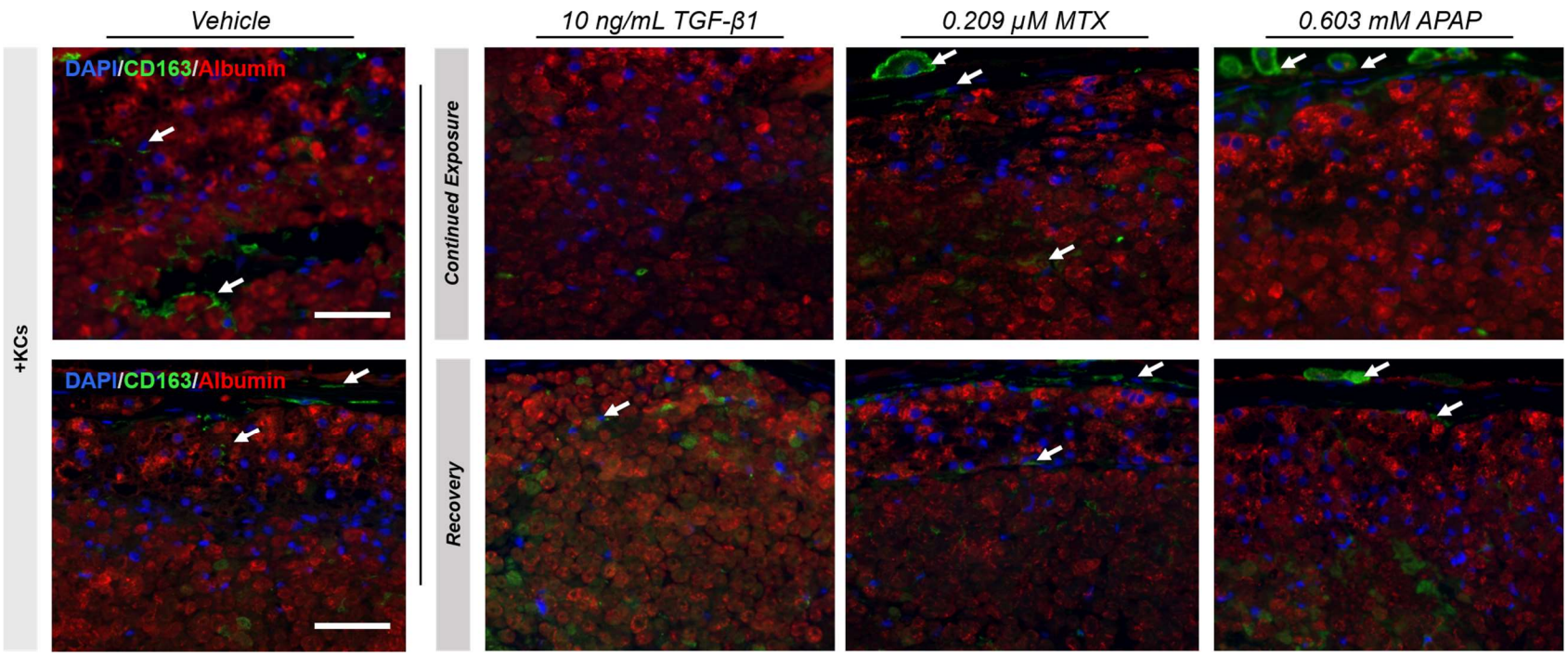

Figure A4.4 *CD163 and albumin staining at treatment day 28 for the modified tissue model (+KCs) following continued exposure or a recovery period.* Mid/apical region of each tissue is shown. CD163-positive cells (white arrows) were mainly localized in the apical region of the tissue in close association with ballooning hepatocytes and the fibrous capsule. Scale bar = 50 μm.

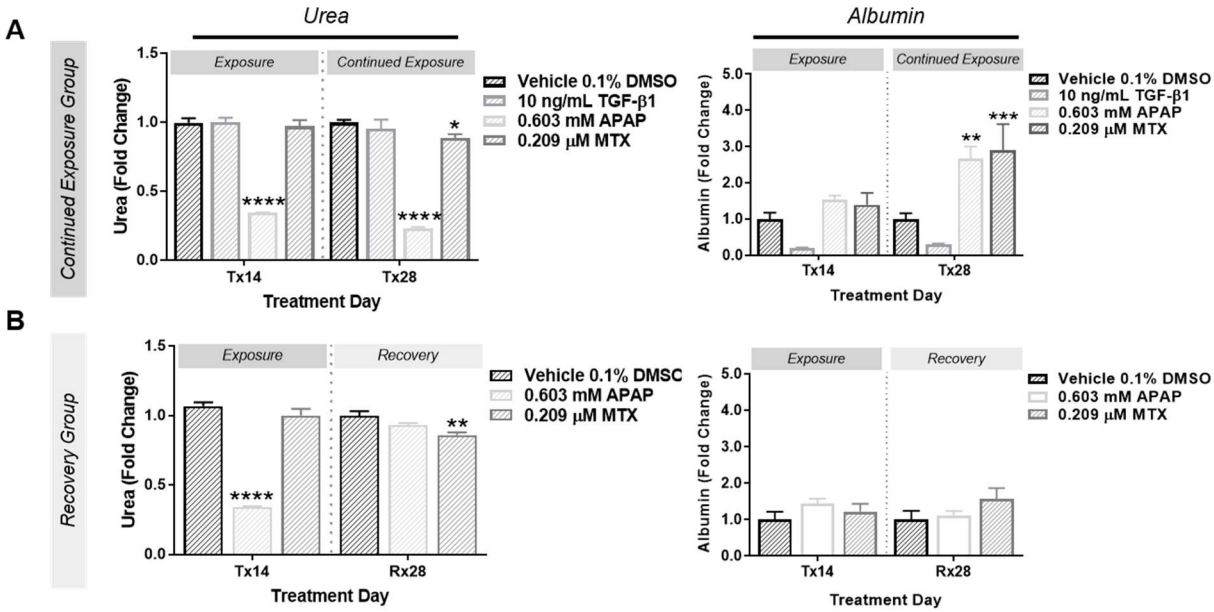

Figure A4.5 *Trends in urea and albumin output for the standard tissue model (-KCs) further suggests tissues retain the biochemical capacity to recover.* (A) Assessment of tissues that underwent continued exposure for 28 days. (B) Assessment of tissues that underwent a 14-day exposure followed by 14 days of recovery. Data represent the mean ± SEM; n = 5. Significance: Two-way ANOVA with post hoc Dunnett's multiple comparisons test (*p<0.05, **p<0.01, ***p<0.001, ****p<0.0001).

REFERENCES

Allyl Alcohol; CID=7858. from National Center for Biotechnology Information: https://pubchem.ncbi.nlm.nih.gov/compound/7858.

Carbon Tetrachloride; CID=5943. National Center for Biotechnology Information, PubChem Compound Database.

"Thioacetamide".(2000). TOXNET : toxicology data network. U.S. National Library of Medicine, Bethesda, MD.

Achilli, T.M., Meyer, J. and Morgan, J.R. (2012). Advances in the formation, use and understanding of multi-cellular spheroids. *Expert opinion on biological therapy,* **12,** 1347-1360.

Akhtar, T. and Sheikh, N. (2013). An overview of thioacetamide-induced hepatotoxicity. *Toxin Reviews,* **32,** 43-46.

Andersen, M.E., Al-Zoughool, M., Croteau, M., Westphal, M. and Krewski, D. (2010). The future of toxicity testing. *J Toxicol Environ Health B Crit Rev,* **13,** 163-196.

Andersen, M.E. and Krewski, D. (2010). The vision of toxicity testing in the 21st century: moving from discussion to action. *Toxicol Sci,* **117,** 17-24.

Ankley, G.T., Bennett, R.S., Erickson, R.J., Hoff, D.J., Hornung, M.W., Johnson, R.D., Mount, D.R., Nichols, J.W., Russom, C.L., Schmieder, P.K., Serrrano, J.A., Tietge, J.E. and Villeneuve, D.L. (2010). Adverse outcome pathways: a conceptual framework to support ecotoxicology research and risk assessment. *Environ Toxicol Chem,* **29,** 730-741.

Arpino, V., Brock, M. and Gill, S.E. (2015). The role of TIMPs in regulation of extracellular matrix proteolysis. *Matrix Biol,* **44-46,** 247-254.

Astashkina, A., Mann, B. and Grainger, D.W. (2012). A critical evaluation of *in vitro* cell culture models for high-throughput drug screening and toxicity. *Pharmacology & therapeutics,* **134,** 82-106.

Attallah, A.M., Mosa, T.E., Omran, M.M., Abo-Zeid, M.M., El-Dosoky, I. and Shaker, Y.M. (2007). Immunodetection of collagen types I, II, III, and IV for differentiation of liver fibrosis stages in patients with chronic HCV. *J Immunoassay Immunochem,* **28,** 155-168.

Baeck, C., Wehr, A., Karlmark, K.R., Heymann, F., Vucur, M., Gassler, N., Huss, S., Klussmann, S., Eulberg, D., Luedde, T., Trautwein, C. and Tacke, F. (2012). Pharmacological inhibition of the chemokine CCL2 (MCP-1) diminishes liver macrophage infiltration and steatohepatitis in chronic hepatic injury. *Gut,* **61,** 416-426.

Ballard, T.E., Wang, S., Cox, L.M., Moen, M.A., Krzyzewski, S., Ukairo, O. and Obach, R.S. (2016). Application of a Micropatterned Cocultured Hepatocyte System To Predict Preclinical and Human-Specific Drug Metabolism. *Drug Metab Dispos,* **44,** 172-179.

Baptista, P.M., Siddiqui, M.M., Lozier, G., Rodriguez, S.R., Atala, A. and Soker, S. (2011). The use of whole organ decellularization for the generation of a vascularized liver organoid. *Hepatology,* **53,** 604-617.

Barker, J., Horn, E.J., Lebwohl, M., Warren, R.B., Nast, A., Rosenberg, W. and Smith, C. (2011). Assessment and management of methotrexate hepatotoxicity in psoriasis patients: report from a consensus conference to evaluate current practice and identify key questions toward optimizing methotrexate use in the clinic. *J Eur Acad Dermatol Venereol,* **25,** 758-764.

Barros, M.H.M., Hauck, F., Dreyer, J.H., Kempkes, B. and Niedobitek, G. (2013). Macrophage Polarisation: an Immunohistochemical Approach for Identifying M1 and M2 Macrophages. *PLOS ONE,* **8,** e80908.

Bataller, R. and Brenner, D.A. (2005). Liver fibrosis. *Journal of Clinical Investigation,* **115,** 209-218.

Bell, C.C., Hendriks, D.F., Moro, S.M., Ellis, E., Walsh, J., Renblom, A., Fredriksson Puigvert, L., Dankers, A.C., Jacobs, F., Snoeys, J., Sison-Young, R.L., Jenkins, R.E., Nordling, A., Mkrtchian, S., Park, B.K., Kitteringham, N.R., Goldring, C.E., Lauschke, V.M. and Ingelman-Sundberg, M. (2016). Characterization of primary human hepatocyte spheroids as a model system for drug-induced liver injury, liver function and disease. *Sci Rep,* **6,** 25187.

Beninson, L.A. and Fleshner, M. (2014). Exosomes: an emerging factor in stress-induced immunomodulation. *Seminars in immunology,* **26,** 394-401.

Bhatia, S.N., Balis, U.J., Yarmush, M.L. and Toner, M. (1999). Effect of cell-cell interactions in preservation of cellular phenotype: cocultivation of hepatocytes and nonparenchymal cells. *FASEB Journal,* **13,** 1883-1900.

Bilzer, M., Roggel, F. and Gerbes, A.L. (2006). Role of Kupffer cells in host defense and liver disease. *Liver Int,* **26,** 1175-1186.

Bioulac-Sage, P., Le Bail, B. and Balabaud, C. (2008). Liver and Biliary Tract Histology In *Textbook of Hepatology*, pp. 9-19. Blackwell Publishing Ltd.

Bjorkman, D.J., Boschert, M., Tolman, K.G., Clegg, D.O. and Ward, J.R. (1993). The effect of long-term methotrexate therapy on hepatic fibrosis in rheumatoid arthritis. *Arthritis & Rheumatism,* **36,** 1697-1701.

Braet, F., De Zanger, R., Jans, D., Spector, I. and Wisse, E. (1996). Microfilament-disrupting agent latrunculin A induces and increased number of fenestrae in rat liver sinusoidal endothelial cells: comparison with cytochalasin B. *Hepatology,* **24,** 627-635.

Busso, N., Chesne, C., Delers, F., Morel, F. and Guillouzo, A. (1990). Transforming growth-factor-β (TGF-β) inhibits albumin synthesis in normal human hepatocytes and in hepatoma HepG2 cells. *Biochemical and Biophysical Research Communications,* **171,** 647-654.

Campion, S.N., Johnson, R., Aleksunes, L.M., Goedken, M.J., van Rooijen, N., Scheffer, G.L., Cherrington, N.J. and Manautou, J.E. (2008). Hepatic Mrp4 induction following acetaminophen exposure is dependent on Kupffer cell function. *Am J Physiol Gastrointest Liver Physiol,* **295,** G294-304.

Canbay, A., Friedman, S. and Gores, G.J. (2004). Apoptosis: the nexus of liver injury and fibrosis. *Hepatology,* **39,** 273-278.

Carpino, G., Morini, S., Ginanni Corradini, S., Franchitto, A., Merli, M., Siciliano, M., Gentili, F., Onetti Muda, A., Berloco, P., Rossi, M., Attili, A.F. and Gaudio, E. (2005). Alpha-SMA expression in hepatic stellate cells and quantitative analysis of hepatic fibrosis in cirrhosis and in recurrent chronic hepatitis after liver transplantation. *Dig Liver Dis,* **37,** 349-356.

Chávez, E., Alcantar, L.K., Moreno, M.G. and Muriel, P. (2006). Gadolinium chloride inhibits the spontaneous resolution of fibrosis in CCl4-induced cirrhosis. *Toxicology Mechanisms and Methods,* **16,** 507-513.

Chen, C.Z. and Raghunath, M. (2009). Focus on collagen: *in vitro* systems to study fibrogenesis and antifibrosis-state of the art. *Fibrogenesis & Tissue Repair,* **2,** 7.

Chilakapati, J., Shankar, K., Korrapati, M.C., Hill, R.A. and Mehendale, H.M. (2005). Saturation toxicokinetics of thioacetamide: role in initiation of liver injury. *Drug Metab Dispos,* **33,** 1877-1885.

Choi, I., Kang, H.S., Yang, Y. and Pyun, K.H. (1994). IL-6 induced hepatic inflammation and collagen synthesis in vitro. *Clin Exp Immunol,* **95,** 530-535.

Chu, X., Bleasby, K. and Evers, R. (2013). Species differences in drug transporters and implications for translating preclinical findings to humans. *Expert Opinion on Drug Metabolism & Toxicology,* **9,** 237-252.

Cogger, V.C., Muller, M., Fraser, R., McLean, A.J., Khan, J. and Le Couteur, D.G. (2004). The effects of oxidative stress on the liver sieve. *J Hepatol,* **41,** 370-376.

Cox, T.R. and Erler, J.T. (2011). Remodeling and homeostasis of the extracellular matrix: implications for fibrotic diseases and cancer. *Disease Models and Mechanisms,* **4,** 165-178.

Crespo Yanguas, S., Cogliati, B., Willebrords, J., Maes, M., Colle, I., van den Bossche, B., de Oliveira, C.P.M.S., Andraus, W., Alves, V.A., Leclercq, I. and Vinken, M. (2016). Experimental models of liver fibrosis. *Archives of Toxicology,* **90,** 1025-1048.

Cronstein, B.N. (2005). Low-dose Methotrexate: A mainstay in the treatment of rheumatoid arthritis. *Pharmacological reviews,* **57,** 163-172.

Czaja, A.J. (2014). Hepatic inflammation and progressive liver fibrosis in chronic liver disease. *World J Gastroenterol,* **20,** 2515-2532.

Davila, J.C., Rodriguez, R.J., Melchert, R.B. and Acosta Jr, D. (1998). Predictive value of in vitro model systems in toxicology. *Annual review of pharmacology and toxicology,* **38,** 63-96.

de Graaf, I.A., Groothuis, G.M. and Olinga, P. (2007). Precision-cut tissue slices as a tool to predict metabolism of novel drugs. *Expert Opinion on Drug Metabolism & Toxicology,* **3,** 879-898.

De Maio, A. (2011). Extracellular heat shock proteins, cellular export vesicles, and the Stress Observation System: a form of communication during injury, infection, and cell damage. *Cell stress & chaperones,* **16,** 235-249.

De Minicis, S., Seki, E., Uchinami, H., Kluwe, J., Zhang, Y., Brenner, D.A. and Schwabe, R.F. (2007). Gene expression profiles during hepatic stellate cell activation in culture and in vivo. *Gastroenterology,* **132,** 1937-1946.

DeLeve, L.D.(2011). *Vascular liver disease and the liver sinusoidal endothelial cells* Springer.

Deleve, L.D., Wang, X. and Guo, Y. (2008). Sinusoidal endothelial cells prevent rat stellate cell activation and promote reversion to quiescence. *Hepatology,* **48,** 920-930.

Deleve, L.D., Wang, X., Hu, L., McCuskey, M.K. and McCuskey, R.S. (2004). Rat liver sinusoidal endothelial phenotype is maintained by paracrine and autocrine regulation. *Am J Physiol Gastrointest Liver Physiol,* **287,** G757-G763.

Dilworth, C., Hamilton, G.A., George, E. and Timbrell, J.A. (2000). The use of liver spheroids as an in vitro model for studying induction of the stress response as a marker of chemical toxicity. *Toxicol In Vitro,* **14,** 169-176.

Domansky, K., Inman, W., Serdy, J., Dash, A., Lim, M.H. and Griffith, L.G. (2010). Perfused multiwell plate for 3D liver tissue engineering. *Lab Chip,* **10,** 51-58.

Dooley, S. and ten Dijke, P. (2012). TGF-β in progression of liver disease. *Cell and Tissue Research,* **347,** 245-256.

Dranoff, J.A. and Wells, R.G. (2010). Portal fibroblasts: Underappreciated mediators of biliary fibrosis. *Hepatology,* **51,** 1438-1444.

Duffield, J.S., Forbes, S.J., Constandinou, C.M., Clay, S., Partolina, M., Vuthoori, S., Wu, S., Lang, R. and Iredale, J.P. (2005). Selective depletion of macrophages reveals distinct, opposing roles during liver injury and repair. *The Journal of Clinical Investigation,* **115,** 56-65.

Ebrahimkhani, M.R., Neiman, J.A., Raredon, M.S., Hughes, D.J. and Griffith, L.G. (2014). Bioreactor technologies to support liver function in vitro. *Advanced drug delivery reviews,* **69-70,** 132-157.

Ekataksin, W. and Kaneda, K. (1999). Liver microvascular architecture: an insight into the pathophysiology of portal hypertension. *Seminars in liver disease,* **19,** 359-382.

Ellis, E.L. and Mann, D.A. (2012). Clinical evidence for the regression of liver fibrosis. *Journal of Hepatology,* **56,** 1171-1180.

Elvevold, K., Smedsrod, B. and Martinez, I. (2008). The liver sinusoidal endothelial cell: a cell type of controversial and confusing identity. *Am J Physiol Gastrointest Liver Physiol,* **294,** G391-400.

Fabriek, B.O., Dijkstra, C.D. and van den Berg, T.K. (2005). The macrophage scavenger receptor CD163. *Immunobiology,* **210,** 153-160.

Fallowfield, J.A., Mizuno, M., Kendall, T.J., Constandinou, C.M., Benyon, R.C., Duffield, J.S. and Iredale, J.P. (2007). Scar-associated macrophages are a major source of hepatic matrix metalloproteinase-13 and facilitate the resolution of murine hepatic fibrosis. *The Journal of Immunology,* **178,** 5288-5295.

Ferslew, B.C. and Brouwer, K.L. (2014). Identification of hepatic phospholipidosis inducers in sandwich-cultured rat hepatocytes, a physiologically relevant model, reveals altered basolateral uptake and biliary excretion of anionic probe substrates. *Toxicol Sci,* **139,** 99-107.

Fogel-Petrovic, M., Long, J.A., Misso, N.L., Foster, P.S., Bhoola, K.D. and Thompson, P.J. (2007). Physiological concentrations of transforming growth factor beta1 selectively inhibit human dendritic cell function. *Int Immunopharmacol,* **7,** 1924-1933.

Forbes, S.J. and Parola, M. (2011). Liver fibrogenic cells. *Best Practice & Research Clinical Gastroenterology,* **25,** 207-217.

Forgacs, G., Jakab, K., Neagu, A. and Mironov, V.(2012). Self-assembling cell aggregates and methods of making engineered tissue using the same. Google Patents.

Forgacs, G., Jakab, K., Neagu, A. and Mironov, V.(2014). Self-assembling cell aggregates and methods of making engineered tissue using the same. Google Patents.

Fraser, R., Dobbs, B.R. and Rogers, G.W. (1995). Lipoproteins and the liver sieve: the role of the fenestrated sinusoidal endothelium in lipoprotein metabolism, atherosclerosis, and cirrhosis. *Hepatology,* **21,** 863-874.

Friedman, S.L. (2000). Molecular regulation of hepatic fibrosis, an integrated cellular response to tissue injury. *The Journal of biological chemistry,* **275,** 2247-2250.

Friedman, S.L. (2008). Hepatic stellate cells: protean, multifunctional, and enigmatic cells of the liver. *Physiol Rev,* **88,** 125-172.

Friedman, S.L. (2012). Fibrogenic cell reversion underlies fibrosis regression in liver. *Proceedings of the National Academy of Sciences,* **109,** 9230-9231.

Friedman, S.L. (2013). Liver fibrosis- from bench to bedside. *Journal of Hepatology,* **38,** 38-53.

Friedman, S.L. and Bansal, M.B. (2006). Reversal of hepatic fibrosis — Fact or fantasy? *Hepatology,* **43,** S82-S88.

Gebhardt, R. (1992). Metabolic zonation of the liver: regulation and implications for liver function. *Pharmacology & therapeutics,* **53,** 275-354.

Gieling, R.G., Wallace, K. and Han, Y.P. (2009). Interleukin-1 participates in the progression from liver injury to fibrosis. *Am J Physiol Gastrointest Liver Physiol,* **296,** G1324-1331.

Godoy, P., Hewitt, N.J., Albrecht, U., Andersen, M.E., Ansari, N., Bhattacharya, S., Bode, J.G., Bolleyn, J., Borner, C., Bottger, J., Braeuning, A., Budinsky, R.A., Burkhardt, B., Cameron, N.R., Camussi, G., Cho, C.S., Choi, Y.J., Craig Rowlands, J., Dahmen, U., Damm, G., Dirsch, O., Donato, M.T., Dong, J., Dooley, S., Drasdo, D., Eakins, R., Ferreira, K.S., Fonsato, V., Fraczek, J., Gebhardt, R., Gibson, A., Glanemann, M., Goldring, C.E., Gomez-Lechon, M.J., Groothuis, G.M., Gustavsson, L., Guyot, C., Hallifax, D., Hammad, S., Hayward, A., Haussinger, D., Hellerbrand, C., Hewitt, P., Hoehme, S., Holzhutter, H.G., Houston, J.B., Hrach, J., Ito, K., Jaeschke, H., Keitel, V., Kelm, J.M., Kevin Park, B., Kordes, C., Kullak-Ublick, G.A., LeCluyse, E.L., Lu, P., Luebke-Wheeler, J., Lutz, A., Maltman, D.J., Matz-Soja, M., McMullen, P., Merfort, I., Messner, S., Meyer, C., Mwinyi, J., Naisbitt, D.J., Nussler, A.K., Olinga, P., Pampaloni, F., Pi, J., Pluta, L., Przyborski, S.A., Ramachandran, A., Rogiers, V., Rowe, C., Schelcher, C., Schmich, K., Schwarz, M., Singh, B., Stelzer, E.H., Stieger, B., Stober, R., Sugiyama, Y., Tetta, C., Thasler, W.E., Vanhaecke, T., Vinken, M., Weiss, T.S., Widera, A., Woods, C.G., Xu, J.J., Yarborough, K.M. and Hengstler, J.G. (2013). Recent advances in 2D and 3D in vitro systems using primary hepatocytes, alternative hepatocyte sources and non-parenchymal liver cells and their use in investigating mechanisms of hepatotoxicity, cell signaling and ADME. *Arch Toxicol,* **87,** 1315-1530.

Gressner, A.M., Gao, C.F. and Gressner, O.A. (2009). Non-invasive biomarkers for monitoring the fibrogenic process in liver: a short survey. *World J Gastroenterol,* **15,** 2433-2440.

Gressner, A.M. and Weiskirchen, R. (2006). Modern pathogenetic concepts of liver fibrosis suggest stellate cells and TGF-β as major players and therapeutic targets. *Journal of Cellular and Molecular Medicine,* **10,** 76-99.

Guillouzo, A., Morel, F., Fardel, O. and Meunier, B. (1993). Use of human hepatocyte cultures for drug metabolism studies. *Toxicology,* **82,** 209-219.

Gutiérrez-Ruiz, M.C. and Gómez-Quiroz, L.E. (2007). Liver fibrosis: searching for cell model answers. *Liver International,* **27,** 434-439.

Hajovsky, H., Hu, G., Koen, Y., Sarma, D., Cui, W., Moore, D.S., Staudinger, J.L. and Hanzlik, R.P. (2012). Metabolism and toxicity of thioacetamide and thioacetamide S-oxide in rat hepatocytes. *Chem Res Toxicol,* **25,** 1955-1963.

Hammond, J.S., Beckingham, I.J. and Shakesheff, K.M. (2006). Scaffolds for liver tissue engineering. *Expert Review of Medical Devices,* **3,** 21-27.

Han, D., Dara, L., Win, S., Than, T.A., Yuan, L., Abbasi, S.Q., Liu, Z.-X. and Kaplowitz, N. (2013). Regulation of drug-induced liver injury by signal transduction pathways: critical role of mitochondria. *Trends in Pharmacological Sciences,* **34,** 243-253.

Hang, T.C., Lauffenburger, D.A., Griffith, L.G. and Stolz, D.B. (2012). Lipids promote survival, proliferation, and maintenance of differentiation of rat liver sinusoidal endothelial cells in vitro. *Am J Physiol Gastrointest Liver Physiol,* **302,** G375-388.

Hernandez-Gea, V. and Friedman, S.L. (2011). Pathogenesis of liver fibrosis. *Annu Rev Pathol,* **6,** 425-456.

Hinz, B. (2013). It has to be the alpha v: myofibroblast integrins activate latent TGF-beta1. *Nat Med,* **19,** 1567-1568.

Hoebe, K.H., Witkamp, R.F., Fink-Gremmels, J., Van Miert, A.S. and Monshouwer, M. (2001). Direct cell-to-cell contact between Kupffer cells and hepatocytes augments endotoxin-induced hepatic injury. *Am J Physiol Gastrointest Liver Physiol,* **280,** G720-728.

Horvat, T., Landesmann, B., Lostia, A., Vinken, M., Munn, S. and Whelan, M. (2017). Adverse outcome pathway development from protein alkylation to liver fibrosis. *Archives of Toxicology,* **91,** 1523-1543.

Ide, M., Kuwamura, M., Kotani, T., Sawamoto, O. and Yamate, J. (2005). Effects of gadolinium chloride (GdCl3) on the appearance of macrophage populations and fibrogenesis in thioacetamide-induced rat hepatic lesions. *Journal of Comparative Pathology,* **133,** 92-102.

Iredale, J.P. (2007). Models of liver fibrosis: exploring the dynamic nature of inflammation and repair in a solid organ. *The Journal of Clinical Investigation,* **117,** 539-548.

Iredale, J.P., Benyon, R.C., Pickering, J., McCullen, M., Northrop, M., Pawley, S., Hovell, C. and Arthur, M.J. (1998). Mechanisms of spontaneous resolution of rat liver fibrosis. Hepatic stellate cell apoptosis and reduced hepatic expression of metalloproteinase inhibitors. *The Journal of Clinical Investigation,* **102,** 538-549.

Ito, R., Takahashi, T., Katano, I. and Ito, M. (2012). Current advances in humanized mouse models. *Cellular and Molecular Immunology,* **9,** 208-214.

Ito, Y., Bethea, N.W., Abril, E.R. and McCuskey, R.S. (2003). Early hepatic microvascular injury in response to acetaminophen toxicity. *Microcirculation (New York, N.Y. : 1994),* **10,** 391-400.

Iwaisako, K., Jiang, C., Zhang, M., Cong, M., Moore-Morris, T.J., Park, T.J., Liu, X., Xu, J., Wang, P., Paik, Y.H., Meng, F., Asagiri, M., Murray, L.A., Hofmann, A.F., Iida, T., Glass, C.K., Brenner, D.A. and Kisseleva, T. (2014). Origin of myofibroblasts in the fibrotic liver in mice. *Proc Natl Acad Sci U S A,* **111,** E3297-3305.

Jackson, M.J., Beaudet, A.L. and O'Brien, W.E. (1986). Mammalian urea cycle enzymes. *Annual review of genetics,* **20,** 431-464.

Jaeschke, H. (2008). Kupffer Cells In *Textbook of Hepatology*, pp. 36-42. Blackwell Publishing Ltd.

Jaeschke, H., McGill, M.R. and Ramachandran, A. (2012). Oxidant stress, mitochondria, and cell death mechanisms in drug-induced liver injury: Lessons learned from acetaminophen hepatotoxicity. *Drug metabolism reviews,* **44,** 88-106.

Jakab, K., Norotte, C., Damon, B., Marga, F., Neagu, A., Besch-Williford, C.L., Kachurin, A., Church, K.H., Park, H., Mironov, V., Markwald, R., Vunjak-Novakovic, G. and Forgacs, G. (2008). Tissue engineering by self-assembly of cells printed into topologically defined structures. *Tissue engineering. Part A,* **14,** 413-421.

Jakab, K., Norotte, C., Marga, F., Murphy, K., Vunjak-Novakovic, G. and Forgacs, G. (2010). Tissue engineering by self-assembly and bio-printing of living cells. *Biofabrication,* **2,** 022001.

Jameel, N.M., Thirunavukkarasu, C., Murase, N., Cascio, M., Prelich, J., Yang, S., Harvey, S.A. and Gandhi, C.R. (2010). Constitutive release of powerful antioxidant-scavenging activity by hepatic stellate cells: protection of hepatocytes from ischemia/reperfusion injury. *Liver Transpl,* **16,** 1400-1409.

Ju, C. and Pohl, L.R. (2005). Tolerogenic role of Kupffer cells in immune-mediated adverse drug reactions. *Toxicology,* **209,** 109-112.

Ju, C., Reilly, T.P., Bourdi, M., Radonovich, M.F., Brady, J.N., George, J.W. and Pohl, L.R. (2002). Protective role of kupffer cells in acetaminophen-induced hepatic injury in mice. *Chemical Research in Toxicology,* **15,** 1504-1513.

Ju, C. and Tacke, F. (2016). Hepatic macrophages in homeostasis and liver diseases: from pathogenesis to novel therapeutic strategies. *Cell Mol Immunol*.

Judson, R., Richard, A., Dix, D.J., Houck, K., Martin, M., Kavlock, R., Dellarco, V., Henry, T., Holderman, T., Sayre, P., Tan, S., Carpenter, T. and Smith, E. (2009). The toxicity data landscape for environmental chemicals. *Environmental health perspectives,* **117,** 685-695.

Kalinichenko, V.V., Bhattacharyya, D., Zhou, Y., Gusarova, G.A., Kim, W., Shin, B. and Costa, R.H. (2003). Foxf1 +/− mice exhibit defective stellate cell activation and abnormal liver regeneration following CCl4 injury. *Hepatology,* **37,** 107-117.

Khatiwala, C., Law, R., Shepherd, B., Dorfman, S. and Csete, M. (2012). 3D Cell Bioprinting for Regenerative Medicine Research and Therapies. *Gene Therapy and Regulation,* **7,** 1230004.

Khetani, S.R. and Bhatia, S.N. (2008). Microscale culture of human liver cells for drug development. *Nature biotechnology,* **26,** 120-126.

Khetani, S.R., Kanchagar, C., Ukairo, O., Krzyzewski, S., Moore, A., Shi, J., Aoyama, S., Aleo, M. and Will, Y. (2013). Use of micropatterned cocultures to detect compounds that cause drug-induced liver injury in humans. *Toxicol Sci,* **132,** 107-117.

Kia, R., Kelly, L., Sison-Young, R.L.C., Zhang, F., Pridgeon, C.S., Heslop, J.A., Metcalfe, P., Kitteringham, N.R., Baxter, M., Harrison, S., Hanley, N.A., Burke, Z.D., Storm, M.P., Welham, M.J., Tosh, D., Küppers-Munther, B., Edsbagge, J., Starkey Lewis, P.J., Bonner, F., Harpur, E., Sidaway, J., Bowes, J., Fenwick, S.W., Malik, H., Goldring, C.E.P. and Park, B.K. (2015). MicroRNA-122: A novel hepatocyte-enriched *in vitro* marker of drug-induced cellular toxicity. *Toxicological Sciences,* **144,** 173-185.

Kim, S., Thiessen, P.A., Bolton, E.E., Chen, J., Fu, G., Gindulyte, A., Han, L., He, J., He, S., Shoemaker, B.A., Wang, J., Yu, B., Zhang, J. and Bryant, S.H. (2016). PubChem Substance and Compound databases. *Nucleic acids research,* **44,** D1202-1213.

Kisseleva, T., Cong, M., Paik, Y., Scholten, D., Jiang, C., Benner, C., Iwaisako, K., Moore-Morris, T., Scott, B., Tsukamoto, H., Evans, S.M., Dillmann, W., Glass, C.K. and Brenner, D.A. (2012). Myofibroblasts revert to an inactive phenotype during regression of liver fibrosis. *Proc Natl Acad Sci U S A,* **109,** 9448-9453.

Klaassen, C.D., Casarett, L.J. and Doull, J.(2013). *Casarett and Doull's toxicology the basic science of poisons,* McGraw-Hill Education, New York.

Kmiec, Z. (2001). Cooperation of liver cells in health and disease. *Advances in anatomy, embryology, and cell biology,* **161,** 1-151.

Knudsen, T.B., Keller, D.A., Sander, M., Carney, E.W., Doerrer, N.G., Eaton, D.L., Fitzpatrick, S.C., Hastings, K.L., Mendrick, D.L., Tice, R.R., Watkins, P.B. and Whelan, M. (2015). FutureTox II: *In vitro* data and *in silico* models for predictive toxicology. *Toxicological Sciences,* **143,** 256-267.

Kolios, G., Valatas, V. and Kouroumalis, E. (2006). Role of Kupffer cells in the pathogenesis of liver disease. *World J Gastroenterol,* **12,** 7413-7420.

Kondo, K., Yamada, N., Suzuki, Y., Toyoda, K., Hashimoto, T., Takahashi, A., Kobayashi, A., Shoda, T., Kuno, H. and Sugai, S. (2012). Enhancement of acetaminophen-induced chronic hepatotoxicity in restricted fed rats: a nonclinical approach to acetaminophen-induced chronic hepatotoxicity in susceptible patients. *The Journal of Toxicological Sciences,* **37,** 911-929.

Kong, X., Horiguchi, N., Mori, M. and Gao, B. (2012). Cytokines and STATs in Liver Fibrosis. *Frontiers in Physiology,* **3**.

Kostadinova, R., Boess, F., Applegate, D., Suter, L., Weiser, T., Singer, T., Naughton, B. and Roth, A. (2013). A long-term three dimensional liver co-culture system for improved prediction of clinically relevant drug-induced hepatotoxicity. *Toxicology and applied pharmacology,* **268,** 1-16.

Krenkel, O. and Tacke, F. (2017). Liver macrophages in tissue homeostasis and disease. *Nat Rev Immunol*.

Krewski, D., Acosta, D., Jr., Andersen, M., Anderson, H., Bailar, J.C., 3rd, Boekelheide, K., Brent, R., Charnley, G., Cheung, V.G., Green, S., Jr., Kelsey, K.T., Kerkvliet, N.I., Li, A.A., McCray, L., Meyer, O., Patterson, R.D., Pennie, W., Scala, R.A., Solomon, G.M., Stephens, M., Yager, J. and Zeise, L. (2010). Toxicity testing in the 21st century: a vision and a strategy. *Journal of toxicology and environmental health. Part B, Critical reviews,* **13,** 51-138.

Landesmann, B.(2016). *Adverse Outcome Pathway on Protein Alkylation Leading to Liver Fibrosis,* OECD Publishing.

Landesmann, B., Mennecozzi, M., Berggren, E. and Whelan, M. (2013). Adverse outcome pathway-based screening strategies for an animal-free safety assessment of chemicals. *Alternatives to laboratory animals : ATLA,* **41,** 461-471.

Leask, A. and Abraham, D.J. (2004). TGF-beta signaling and the fibrotic response. *FASEB J,* **18,** 816-827.

LeCluyse, E.L., Witek, R.P., Andersen, M.E. and Powers, M.J. (2012). Organotypic liver culture models: meeting current challenges in toxicity testing. *Crit Rev Toxicol,* **42,** 501-548.

Lee, U.E. and Friedman, S.L. (2011). Mechanisms of hepatic fibrogenesis. *Best Pract Res Clin Gastroenterol,* **25,** 195-206.

Leite, S.B., Roosens, T., El Taghdouini, A., Mannaerts, I., Smout, A.J., Najimi, M., Sokal, E., Noor, F., Chesne, C. and van Grunsven, L.A. (2016). Novel human hepatic organoid model enables testing of drug-induced liver fibrosis in vitro. *Biomaterials,* **78,** 1-10.

Liedtke, C., Luedde, T., Sauerbruch, T., Scholten, D., Streetz, K., Tacke, F., Tolba, R., Trautwein, C., Trebicka, J. and Weiskirchen, R. (2013). Experimental liver fibrosis research: update on animal models, legal issues and translational aspects. *Fibrogenesis & Tissue Repair,* **6,** 1-24.

Lin, C., Shi, J., Moore, A. and Khetani, S.R. (2016). Prediction of Drug Clearance and Drug-Drug Interactions in Microscale Cultures of Human Hepatocytes. *Drug Metab Dispos,* **44,** 127-136.

Lindros, K.O. (1997). Zonation of cytochrome P450 expression, drug metabolism and toxicity in liver. *General pharmacology,* **28,** 191-196.

Lindsay, K., Fraser, A.D., Layton, A., Goodfield, M., Gruss, H. and Gough, A. (2009). Liver fibrosis in patients with psoriasis and psoriatic arthritis on long-term, high cumulative dose methotrexate therapy. *Rheumatology (Oxford),* **48,** 569-572.

Liu, X., Xu, J., Brenner, D.A. and Kisseleva, T. (2013). Reversibility of Liver Fibrosis and Inactivation of Fibrogenic Myofibroblasts. *Current Pathobiology Reports,* **1,** 209-214.

Lozano, R., Naghavi, M., Foreman, K., Lim, S. and Shibuya, K. (2012). Global and regional mortality from 235 causes of death for 20 age groups in 1990 and 2010: A systematic analysis for the Global Burden of Disease Study 2010. *Lancet,* **380,** 2095-2128.

Lu, J., Einhorn, S., Venkatarangan, L., Miller, M., Mann, D.A., Watkins, P.B. and LeCluyse, E. (2015). Morphological and functional characterization and assessment of iPSC-derived hepatocytes for *in vitro* toxicity Testing. *Toxicol Sci,* **147,** 39-54.

Maemura, K., Zheng, Q., Wada, T., Ozaki, M., Takao, S., Aikou, T., Bulkley, G.B., Klein, A.S. and Sun, Z. (2005). Reactive oxygen species are essential mediators in antigen presentation by Kupffer cells. *Immunol Cell Biol,* **83,** 336-343.

Marcellin, P., Gane, E., Buti, M., Afdhal, N., Sievert, W., Jacobson, I.M., Washington, M.K., Germanidis, G., Flaherty, J.F., Schall, R.A., Bornstein, J.D., Kitrinos, K.M., Subramanian, G.M., McHutchison, J.G. and Heathcote, E.J. (2013). Regression of cirrhosis during treatment with tenofovir disoproxil fumarate for chronic hepatitis B: a 5-year open-label follow-up study. *The Lancet,* **381,** 468-475.

Martignoni, M., Groothuis, G.M. and de Kanter, R. (2006). Species differences between mouse, rat, dog, monkey and human CYP-mediated drug metabolism, inhibition and induction. *Expert Opin Drug Metab Toxicol,* **2,** 875-894.

Matsukura, S., Odaka, M., Kurokawa, M., Kuga, H., Homma, T. and al., e. (2010). Tranforming growth factor-B stimulates the expression of eotaxin/CC chemokine ligand 11 and its promoter activity through binding site for nuclear factor-kB in airway smooth muscle cells. *Clin Exp Allergy,* **40,** 763-771.

Maybury, C.M., Jabbar-Lopez, Z.K., Wong, T., Dhillon, A.P., Barker, J.N. and Smith, C.H. (2014). Methotrexate and liver fibrosis in people with psoriasis: a systematic review of observational studies. *Br J Dermatol,* **171,** 17-29.

McGill, M.R., Williams, C.D., Xie, Y., Ramachandran, A. and Jaeschke, H. (2012). Acetaminophen-induced liver injury in rats and mice: comparison of protein adducts, mitochondrial dysfunction, and oxidative stress in the mechanism of toxicity. *Toxicology and applied pharmacology,* **264,** 387-394.

Mederacke, I., Hsu, C.C., Troeger, J.S., Huebener, P., Mu, X., Dapito, D.H., Pradere, J.P. and Schwabe, R.F. (2013). Fate tracing reveals hepatic stellate cells as dominant contributors to liver fibrosis independent of its aetiology. *Nat Commun,* **4,** 2823.

Mehal, W.Z., Iredale, J. and Friedman, S.L. (2011). Scraping fibrosis: Expressway to the core of fibrosis. *Nat Med,* **17,** 552-553.

Messner, S., Agarkova, I., Moritz, W. and Kelm, J.M. (2013). Multi-cell type human liver microtissues for hepatotoxicity testing. *Arch Toxicol,* **87,** 209-213.

Mezey, E. (1982). Liver Disease and Protein Needs. *Annual Review of Nutrition,* **2,** 21-50.

Michaut, A., Moreau, C., Robin, M.-A. and Fromenty, B. (2014). Acetaminophen-induced liver injury in obesity and nonalcoholic fatty liver disease. *Liver International,* **34,** e171-e179.

Morgan, E.T. (2009). Impact of infectious and inflammatory disease on cytochrome P450-mediated drug metabolism and pharmacokinetics. *Clin Pharmacol Ther,* **85,** 434-438.

Motomura, Y., Kanbayashi, H., Khan, W.I., Deng, Y., Blennerhassett, P.A., Margetts, P.J., Gauldie, J., Egashira, K. and Collins, S.M. (2005). The gene transfer of soluble VEGF type I receptor (Flt-1) attenuates peritoneal fibrosis formation in mice but not soluble TGF-beta type II receptor gene transfer. *Am J Physiol Gastrointest Liver Physiol,* **288,** G143-150.

Müller, A., Machnik, F., Zimmermann, T. and Schubert, H. (1988). Thioacetamide-induced cirrhosis-like liver lesions in rats usefulness and reliability of this animal model. *Experimental pathology,* **34,** 229-236.

Muriel, P., Alba, N., Pérez-Álvarez, V.M., Shibayama, M. and Tsutsumi, V.K. (2001). Kupffer cells inhibition prevents hepatic lipid peroxidation and damage induced by carbon tetrachloride. *Comparative Biochemistry and Physiology Part C: Toxicology & Pharmacology,* **130,** 219-226.

Muriel, P. and Escobar, Y. (2003). Kupffer cells are responsible for liver cirrhosis induced by carbon tetrachloride. *Journal of Applied Toxicology,* **23,** 103-108.

Murphy, K., Dorfman, S., Smith, N., Bauwens, L., Sohn, I., McDonald, T., Leigh-Lancaster, C. and Law, R.J.(2015). Devices, systems, and methods for the fabrication of tissue. Google Patents.

Murphy, S.V. and Atala, A. (2014). 3D bioprinting of tissues and organs. *Nature biotechnology,* **32,** 773-785.

Murray, C.J., Vos, T., Lozano, R., Naghavi, M. and al., e. (2012). Disability-adjusted life years (DALYs) for 291 diseases and injuries in 21 regions, 1990-2010: a systematic analysis for the Global Burden of Disease Study 2010. *Lancet,* **380,** 2197-2223.

Nguyen, D.G., Funk, J., Robbins, J.B., Crogan-Grundy, C., Presnell, S.C., Singer, T. and Roth, A.B. (2016). Bioprinted 3D Primary Liver Tissues Allow Assessment of Organ-Level Response to Clinical Drug Induced Toxicity *In Vitro*. *PLoS ONE,* **11,** e0158674.

Norona, L.M., Nguyen, D.G., Gerber, D.A., Presnell, S.C. and LeCluyse, E.L. (2016). Editor's Highlight: Modeling Compound-Induced Fibrogenesis In Vitro Using Three-Dimensional Bioprinted Human Liver Tissues. *Toxicological Sciences,* **154,** 354-367.

Olinga, P. and Schuppan, D. (2013). Precision-cut liver slices: A tool to model the liver ex vivo. *Journal of Hepatology,* **58,** 1252-1253.

Olsen, A.L., Bloomer, S.A., Chan, E.P., Gaca, M.D., Georges, P.C., Sackey, B., Uemura, M., Janmey, P.A. and Wells, R.G. (2011). Hepatic stellate cells require a stiff environment for myofibroblastic differentiation. *Am J Physiol Gastrointest Liver Physiol,* **301,** G110-118.

Olson, H., Betton, G., Robinson, D., Thomas, K., Monro, A., Kolaja, G., Lilly, P., Sanders, J., Sipes, G., Bracken, W., Dorato, M., Van Deun, K., Smith, P., Berger, B. and Heller, A. (2000). Concordance of the toxicity of pharmaceuticals in humans and in animals. *Regulatory toxicology and pharmacology : RTP,* **32,** 56-67.

Osuga, T., Ikura, Y., Kadota, C., Hirano, S., Iwai, Y. and Hayakumo, T. (2015). Significance of liver biopsy for the evaluation of methotrexate-induced liver damage in patients with rheumatoid arthritis. *Int J Clin Exp Pathol,* **8,** 1961-1966.

Parks, W.C., Wilson, C.L. and Lopez-Boado, Y.S. (2004). Matrix metalloproteinases as modulators of inflammation and innate immunity. *Nat Rev Immunol,* **4,** 617-629.

Pellicoro, A., Ramachandran, P., Iredale, J.P. and Fallowfield, J.A. (2014). Liver fibrosis and repair: immune regulation of wound healing in a solid organ. *Nat Rev Immunol,* **14,** 181-194.

Pintilie, D.G., Shupe, T.D., Oh, S.H., Salganik, S.V., Darwiche, H. and Petersen, B.E. (2010). Hepatic stellate cells' involvement in progenitor-mediated liver regeneration. *Lab Invest,* **90,** 1199-1208.

Puche, J.E., Saiman, Y. and Friedman, S.L. (2013). Hepatic stellate cells and liver fibrosis. *Compr Physiol,* **3,** 1473-1492.

Qazi, B.S., Tang, K. and Qazi, A. (2011). Recent advances in underlying pathologies provide insight into interleukin-8 expression-mediated inflammation and angiogenesis. *Int J Inflam***,** 908468.

Ramachandran, P. and Iredale, J.P. (2012). Macrophages: Central regulators of hepatic fibrogenesis and fibrosis resolution. *Journal of Hepatology,* **56,** 1417-1419.

Ramaiahgari, S.C., den Braver, M.W., Herpers, B., Terpstra, V., Commandeur, J.N.M., van de Water, B. and Price, L.S. (2014). A 3D in vitro model of differentiated HepG2 cell spheroids with improved liver-like properties for repeated dose high-throughput toxicity studies. *Archives of Toxicology,* **88,** 1083-1095.

Ramsden, D., Tweedie, D.J., Chan, T.S., Taub, M.E. and Li, Y. (2014). Bridging in vitro and in vivo metabolism and transport of faldaprevir in human using a novel cocultured human hepatocyte system, HepatoPac. *Drug Metab Dispos,* **42,** 394-406.

Rausch, O. (2006). High content cellular screening. *Current Opinion in Chemical Biology,* **10,** 316-320.

Reid, L.M., Fiorino, A.S., Sigal, S.H., Brill, S. and Holst, P.A. (1992). Extracellular matrix gradients in the space of disse: Relevance to liver biology. *Hepatology,* **15,** 1198-1203.

Rieder, H., Armbrust, T., Meyer zum Buschenfelde, K.H. and Ramadori, G. (1993). Contribution of sinusoidal endothelial liver cells to liver fibrosis: expression of transforming growth factor-beta 1 receptors and modulation of plasmin-generating enzymes by transforming growth factor-beta 1. *Hepatology,* **18,** 937-944.

Robbins, P.D. and Morelli, A.E. (2014). Regulation of immune responses by extracellular vesicles. *Nat Rev Immunol,* **14,** 195-208.

Roberts, R.A., Ganey, P.E., Ju, C., Kamendulis, L.M., Rusyn, I. and Klaunig, J.E. (2007). Role of the Kupffer Cell in Mediating Hepatic Toxicity and Carcinogenesis. *Toxicological Sciences,* **96,** 2-15.

Rockey, D.C. (2001). Hepatic blood flow regulation by stellate cells in normal and injured liver. *Seminars in liver disease,* **21,** 337-349.

Rodés, J.(2007). *Textbook of hepatology : from basic science to clinical practice,* Blackwell, Malden, Mass.

Rogiers V., a.V.V. (1993). Rat hepatocyte cultures and co-cultures in biotransformation studies of xenobiotics. *Toxicology,* **82,** 193-208.

Rose, K.A., Holman, N.S., Green, A.M., Andersen, M.E. and LeCluyse, E.L. (2016). Co-culture of Hepatocytes and Kupffer Cells as an In Vitro Model of Inflammation and Drug-Induced Hepatotoxicity. *Journal of Pharmaceutical Sciences,* **105,** 950-964.

Roskos, K., Stuiver, I., Pentoney, S. and Presnell, S. (2015). Bioprinting: An Industrial Perspective In *Essentials of 3D Biofabrication and Translation* (Yoo, J.J. ed.), pp. 395-411. Academic Press, Boston.

Roth, A. and Singer, T. (2014). The application of 3D cell models to support drug safety assessment: opportunities & challenges. *Advanced drug delivery reviews,* **69-70,** 179-189.

Schmitt-Graff, A., Kruger, S., Bochard, F., Gabbiani, G. and Denk, H. (1991). Modulation of Alpha Smooth Muscle Actin and Desmin Expression in Perisinusoidal Cells of Normal and Diseased Human Livers. *American Journal of Pathology,* **138,** 1233-1242.

Schneider, C.A., Rasband, W.S. and Eliceiri, K.W. (2012). NIH Image to ImageJ: 25 years of image analysis. *Nature Methods,* **9,** 671-675.

Sebastiani, G. and Alberti, A. (2006). Noninvasive fibrosis markers reduce but not substitute the need for liver biopsy. *World J Gastroenterol,* **12,** 3682-3694
Shepherd, B.R., Robbins, J.B., Gorgen, V.A. and Presnell, S.C.(2015). Engineered liver tissues, arrays thereof, and methods of making the same. Google Patents.

Shergy, W.J., Polisson, R.P., Caldwell, D.S., Rice, J.R., Pisetsky, D.S. and Allen, N.B. (1988). Methotrexate-Associated Hepatotoxicity: Retrospective Analysis of 210 Patients with Rheumatoid Arthritis. *The American Journal of Medicine,* **85,** 771-774.

Sherman, M. (2009). Vinyl chloride and the liver. *Journal of Hepatology,* **51,** 1074-1081.

Shiozawa, K., Tanaka, Y., Yoshihara, R., Imura, S., Murata, M., Yamane, T., Miura, Y., Hashiramoto, A. and Shiozawa, S. (2005). Serum levels and pharmacodynamics of methotrexate and its metabolite 7-hydroxy methotrexate in Japanese patients with rheumatoid arthritis treated with 2-mg capsule of methotrexate three times per week. *Mod Rheumatol,* **15,** 405-409.

Shiratori, Y., Tananka, M., Kawase, T., Shiina, S., Komatsu, Y. and Omata, M. (1993). Quantification of sinusoidal cell function in vivo. *Seminars in liver disease,* **13,** 39-49.

Smedsrod, B., Pertoft, H., Gustafson, S. and Laurent, T.C. (1990). Scavenger functions of the liver endothelial cell. *The Biochemical journal,* **266,** 313-327.

Smith, M.T. and Wills, E.D. (1981). Effects of dietary lipid and phenobarbitone on the distribution and concentration of cytochrome P-450 in the liver studied by quantitative cytochemistry. *FEBS letters,* **127,** 33-36.

Soldatow, V.Y., Lecluyse, E.L., Griffith, L.G. and Rusyn, I. (2013). *In vitro* models for liver toxicity testing. *Toxicol Res,* **2,** 23-39.

Starkel, P. and Leclercq, I.A. (2011). Animal models for the study of hepatic fibrosis. *Best Pract Res Clin Gastroenterol,* **25,** 319-333.

Stolz, D.B. (2011). Sinusoidal Endothelial Cells. *Molecular Pathology of Liver Diseases,* **5,** 97-107.

Sziksz, E., Domonkos, P., Lippai, R., Beres, N.J., Fekete, A., Szabo, A.J. and Vannay, A. (2015). Fibrosis Related Inflammatory Mediators: Role of the IL-10 cytokine family. *Mediators of Inflammation,* **2015,** 15.

Tacke, F. and Zimmermann, H.W. (2014). Macrophage heterogeneity in liver injury and fibrosis. *J Hepatol,* **60,** 1090-1096.

Taghdouini, A.E., Najimi, M., Sancho-Bru, P., Sokal, E. and van Grunsven, L.A. (2015). In vitro reversion of activated primary human hepatic stellate cells. *Fibrogenesis Tissue Repair,* **8,** 14.

Takezawa, T., Yamazaki, M., Mori, Y., Yonaha, T. and Yoshizato, K. (1992). Morphological and immuno-cytochemical characterization of a hetero-spheroid composed of fibroblasts and hepatocytes. *Journal of cell science,* **101,** 495-501.

Taura, K., Miura, K., Iwaisako, K., Osterreicher, C.H., Kodama, Y., Penz-Osterreicher, M. and Brenner, D.A. (2010). Hepatocytes do not undergo epithelial-mesenchymal transition in liver fibrosis in mice. *Hepatology,* **51,** 1027-1036.

Thiele, G.M., Duryee, M.J., Thiele, G.E., Tuma, D.J. and Klassen, L.W. (2015). Review: Precision Cut Liver Slices for the Evaluation of Fatty Liver and Fibrosis. *Current molecular pharmacology*.

Thomas, R.J., Bhandari, R., Barrett, D.A., Bennett, A.J., Fry, J.R., Powe, D., Thomson, B.J. and Shakesheff, K.M. (2005). The effect of three-dimensional co-culture of hepatocytes and hepatic stellate cells on key hepatocyte functions in vitro. *Cells Tissues Organs,* **181,** 67-79.

Tolosa, L., Gomez-Lechon, M.J. and Donato, M.T. (2015). High-content screening technology for studying drug-induced hepatotoxicity in cell models. *Arch Toxicol,* **89,** 1007-1022.

Tong, H.Y., Medrano, N., Borobia, A.M., Martínez, A.M., Martín, J., Ruiz, J.A., García, S., Quintana, M., Carcas, A.J., Frías, J. and Ramírez, E. (2015). Hepatotoxicity induced by acute and chronic paracetamol overdose in adults. Where do we stand? *Regulatory Toxicology and Pharmacology,* **72,** 370-378.

Traber, P.G., Chou, H., Zomer, E., Hong, F., Klyosov, A., Fiel, M.I. and Friedman, S.L. (2013). Regression of fibrosis and reversal of cirrhosis in rats by galectin inhibitors in thioacetamide-induced liver disease. *PLoS One,* **8,** e75361.

Trask, O.J., Jr., Moore, A. and LeCluyse, E.L. (2014). A micropatterned hepatocyte coculture model for assessment of liver toxicity using high-content imaging analysis. *Assay and drug development technologies,* **12,** 16-27.

Troeger, J.S., Mederacke, I., Gwak, G.Y., Dapito, D.H., Mu, X., Hsu, C.C., Pradere, J.P., Friedman, R.A. and Schwabe, R.F. (2012). Deactivation of hepatic stellate cells during liver fibrosis resolution in mice. *Gastroenterology,* **143,** 1073-1083 e1022.

Turner, R., Lozoya, O., Wang, Y., Cardinale, V., Gaudio, E., Alpini, G., Mendel, G., Wauthier, E., Barbier, C., Alvaro, D. and Reid, L.M. (2011). Human hepatic stem cell and maturational liver lineage biology. *Hepatology,* **53,** 1035-1045.

Ugele, B., Kempen, H.J., Kempen, J.M., Gebhardt, R., Meijer, P., Burger, H.J. and Princen, H.M. (1991). Heterogeneity of rat liver parenchyma in cholesterol 7 alpha-hydroxylase and bile acid synthesis. *The Biochemical journal,* **276 (Pt 1),** 73-77.

Ukairo, O., Kanchagar, C., Moore, A., Shi, J., Gaffney, J., Aoyama, S., Rose, K., Krzyzewski, S., McGeehan, J., Andersen, M.E., Khetani, S.R. and Lecluyse, E.L. (2013). Long-term stability of primary rat hepatocytes in micropatterned cocultures. *Journal of biochemical and molecular toxicology,* **27,** 204-212.

Van de Bovenkamp, M., Groothuis, G.M., Meijer, D.K. and Olinga, P. (2007). Liver fibrosis in vitro: cell culture models and precision-cut liver slices. *Toxicol In Vitro,* **21,** 545-557.

Veidal, S.S., Karsdal, M.A., Nawrocki, A., Larsen, M.R., Dai, Y., Zheng, Q., Hagglund, P., Vainer, B., Skjot-Arkil, S. and Leeming, D.J. (2011). Assessment of proteolytic degradation of the basement membrane: a fragment of type IV collagen as a biochemical marker of liver fibrosis. *Fibrogenesis & Tissue Repair,* **4,** 1-11.

Wang, Y., Cui, C.B., Yamauchi, M., Miguez, P., Roach, M., Malavarca, R., Costello, M.J., Cardinale, V., Wauthier, E., Barbier, C., Gerber, D.A., Alvaro, D. and Reid, L.M. (2011). Lineage restriction of human hepatic stem cells to mature fates is made efficient by tissue-specific biomatrix scaffolds. *Hepatology,* **53,** 293-305.

Watelet, J., Laurent, V., Bressenot, A., Bronowicki, J.P., Larrey, D. and Peyrin-Biroulet, L. (2007). Toxicity of chronic paracetamol ingestion. *Alimentary Pharmacology & Therapeutics,* **26,** 1543-1544.

Westra, I.M., Mutsaers, H.A., Luangmonkong, T., Hadi, M., Oosterhuis, D., de Jong, K.P., Groothuis, G.M. and Olinga, P. (2016). Human precision-cut liver slices as a model to test antifibrotic drugs in the early onset of liver fibrosis. *Toxicol In Vitro,* **35,** 77-85.

Xu, L., Hui, A.Y., Albanis, E., Arthur, M.J., O'Byrne, S.M., Blaner, W.S., Mukherjee, P., Friedman, S.L. and Eng, F.J. (2005). Human hepatic stellate cell lines, LX-1 and LX-2: new tools for analysis of hepatic fibrosis. *Gut,* **54,** 142-151.

Yin, C., Evason, K.J., Asahina, K. and Stainier, D.Y. (2013). Hepatic stellate cells in liver development, regeneration, and cancer. *J Clin Invest,* **123,** 1902-1910.

You, Q., Cheng, L., Kedl, R.M. and Ju, C. (2008). Mechanism of T cell tolerance induction by murine hepatic Kupffer cells. *Hepatology,* **48,** 978-990.

Zinchenko, Y.S., Culberson, C.R. and Coger, R.N. (2006). Contribution of non-parenchymal cells to the performance of micropatterned hepatocytes. *Tissue engineering,* **12,** 2241-1251.